Report No. FAA-RD-77-38

WIND SHEAR MODELING FOR AIRCRAFT HAZARD DEFINITION

Walter Frost
Dennis W. Camp

March 1977
Interim Report

Prepared for

U.S. DEPARTMENT OF TRANSPORTATION
FEDERAL AVIATION ADMINISTRATION
Systems Research & Development Service
Washington, D.C. 20590

NOTICE

This document is disseminated under the sponsorship of the Department of Transportation in the interest of information exchange. The United States Government assumes no liability for its contents or use thereof.

Technical Report Documentation Page

1. Report No.	2. Government Accession No.	3. Recipient's Catalog No.
FAA-RD-77-36		

4. Title and Subtitle: Wind Shear Modeling for Aircraft Hazard Definition

5. Report Date: March 1977

6. Performing Organization Code:

7. Author(s): Walter Frost (1) / Dennis W. Camp

8. Performing Organization Report No.: 16 p.

9. Performing Organization Name and Address:
National Aeronautics & Space Adm.
Atmospheric Sciences Division
Space Sciences Laboratory
Marshall Space Flight Center, AL 35812
(1) FWG Assoc., Inc.
Tullahoma, TN
37388

10. Work Unit No. (TRAIS): 154-451-014A

11. Contract or Grant No.: DOT-FA76-WAI-620

12. Sponsoring Agency Name and Address:
U. S. Department of Transportation
Federal Aviation Administration
Systems Research and Development Service, Airport Div.
Washington, D.C. 20590

13. Type of Report and Period Covered: Interim Report, for April 1976 — March 1977

14. Sponsoring Agency Code: FAA/ARD-450

15. Supplementary Notes: Prepared under FAA Interagency Agreement No. DOT-FA76WAI-620, managed by the Aviation Weather Systems Branch, ARD-450. Contracted by MSFC (NAS8-32217) to FWG Assoc., Tullahoma, TN 37388

16. Abstract

This document presents a discussion of the various types of wind shear which cause problems to aircraft operations. The presentation is limited to low-level wind shear such as could be encountered in the vicinity of airports by aircraft on approach to landing and on takeoff. The types of shear discussed are primarily limited to frontal, thunderstorm and shears associated with stable and neutral boundary layers. The discussions emphasize modeling of the wind shear for simulation purposes.

Wind shear is discussed not only as a change in absolute wind speed but also as a result of wind direction change. Some insight is given relative to a combination of wind speed and direction change. It is to be noted that the condition affecting aircraft operations is not one shear parameter but is a combination of several, e.g. horizontal shear, vertical shear, wind direction change and height of shear above ground level.

17. Key Words	18. Distribution Statement
Wind Shear Thunderstorm Gust Fronts Frontal Wind Shear	Document is available to the U.S. public through the National Technical Information Service, Springfield, Virginia 22151.

19. Security Classif. (of this report)	20. Security Classif. (of this page)	21. No. of Pages	22. Price
Unclassified	Unclassified	152	

Form DOT F 1700.7 (8-72) Reproduction of completed page authorized

PREFACE

The authors are grateful for the many people who were helpful in the preparation of this report. A complete acknowledgment list would be too lengthy; however, there are some individuals we feel we must recognize. These are Messrs. Frank Coons, Guice Tinsley, and Frank Melewicz of the FAA for many helpful discussions and especially for their patience in critiquing the report; Messrs. R. Craig Goff* and Jean Lee of NSSL for discussions and providing thunderstorm data; Mr. Hubert McCaleb and other members of NTSB for providing needed information and reports; Mr. Paul Jernigan of Douglas Aircraft for discussion on how data are used in aircraft simulators; Messrs. Mike Kennan and Dean Babock of SRI for many helpful discussions and comments; Drs. John McCarthy and Edward Blick of the University of Oklahoma for discussions and providing data; and we especially wish to recognize Dr. George Fichtl without whose help and assistance the report would not have been possible. The authors are indebted to Mrs. Judy Wright for typing the report.

*Mr. R. Craig Goff's present affiliation is FAA/NAFEC.

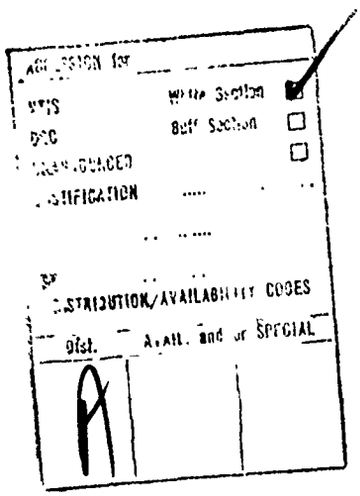

METRIC CONVERSION FACTORS

Approximate Conversions to Metric Measures

Symbol	When You Know	Multiply by	To Find	Symbol
	LENGTH			
	inches	*2.5	centimeters	cm
	feet	30	centimeters	cm
	yards	0.9	meters	m
mi	miles	1.6	kilometers	km
	AREA			
in^2	square inches	6.5	square centimeters	cm^2
ft^2	square feet	0.09	square meters	m^2
yd^2	square yards	0.8	square meters	m^2
mi^2	square miles	2.6	square kilometers	km^2
	acres	0.4	hectares	ha
	MASS (weight)			
oz	ounces	28	grams	g
lb	pounds	0.45	kilograms	kg
	short tons (2000 lb)	0.9	tonnes	t
	VOLUME			
tsp	teaspoons	5	milliliters	ml
tbsp	tablespoons	15	milliliters	ml
fl oz	fluid ounces	30	milliliters	ml
c	cups	0.24	liters	l
pt	pints	0.47	liters	l
qt	quarts	0.95	liters	l
gal	gallons	3.8	liters	l
ft^3	cubic feet	0.03	cubic meters	m^3
yd^3	cubic yards	0.76	cubic meters	m^3
	TEMPERATURE (exact)			
°F	Fahrenheit temperature	5/9 (after subtracting 32)	Celsius temperature	°C

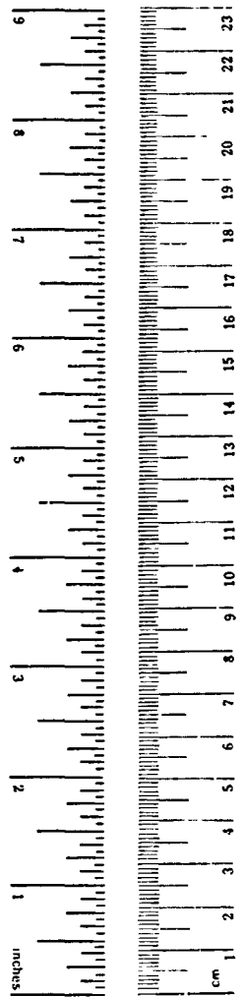

Approximate Conversions from Metric Measures

Symbol	When You Know	Multiply by	To Find	Symbol
	LENGTH			
mm	millimeters	0.04	inches	in
cm	centimeters	0.4	inches	in
m	meters	3.3	feet	ft
m	meters	1.1	yards	yd
km	kilometers	0.6	miles	mi
	AREA			
cm^2	square centimeters	0.16	square inches	in^2
m^2	square meters	1.2	square yards	yd^2
km^2	square kilometers	0.4	square miles	mi^2
ha	hectares (10,000 m^2)	2.5	acres	
	MASS (weight)			
g	grams	0.035	ounces	oz
kg	kilograms	2.2	pounds	lb
t	tonnes (1000 kg)	1.1	short tons	
	VOLUME			
ml	milliliters	0.03	fluid ounces	fl oz
l	liters	2.1	pints	pt
l	liters	1.06	quarts	qt
l	liters	0.26	gallons	gal
m^3	cubic meters	35	cubic feet	ft^3
m^3	cubic meters	1.3	cubic yards	yd^3
	TEMPERATURE (exact)			
°C	Celsius temperature	9/5 (then add 32)	Fahrenheit temperature	°F

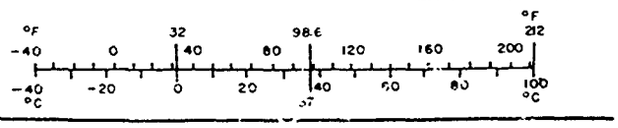

TABLE OF CONTENTS

LIST OF ILLUSTRATIONS

LIST OF TABLES

LIST OF ABBREVIATIONS AND SYMBOLS

A(h/L)	Empirically determined stability functions
B(h/L)	Empirically determined stability functions
C	Gust front speed
C_p	Specific heat
f	Coriolis parameter
H	Heat flux
h	Height scale
k	von Karmans constant
L	Monin-Obukhov stability length
L'	Alternate scaling length (see Equation 5.6)
R	Average slope of gust front
Ri	Richardson's number
Ro	Rossby number
t	Time
T	Temperature
u_c	Cold air velocity component
u_w	Warm air velocity component
u_*	Friction velocity
W_g	Geostrophic wind
W_x	Wind speed in horizontal direction
W_y	Wind speed in lateral direction
W_z	Wind speed in vertical direction

x	Horizontal distance
y	Lateral distance
z	Vertical distance
z_o	Surface roughness
δ	Atmospheric boundary layer thickness
ρ	Density

1.0 INFLUENCE OF WIND SHEAR ON AIRCRAFT OPERATIONS

1.1 Introduction

Wind is an important consideration in the analysis of airplane flight in the atmospheric boundary layer, both because of short scale gusts or turbulence and because of large scale variations of the mean wind. In the planetary boundary layer, the mean wind decays toward the ground and has considerable horizontal variations due to irregularities in terrain. Thus, both spatial and temporal variations occur in mean surface winds encountered along ascending and descending flight paths.

Many analyses of airplane motion have been carried out (1-1, 2, 3) which, in general, consider only constant winds and thus neglect effect of wind shear. Recent reports of commercial airline accidents, however, have identified wind shear in the planetary boundary layer as being a significant factor in the cause of these accidents, illustrating that variable winds are an importa design consideration.

This report begins with a review of the reported influence of wind shear on aircraft accidents. Recent major accidents where wind shear was a primary factor are described.

State of the art mathematical models, tabulated data of mean wind profiles and fields which can be generally used in computer simulation of aircraft flight through the wind shears associated with these meteorological conditions are presented.

1.2 Problems of Wind Shear in Aircraft Operations

Accidents caused by encountering strong wind shear, turbulence and gusts during terminal flight operations are becoming increasingly more evident as improved documentation of these conditions is achieved through advanced instrument technology, such as digital flight data recorders. Reference [1-4] reports that weather conditions were significant factors in air carrier accidents within the last two years and Wyatt [1-5] reports weather to be a factor in approximately 39% of all fatal accidents which occurred in general aviation between 1964 to 1973.

To what degree these were due to wind effects is uncertain. However, many missed approaches which have simply been classified as pilot error may, in the light of today's knowledge, be traceable to wind shear.

Recently, a number of well-defined incidents where wind shear has been a major factor contributing to serious accidents have been documented. Laynor [1-6] reports that an Iberian Airlines' DC 10-30 crashed on December 17, 1973, about 500 feet short of the runway while making an Instrument Landing System (ILS) approach to Logan International

Airport, Boston, Massachusetts.

The meteorological data indicated that the winds aloft at altitudes above 1000 feet in the Boston area were generally from the south at speeds approximately 40 kts. The surface wind measured at Logan Airport was from a westerly direction at 9 kts. These data suggest that wind shear existed at the time of the accident.

Examination of the data recorded on the aircraft digital flight data recorder generally verified that the aircraft penetrated an altitude band where a sudden change in wind direction and speed occurred. The results of reconstructing the approach in a Douglas DC-10 simulator disclosed that a wind shear, characterized by a diminishing tailwind component, encountered at low altitudes during the period of approach where the pilot is transitioning from automatic to manual flight, produced a situation in which the aircraft descended below the glide path. Winds representative of those experienced during the accident are shown in Table 1-1.

On January 4, 1971, a FAA Douglas DC-3C, N7 crashed at LaGuardia Airport, New York, approximately 2000 feet short of the approach threshold. The probable cause of the accident was reported [1-7] as the failure of the pilot to recognize the wind shear conditions and compensate for them. The meteorological conditions which prevailed the day of the crash were a warm front between the Kennedy and LaGuardia airports and the winds aloft were southwesterly and quite strong while the surface winds were from the northeast and relatively gentle.

TABLE 1-1

REPRESENTATIVE WINDS ALONG FLIGHT PATH OF DC 10-30 AIRLINER WHICH CRASHED AT LOGAN AIRPORT, DECEMBER 19, 1973 [1-6]

Altitude ft.	Longitudinal Component kt	Lateral Component kt	Direction/Speed North/kt
1600	25 tail	26 left	169/36
1000	23 tail	26 left	176/35
650	21.5 tail	25 left	176/33
500	18.0 tail	23 left	179/29
420	12.5 tail	18.5 left	183/23
350	9 tail	14.5 left	190/17
255	3 tail	10 left	229/9
180	6 head	2 left	270/5
100	6 head	2 left	296/6
0	4 head	2 left	296/5

Sowa [1-8] reports four cases of wind shear ranging from a catastrophic accident to a frightening experience for which the primary cause can be attributed to wind shear. Figure 1-1 from [1-8] illustrates the flight recorder traces of two dissimilar aircrafts at widely separated regions of the earth. The figures suggest that the aircraft most likely encountered a strong headwind near 3000 feet resulting in a pitched-up attitude and a high rate of ascent. At 8000 feet with the throttle and altitude probably adjusted to trim out

the high climb rate, a tailwind was presumably encountered, resulting in a very low pitch attitude and a rapid rate of descent over a distance on the order of 7000 feet. Another 1000 feet and the incident may well have been fatal.

Nine missed approaches (see Table 1-2 from [1-8]) made at J. F. Kennedy Airport, New York, between 2152Z and 2354Z on January 4, 1971, highlight a problem also associated with wind shear. Chambers [1-9] reports a warm front approached JFK from the south arriving approximately 2300Z. At 2330Z, winds were as indicated in Table 1-3.

The wind speeds shown demonstrate that a wind shear of 2 kts/100 ft was present. Prior to the passage of the front, the surface wind was 040°/7 kts. During approach under these shear conditions, a decreasing tailwind with decreasing altitude was encountered and heavy (slow response) aircraft were unable to prevent a speed overrun. They were also high on the glide slope. This conceivably caused many of the missed approaches shown in Table 1-2. Difficulties occurred during takeoff as well since departing airplanes experienced loss of air speed due to the wind shear and also a thrust loss due to flying into warmer air aloft.

Chambers [1-9] points out that British Overseas Airline Company pilots have reported other cases of marked wind shear at New York. Additionally, he notes that BOAC lost an airplane shortly after takeoff from Kano, Nigeria in 1965 due to wind shear from a cold air down draft accompanying a thunderstorm.

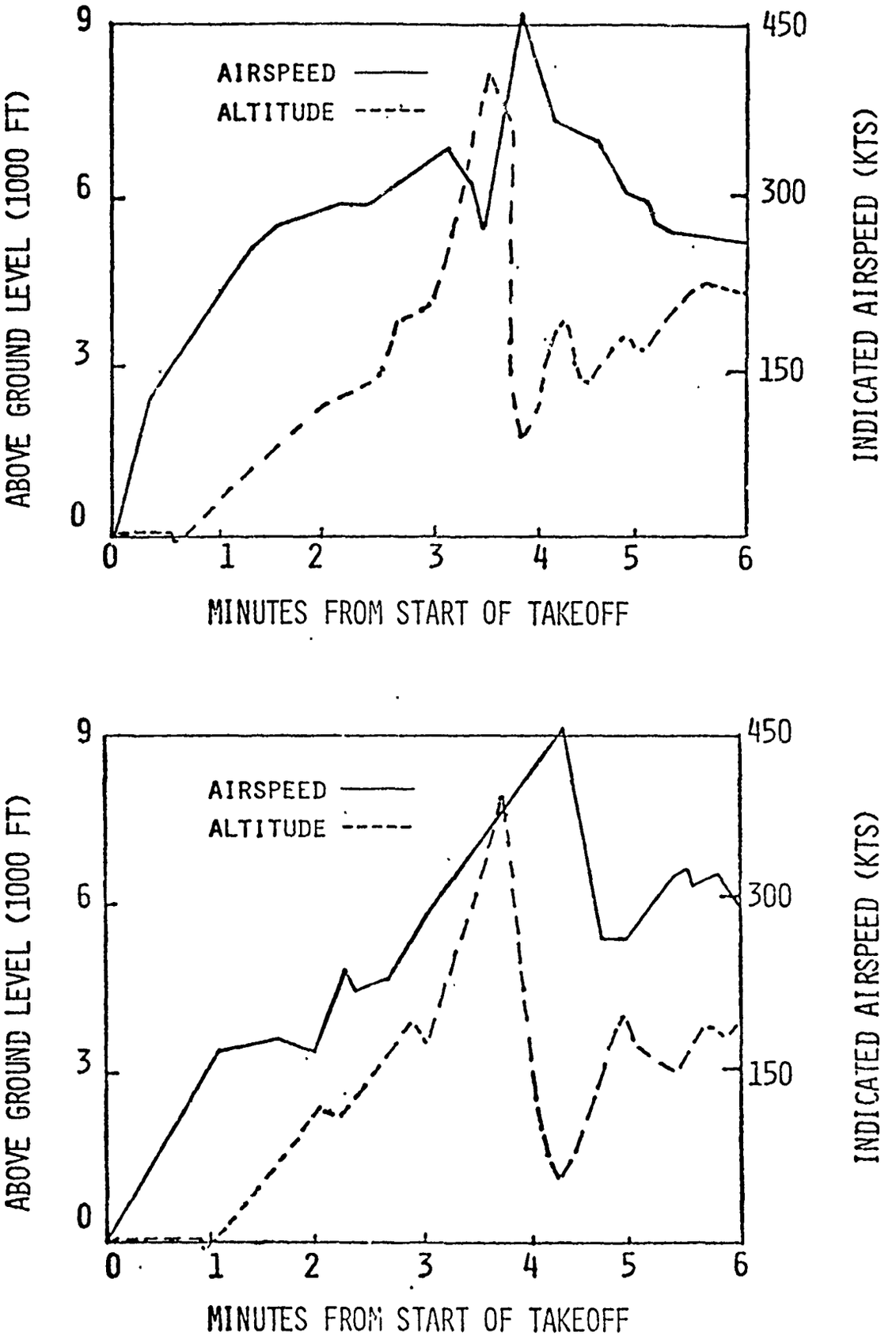

FIGURE 1-1 FLIGHT RECORDER TRACES OF TWO DIFFERENT AIRCRAFT PASSING THROUGH UNEXPECTED WIND SHEAR [1-8].

TABLE 1-2

DATA FROM TOWER LOG OF A MAJOR AIRPORT [1-8]

Time (Z)	Aircraft	Comment
2152	Twin Turbo	Missed approach & diverted
2200	Wide-body	Landed
2237	4-Engine Jet	Missed approach
2300	4-Engine Jet	Landed second approach
2302	Wide-body	Missed approach & diverted
2304	4-Engine Jet	Missed approach
2329	Tri-Jet	Missed approach
2333	4-Engine Jet	Missed approach
2341	4-Engine Jet	Landed second approach
2346	Tri-Jet	Landed second approach
2349	Wide-body	Missed approach
2353	4-Engine Jet	Landed second approach
2354	Wide-body	Missed approach
0013		Changed from runway 04R to 22
0020	Wide-body	Landed second approach
0023	Wide-body	Landed second approach

TABLE 1-3

WINDS OVER JFK ON JANUARY 4, 1971 [1-9]

Direction/Speed (kts)	Altitude
220/05	Surface
215/26	1000 ft.
220/46	2600 ft.

Wind shear is also considered a major factor in two recent airline crashes. A Continental Airlines 727 crashed on takeoff at Stapleton Airport in Denver on August 8, 1975, with no fatalities, but a more ill-fated Boeing 727, Eastern Airlines Flight 66, crashed on landing at J. F. Kennedy Airport in New York June 24, 1975, resulting in 112 deaths.

Wind shear is now being recognized as a hazard to terminal flight operations. Section 1.3 describes qualitatively how wind shear influences the aircraft during approach and departure.

1.3 Effects of Wind Shear on Aircraft Flight

Basically, there are two potentially hazardous shear situations [1-10]. First, a tailwind may shear to either a calm or headwind component. In this instance, initially the airspeed increases, the aircraft pitches up and the altitude increases (Figure 1-2). Second, a headwind may shear to a calm or tailwind component. Initially, the airspeed decreases, the aircraft pitches down and the altitude decreases (Figure 1-3). Aircraft speed, aerodynamic characteristics, power/weight ratio, powerplant response time and pilot reactions along with other factors have a bearing on the severity of wind shear effects.

The potential hazards of wind shear therefore suggest that manned flight simulators should be programmed to train flight crews to cope with shear conditions and for fast time computer analysis to relate the potential hazards posed by

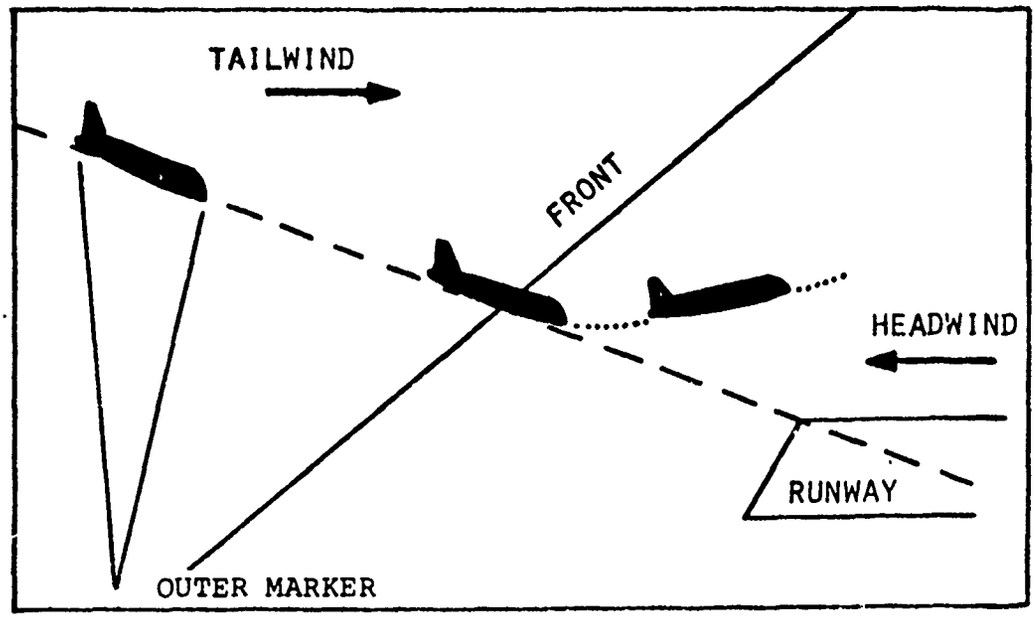

FIGURE 1-2 APPROACH IN TAILWIND WITH SHEAR

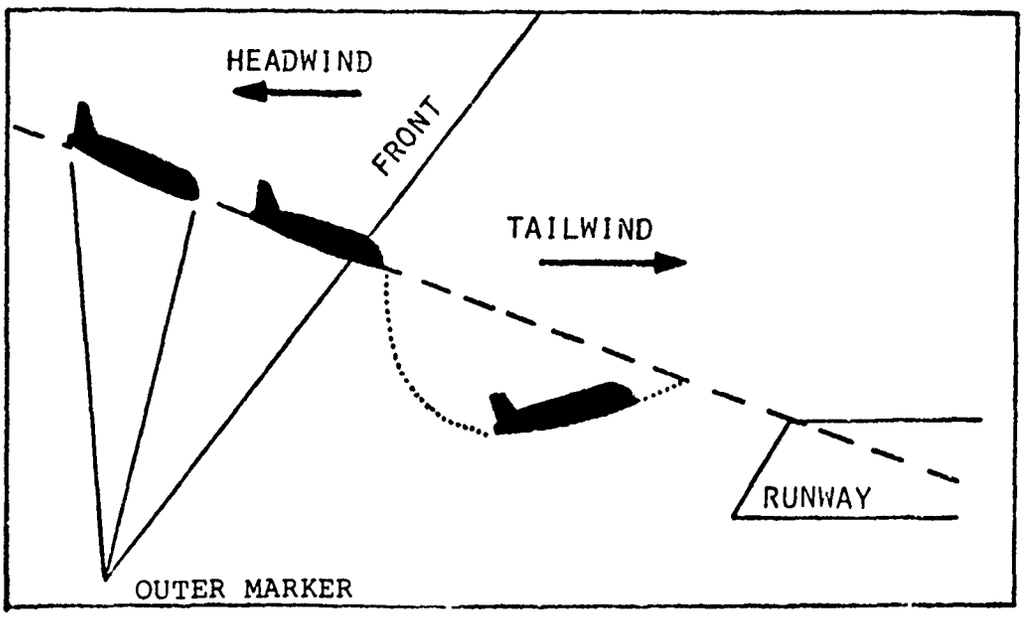

FIGURE 1-3 APPROACH IN HEADWIND WITH SHEAR [1-10].

the wind shear phenomenon to different types of aircraft and control systems. Section 2.0, which follows, identifies the various wind shear regimes while Sections 3.0, 4.0 and 5.0 provide a concise review of the state-of-the-art knowledge of frontal wind shears, thunderstorm wind shears and wind shears found in stable and neutral atmospheric boundary layers, respectively. Formulation of existing models and/or wind data into mathematical expressions is given in these sections for later applications to the engineering models to be developed in the final report.

2.0 TYPES OF WIND SHEAR

2.1 Introduction

Wind shear is caused by several different motions of atmospheric air masses. The atmospheric boundary layer in its natural state always contains some degree of wind shear. The geostrophic wind* aloft which flows parallel to the isobars is turned and retarded by frictional forces as the earth surface is approached. This creates the atmospheric turning layer which has both directional and speed variation with height resulting in vertical wind shear. Near the earth, horizontal variation in winds occur due to terrain irregularities, creating horizontal wind shear. Thus, during most approach and takeoff operations, some degree of wind shear is encountered. The strength of the shear and the degree to which it becomes hazardous is dependent upon the existing combination of meteorological conditions. Under conditions of strong nighttime temperature inversions, which may have in addition a low level jet near the top of the inversion, severe shears can be created, whereas, under conditions of a super adiabatic lapse rate, shear may be destroyed by vigorous turbulent mixing. Wind shear can occur in land/sea

*The geostrophic wind results from a balance of the horizontal pressure gradient and the Coriolis force, and it blows along straight parallel isobars above the boundary layer.

breezes and in anabatic/katabatic winds associated with local topography.

Large wind shear occurs in association with cold air downdrafts spreading over the ground outwards from a thunderstorm (gust front) which may precede the storm by as much as 10 miles. Slowly moving warm and cold fronts create wind shear primarily of a directional variation but also at times of a wind speed variation. Cases of low level jets with accompanying strong shear have been noted in warm sectors near cold fronts.

Sections 3.0, 4.0 and 5.0 of this report provide insight into the current understanding and prediction schemes available for the three major sources of wind shear, i.e., frontal wind shear, thunderstorm wind shear and wind shear associated with stable and neutral boundary layers.

3.0 FRONTAL WIND SHEAR

Fronts, as described in this section, refer to warm and cold frontal surfaces in motion and not to the thunderstorm gust front discussed later. Not all fronts produce significant shear and, in fact, many have gradual transitions in wind speed over broad transition regions. Those cold and warm fronts which do have sharp, narrow transition zones generate significant wind shear that is particularly disturbing due to associated bad weather. It was wind shear created by a slowly moving warm front that caused the numerous missed approaches reported at J. F. Kennedy Airport January 4, 1971.

Mathematical expressions for the structure of wind fields accompanying fronts are not presently available, but criteria for those fronts which contain significant wind shear is given by Sowa [1-8] as: 1) fronts which have a 10°F (5°C) or more temperature difference immediately across the front at surface level; and/or 2) fronts which are moving at 30 kts or faster.

Wind shear associated with fronts can be either directional shear or speed shear. Figure 3-1 illustrates two cases of directional shear. The large solid line in Figure 3-1a indicates the cold front. The wind below the front at A (surface wind) is from 320° and the wind above the front

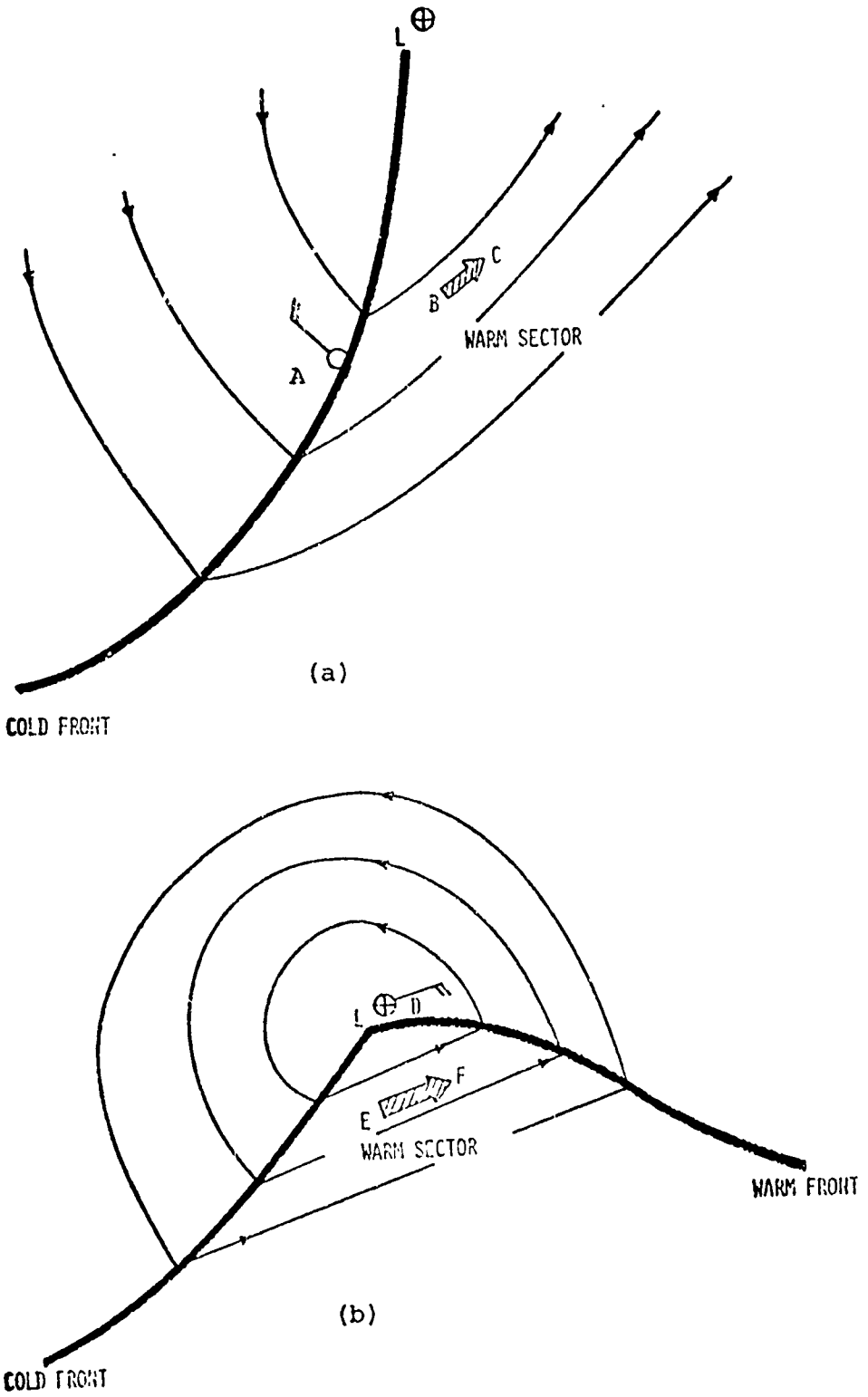

FIGURE 3-1 CASES OF DIRECTIONAL WIND SHEAR ASSOCIATED WITH A FRONT, [1-8].

(which is paralled to the isobars) is from 220°. Similarly, point D in Figure 3-1b which has a warm front sloping over it, has a surface wind from 040°. Above the front, the wind is paralled to the isobars from 230°. The height above the landing surface at which the directional change occurs is difficult to determine. A cold front moving at 30 kts or more might reasonably be expected to have a frontal slope such that the front is 5000 feet above the airport three hours after the passage of the front. Figure 3-2 shows a linear extrapolation of the above observation. The shear associated with a warm front usually exists below 5000 feet and for approximately six hours prior to the warm front passing the airport. The shear becomes negligible once the warm front has gone by.

Wind speed changes as opposed to wind directional changes occur most frequently with slow moving warm fronts having large temperature differences. Very little information on predicting these speed changes is available.

The presence of turbulence with the frontal wind shear may or may not occur. Figure 3-3 indicates the approximate conditions of speed and temperature difference which will induce turbulence along with the wind shear.

Recent data available from the Atmospheric Variability Experiment Number IV (AVE IV) provides three hour soundings of wind speed and direction at 25 m increments in elevation.

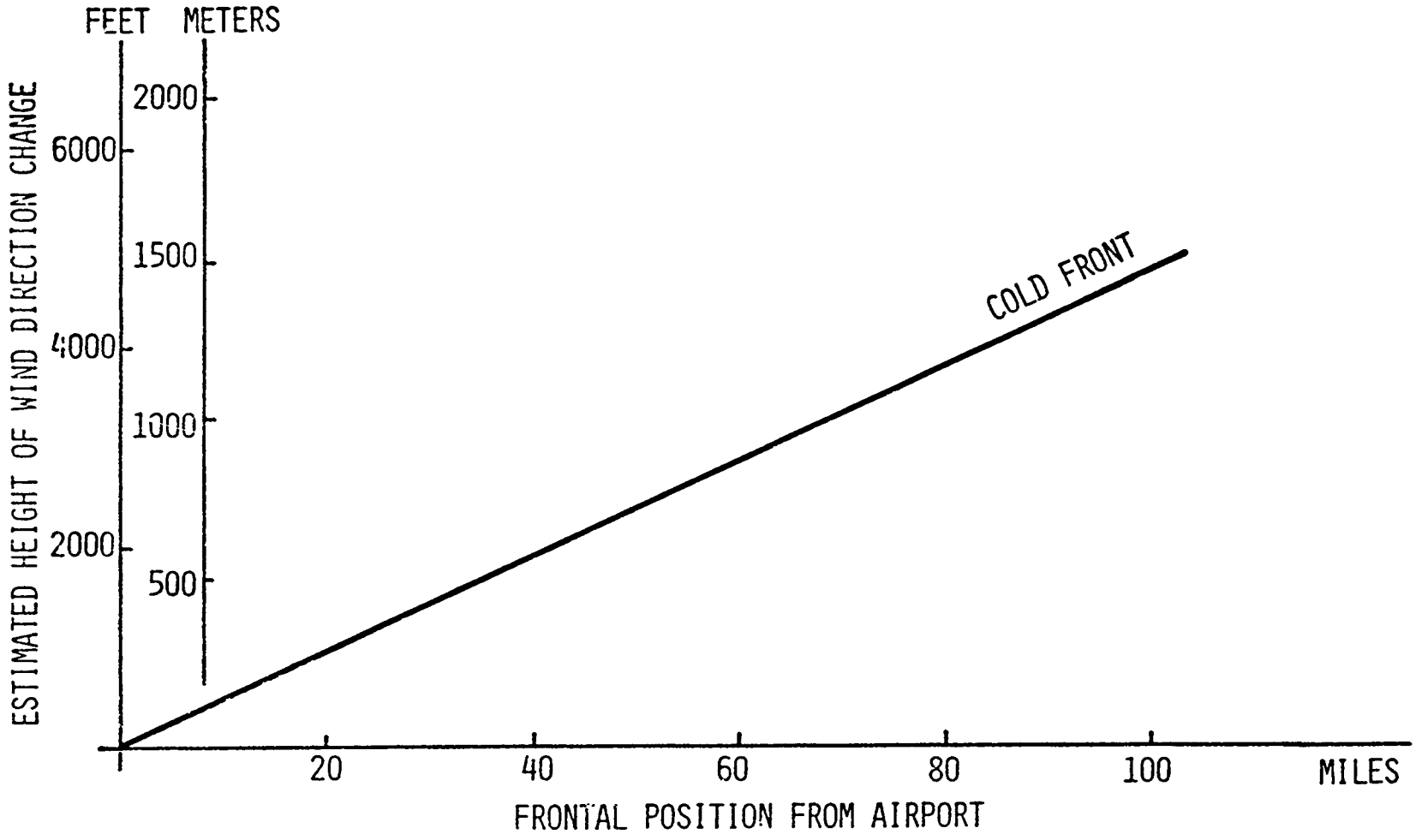

FIGURE 3-2 ESTIMATED POSITION OF COLD FRONT RELATIVE TO THE DISTANCE OF THE FRONT FROM THE AIRPORT.

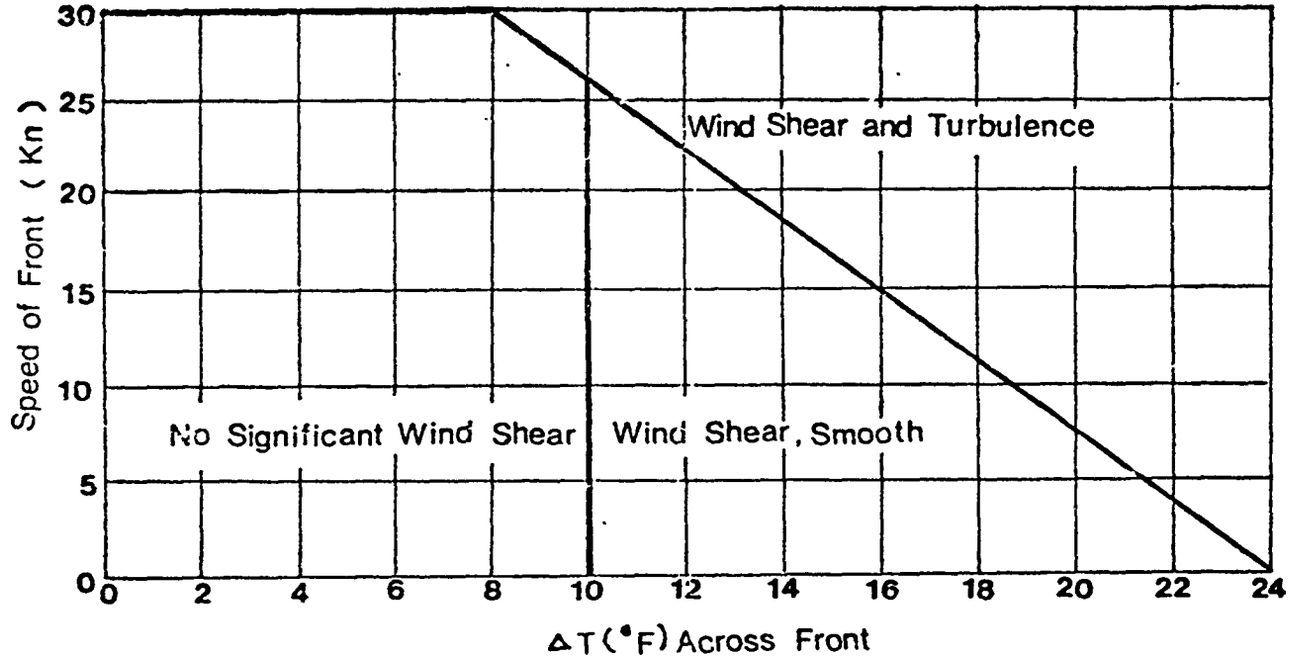

FIGURE 3-3 APPROXIMATE CONDITIONS OF WIND SPEED AND TEMPERATURE DIFFERENCE WHICH WILL INDUCE TURBULENCE ALONG WITH WIND SHEAR, [1-8].

These data are available for 23 stations throughout the eastern half of the United States. Analysis of these data to extract detailed structure of fronts and to develop a predictive model of frontal winds should be carried out.

4.0 THUNDERSTORM GUST FRONTS

4.1 Introduction

One of the most common causes of significant wind shear is the gust front associated with thunderstorms. The thunderstorm gust front is believed responsible for the Eastern 66 crash in New York in 1975, and for the BOAC crash in Kano, Nigeria in 1965, among others. The severe wind shear accompanying thunderstorms is generated by a vigorous rain-cooled downdraft, which spreads out horizontally from the storm cell as it approaches the ground. The cold outflow is led by a strong gusty wind which often occurs as much as 20 km ahead of the storm, called the gust front. During the passing of the front, winds may increase from a relative calm to significant values in a very short time and then decrease as suddenly. This sudden increase in wind is called the gust size and the time over which it occurs is called the gust length.

4.2 Storm Cells

The salient kinematic features of a thunderstorm are best described by considering a particular storm reported by Kropfli and Miller [4-1]. The storm extends to a height of approximately 13 km and covers an area of approximately 324 km^2. Figure 4-1 schematically illustrates four typical features common to most thunderstorms which are: mid-level (6 km in this case), entrainment of cool dry air from behind the storm, a precipitation-filled downdraft, a gust front

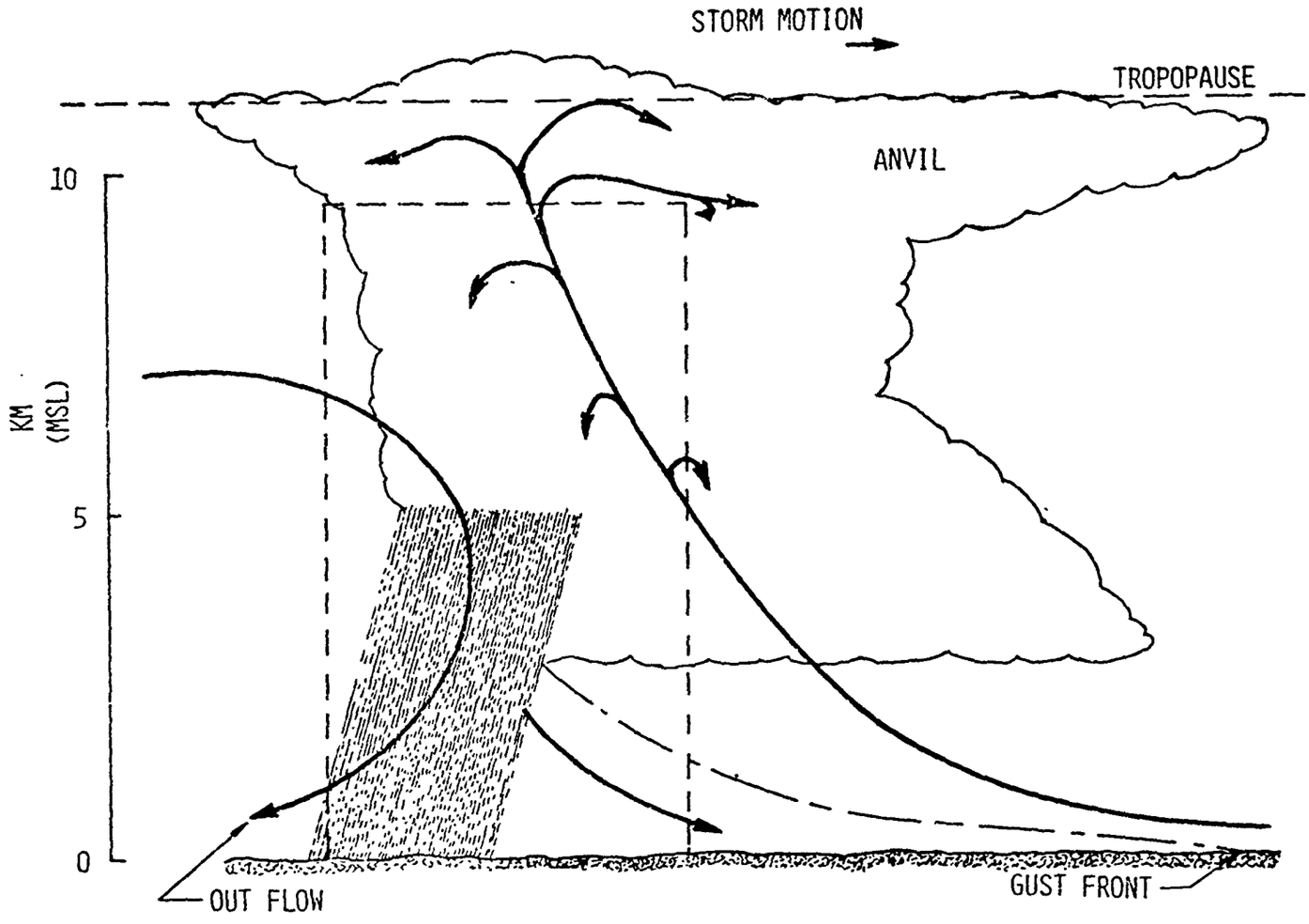

FIGURE 4-1 TYPICAL FEATURES OF A THUNDERSTORM.

consisting of air originating from the middle level and a warm air updraft ahead of the storm. Figure 4-2 from [4-1] shows the approximate three-dimensional motion of air parcels in the storm. This figure illustrates that the gust front at the surface on the right forward flank has its source of air from the left rear flank and exits at the surface under the updraft. The source of air for the northern portion of the gust front comes mainly from air entrained at the left forward flank and partially from the left rearward flank. Air entering at mid-level on the right rear flank descends and exits at the rear about 0.5 km above the ground. This downdraft cut the backside is also supplemented with inflowing air which starts at the lower edge of the updraft. Air entering from the right side and the right forward flank moves upward with cyclonic curvature and exits near the 11 km level. Most of the upward moving warm air inflow from the forward central edge of the storm enters at a 25° backward tilt (the direction of this sheet of air is often called the gust front slope) and ascends with little rotation, exiting near the 11 km level. Part of this air splits off, however, and exits from the left side near the 9 km level.

Contours of vertical velocity relative to the storm motion in horizontal planes through the storm at three elevations are shown in Figure 4-3. Three kilometers above the surface

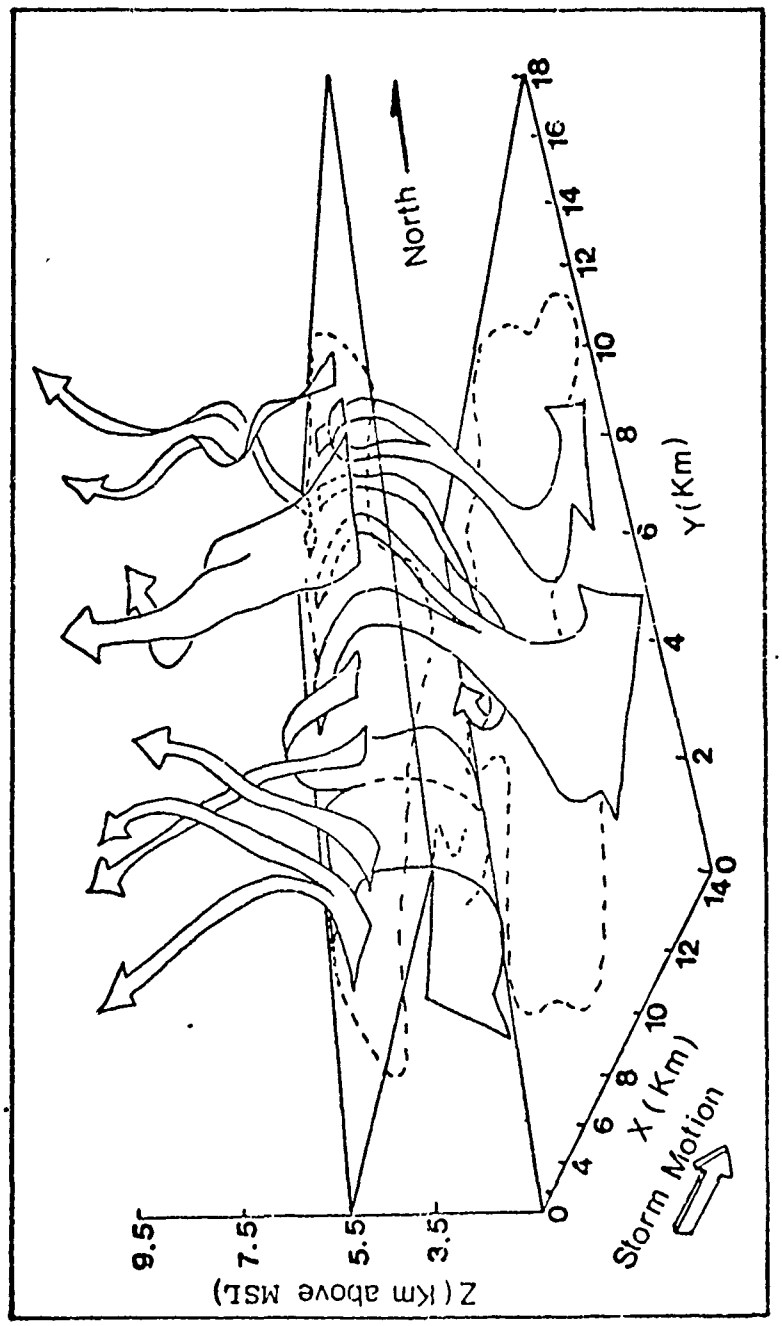

FIGURE 4-2 THREE-DIMENSIONAL MOTIONS OF AIR PARCELS IN A THUNDERSTORM CELL, [4-1].

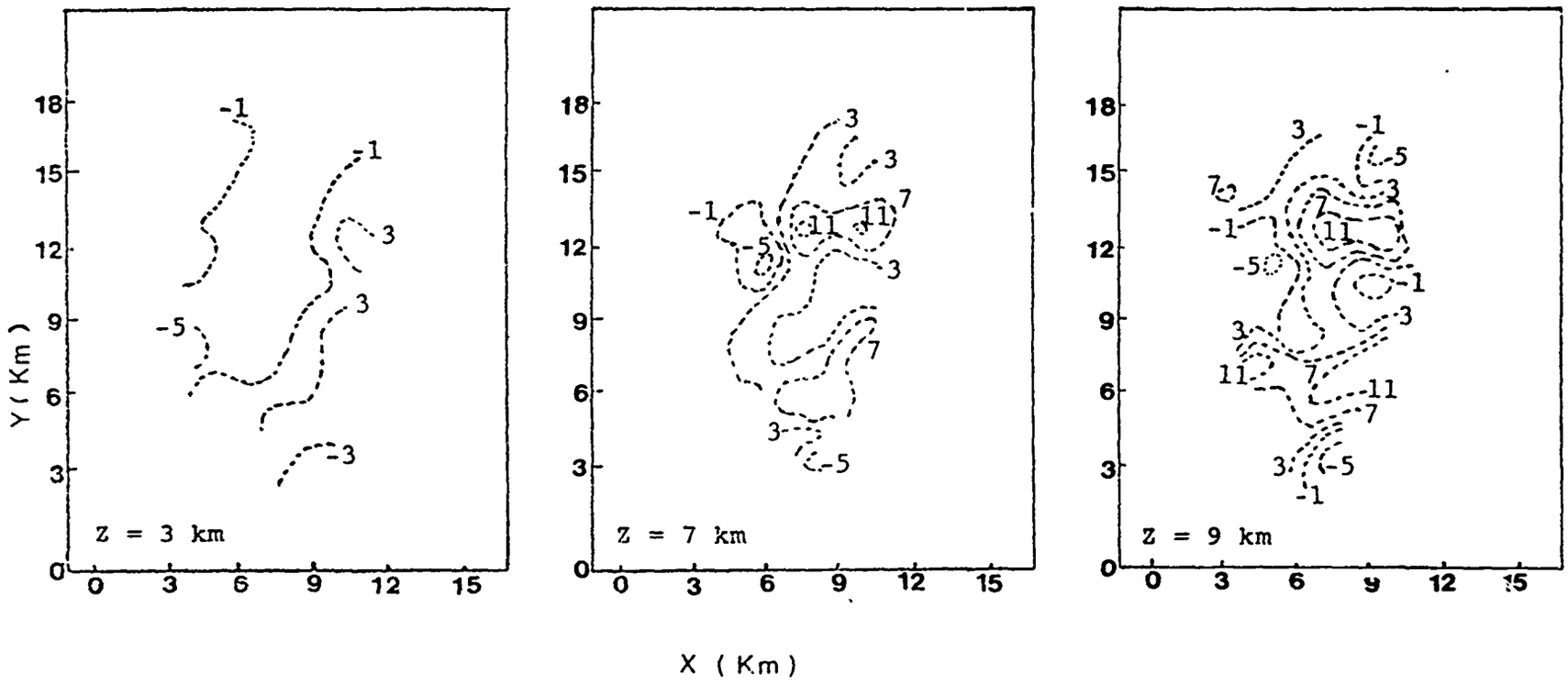

FIGURE 4-3 CONTOURS OF VERTICAL VELOCITY IN METERS PER SECOND RELATIVE TO THE STORM MOTION, [4-1].

the inflow air is moving upward at approximately 3 m/s whereas, the downdraft descends in the center at 4 m/s. At 7 km the inflow has penetrated the storm with vertical velocities reaching 11 m/s. The highest updraft reported during the life of the storm occured near the top and was observed to have attained a speed of 19 m/s. The nature of the relative velocity in the horizontal planes is indicated in the hodograph shown in Figure 4-4. These velocity contours correspond to a particular instant of time and, although retaining similar features, will show strengthening or weakening as the storm matures and decays.

The foregoing comments were intended to describe the large scale characteristics of a thunderstorm.

It is the air motion in the gust front of the thunderstorm below the 2 km level which is of most significance to aeronautical operation in terminal areas. Some relatively detailed wind tower measurements of gust fronts are reported [4-2, 3, 4, 5] although a complete understanding of the physical mechanism and a predictive mathematical model of the three-dimensional motion is still needed.

4.3 Gust Fronts

4.3.1. Gust Front Types

Figure 4-5 illustrates the common features of a gust front.

The figure shows that the pre-storm warm moist air is

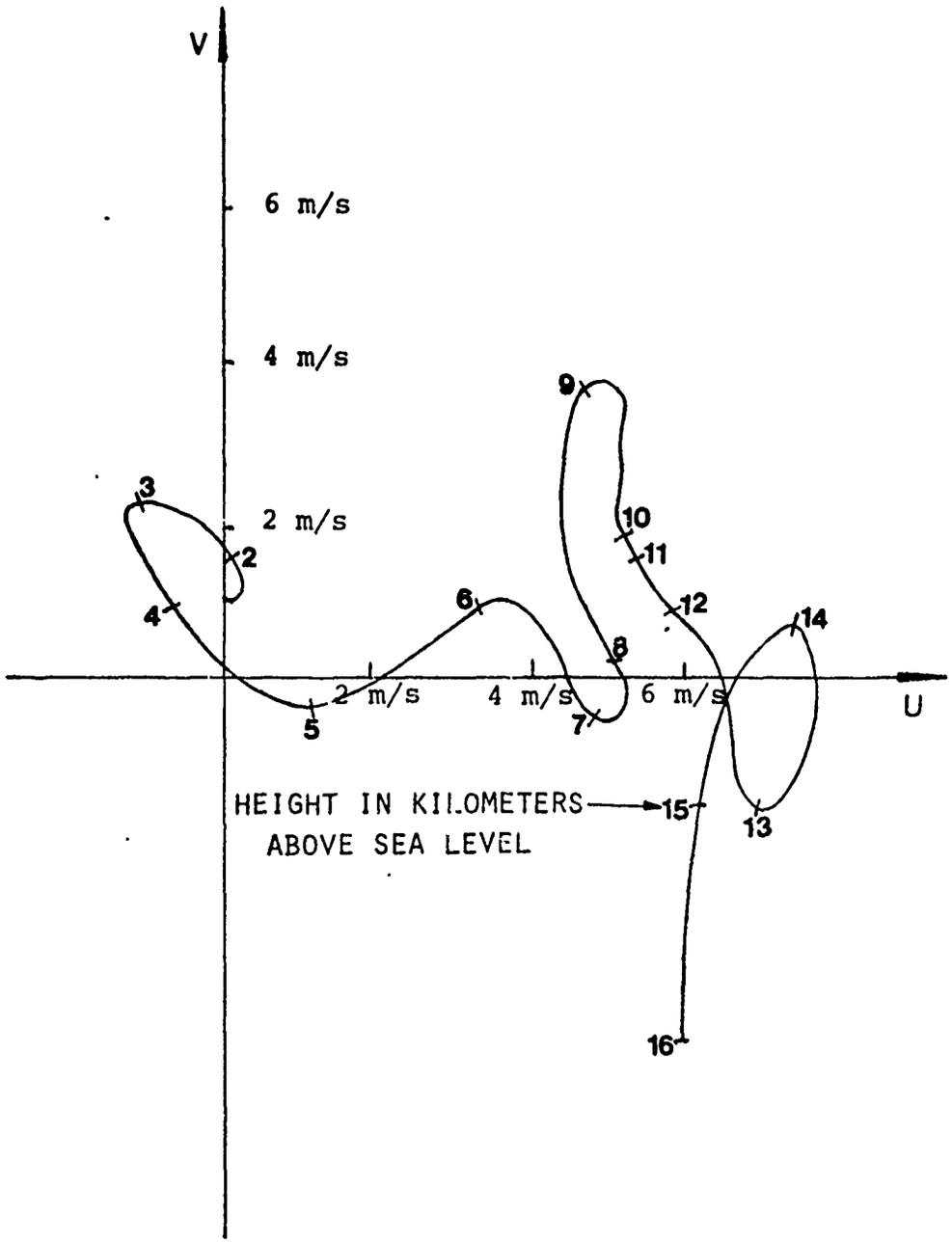

FIGURE 4-4 HODOGRAPH OF HORIZONTAL VELOCITY IN THE THUNDERSTORM CELL, [4-1].

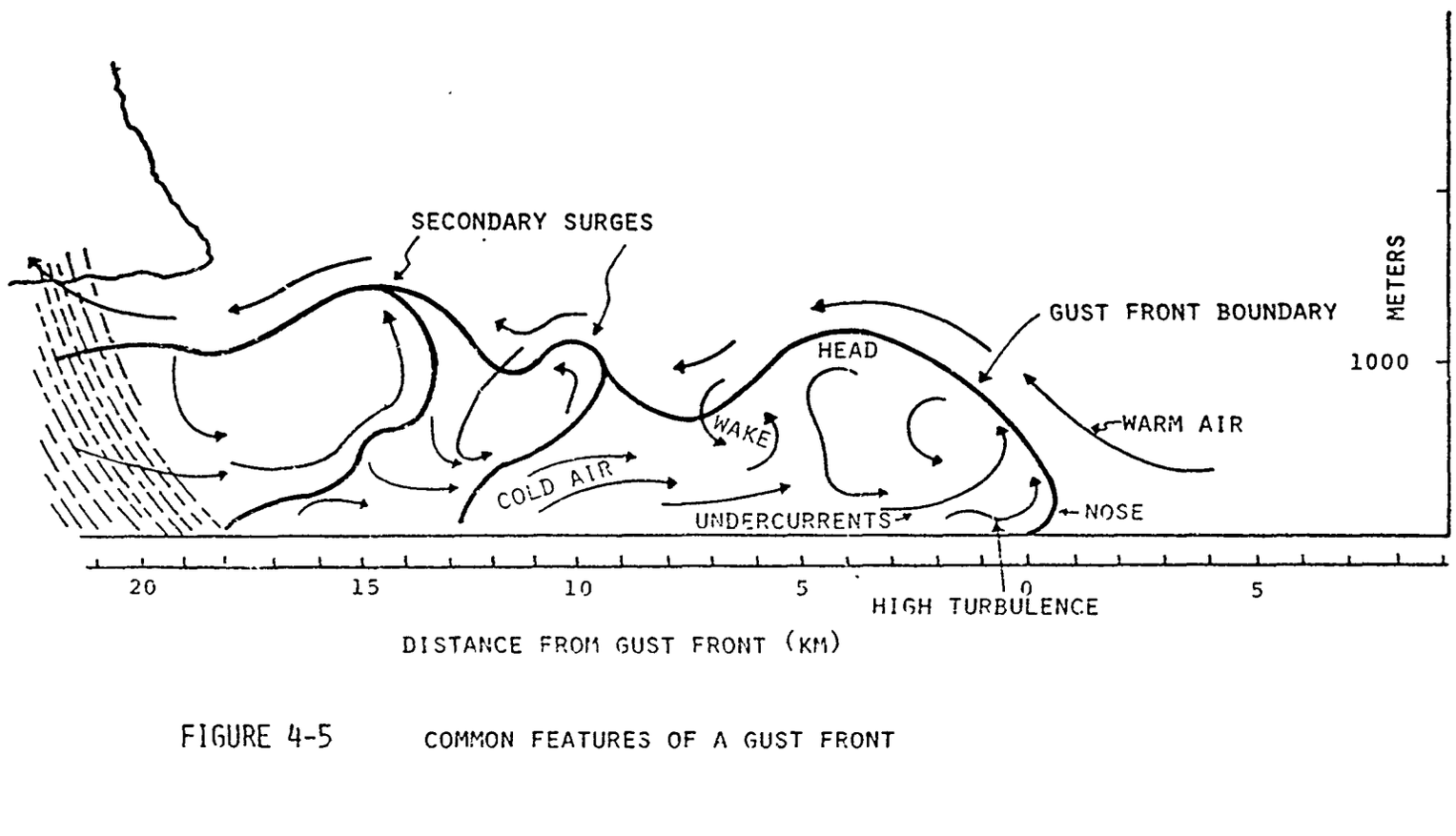

FIGURE 4-5 COMMON FEATURES OF A GUST FRONT

displaced upward by the more dense outflow from the thunderstorm. The mechanical forcing occurs in a 1 km wide band in advance of the gust front. After rising about 800 m over the head, gravitational instability forces the uplifted air down in the wake of the gravity current and horizontal divergence assists entrainment of warm air across the inversion boundary into the cold outflow. This wake, then, is a highly turbulent zone frequently characterized by large shears in the horizontal wind and large oscillations in vertical motion. Similar characteristics are observed in secondary outflow surges. Horizontal divergence has been observed to be so strong in the wake of these secondary surges that large volumes of air may descend almost to the surface.

The extent and intensity to which the features illustrated in Figure 4-5 may be present depend upon the evolution of the thunderstorm. Goff [4-2] has grouped his data into four frontal cases. These are:

1. Gust fronts associated with intensifying storms or accelerating outflow.
2. Gust fronts associated with mature intense storms or strong outflow.
3. Gust fronts associated with dissipating storms or outflow decelerating with respect to the storm.
4. Gust fronts in the final stage of life cycle.

4.3.2 Gust Front Speed

Table 4-1 lists the gust front speed of the 17 thunderstorms reported in [4-2]. Gust fronts associated with intensifying and accelerating outflow tend to move more slowly relative to the ground than those associated with storms in the state of final dissipation which move more rapidly. The gust front speed has been related to the velocity component in the cold air by Clarke [4-6] as:

$$c = 0.67\ u_c \qquad 4.1$$

Frank [4-5] gives $c = 0.62\ u_c$ and Colmer's [4-3] data from a visual inspection seem to support a value on the order of 0.67. Goff [4-2] finds Equation 4.1 suitable for case 1 type storms, but that

$$c = 0.7\ u_c + 0.3\ u_w \qquad 4.2$$

where u_w is the velocity component in the warm air (normally negative) correlates types 2 and 3 storms somewhat better. Type 4 storms appear to have a different propagation mechanism and are not well predicted by either Equation 4.1 or 4.2.

4.3.3 Gust Front Characteristics

Most all gust front passages are either dry, or almost coincident with the onset of rain. The dry gust front may move as far as 10 to 12 km ahead of the precipitation and

TABLE 4-1

GUST FRONT SPEEDS OF 17 DIFFERENT STORMS

Type	No. of Storms	Gust Front Speed (m/s^{-1})
1	4	6.1, 5.0, 8.6, 11.6
2	8	16.7, 11.0, 11.8, 8.5 11.5, 13.1, 12.4, 5.5
3	4	9.6, 8.0, 11.4, 6.9
4	1	17.5

can travel this distance from the cell center in 15 to 20 min. [4-7]. Goff [4-2] reports that the separation distance between precipitation and the gust front is largest for mature storms, case 2, whereas Colmer [4-3] reports that for the 11 thunderstorms he studied, the gust fronts remain beteen 0 to 7 km from the storm center while the storm is in the mature and developing phases and then move ahead of the storm by 8 to 20 km during the decay phase. Goff [4-2] reports that the storm overruns the gust front in the decaying stages and precipitation tends to coincide with the gust front passage. It appears that the definitions of the storm life by these two authors may be inconsistent or that the storms are different. Note the average separation distance for case 1 storms, from Goff, is 7.6 km; case 2 storms is 10 km which correspond roughly to Colmer's 0-7 km and 8-20 km range.

The important observation from the above is that gust fronts with sudden wind changes may pass over an airport several miles ahead of any indicated precipitation or storm activity. This creates unexpected wind hazards.

4.3.4 Gust Front Shape

The gust front boundary is defined as the boundary separating the flow originating from a cold source and the flow of air originating from a warm air source. The boundary is generally shaped with a nose protruding ahead of the front. Surface drag tends to retard the outward rushing cold air near the ground causing it to overrun itself above. The point of the nose is on the order of 100 to 300 m above the surface (both Colmer [4-3] and Frank [4-5] report the peak at 250 m), and can extend horizontally as far as 200 m into the warm air.

The lag of ground level air behind the foremost part of the front is expected to be intermittent with the cold air falling through the warm air entrained beneath the nose and again reforming due to surface stress. This over-turning implies high turbulence in the nose region. The bulging gust front is most prevalent in mature storms.

Above the peak of the nose the gust front boundary slopes backward. Goff gives angles of 45° for case 1 storms and 45° to 75° for case 2 storms. A time-height plot of streamlines shown in Figure 4-6 clearly illustrates this

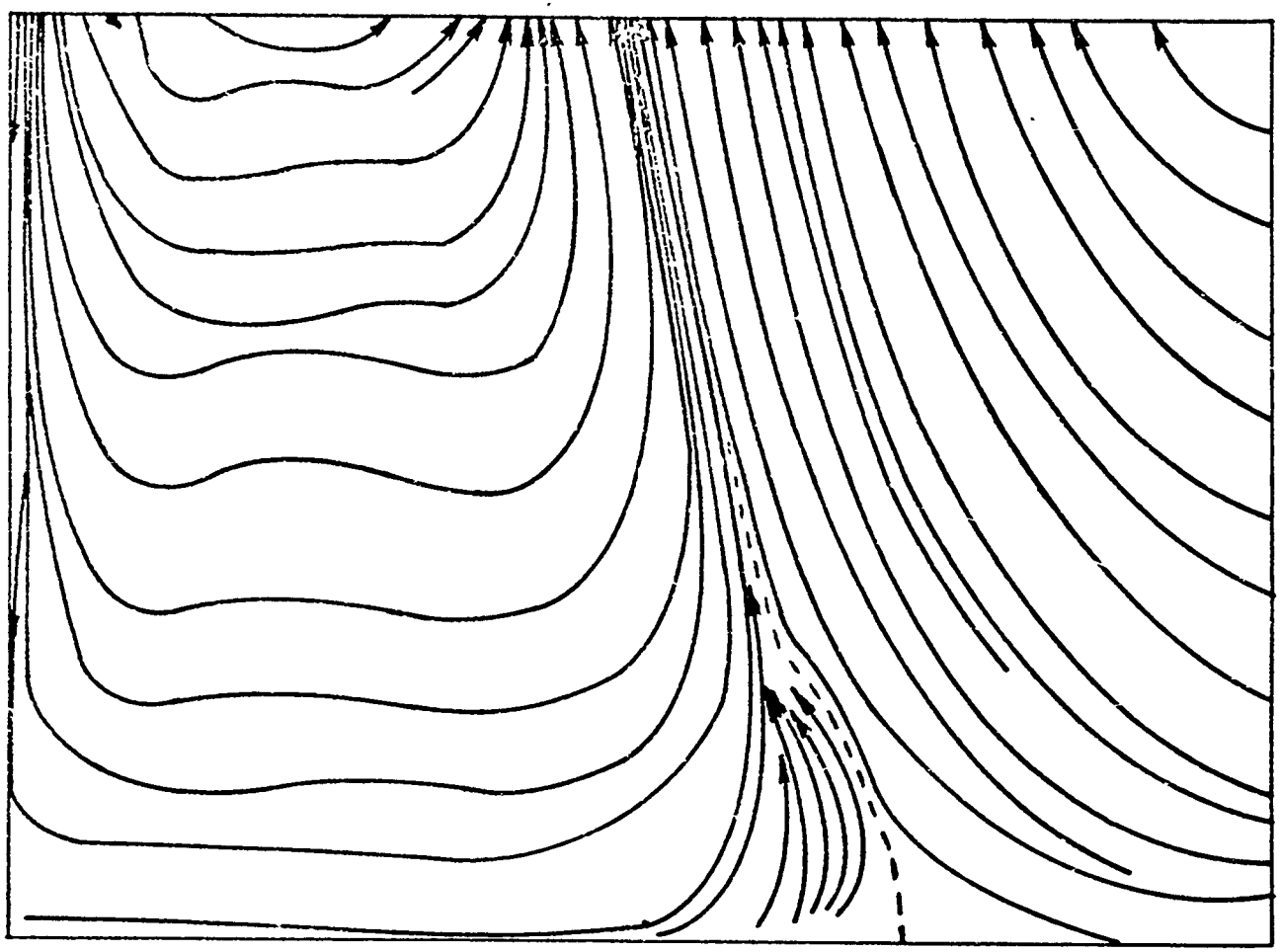

FIGURE 4-6 STREAMLINE PATTERN ASSOCIATED WITH A GUST FRONT, [4-2], ZERO STREAMLINE ---.

slope which coincides with the zero streamline. As previously mentioned, Kropfli and Miller [4-1] report a 25° slope which corresponds to the decaying stages of their storm. Colmer [4-3] notes that the frontal slope is not linear and parts of the gust front will have much larger slopes than the average (see Figure 4-7). He correlates the ratio of maximum slope over a 30 sec. period to the average slope, R, with the gust length, H, by the relationship

$$\log R = 0.667 \log H + \text{const.} \qquad 4.3$$

Depending on the relative position of the storm to the airport, a landing aircraft will encounter the most severe wind shear at different heights above the ground. Also, the rain typically follows some distance behind the gust front and the pilot may or may not land in rain. Since for simulation purposes it is useful to relate the location of the shear and the probability of rain to the position of the airport, Figure 4-8 has been prepared from limited data.

Figure 4-8 illustrates the altitude at which an aircraft approaching an airport on a 3° glide slope might expect to encounter a gust front which has passed over the airport at the time indicated on the horizontal scale. The probability of rain at the airport relative to the position of encountering shear is also shown. As an example, the curve shows that if the gust front had passed the airport 10 min. prior to the airplane's approach, the pilot could

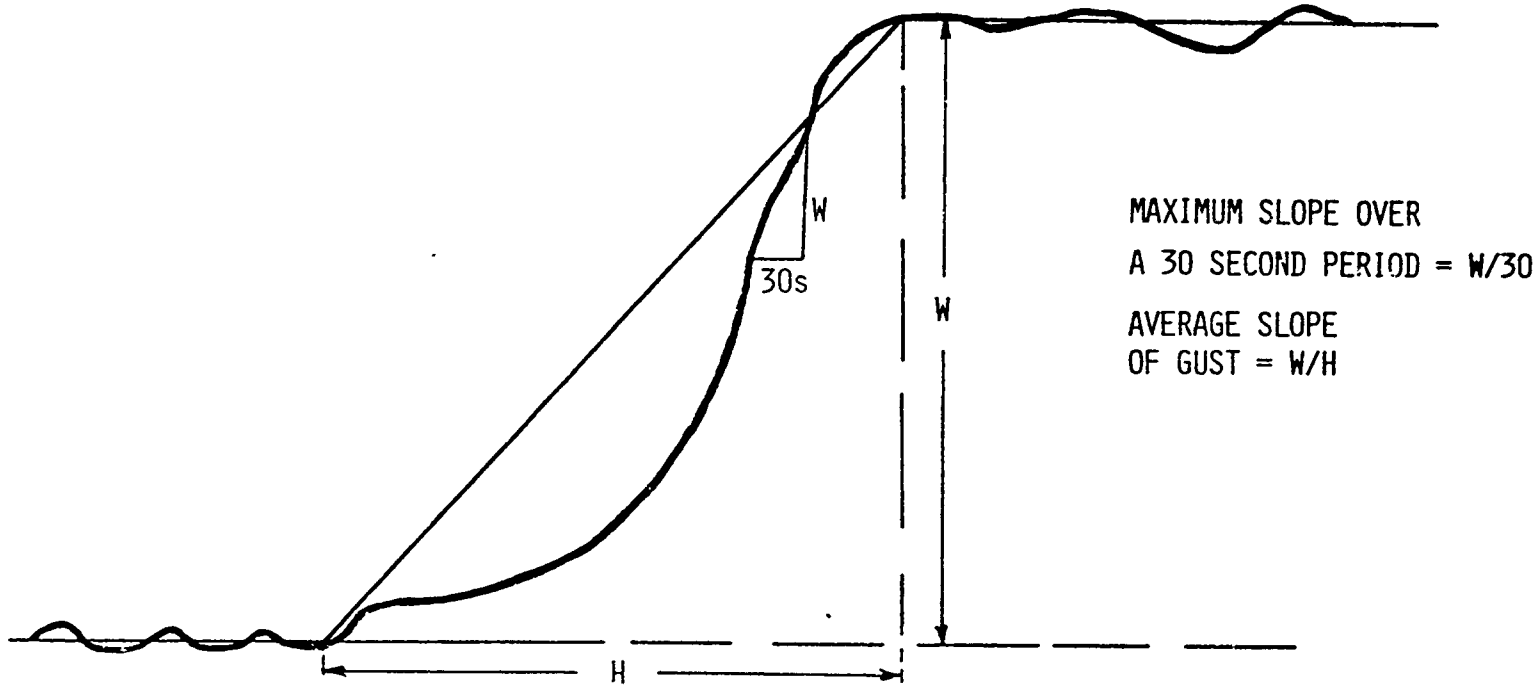

FIGURE 4-7 NONLINEAR FRONTAL SLOPE AS DESCRIBED BY COLMER, [4-3].

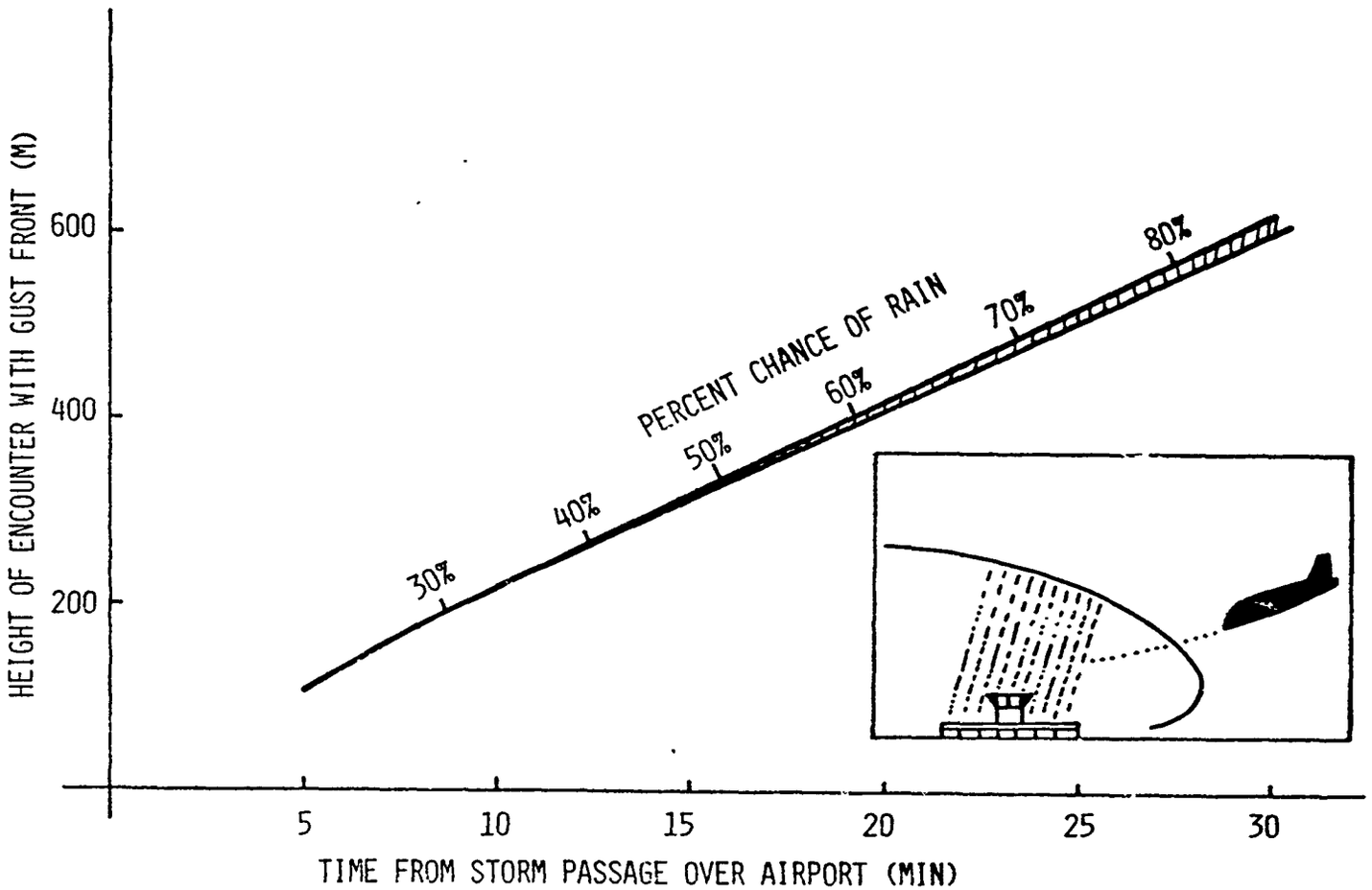

FIGURE 4-8 ALTITUDE AT WHICH AN AIRCRAFT APPROACHING AN AIRPORT MIGHT EXPECT TO ENCOUNTER A GUST FRONT WHICH PASSED THE AIRPORT EARLIER.

expect shear at 210 m and a 33% chance of landing in rain. This curve is interpolated from the data of the preceeding discussion and should be used only as a rough estimate.

4.3.5 Gust Characteristics

The gust size (magnitude of wind increase) and the gust length (length of time over which the wind increases) were plotted by Colmer for 11 case studies. On an average, the gust size increases by 50% between the surface and 500 m with the most increase occurring in the first 50 m. This is a significant observation since a ground based anemometer will read winds considerably less than those a hundred or so meters above.

Note, however, that the gust size profile exhibits considerable variability. The gust length on the other hand shows less variability and an almost linear decrease with height. Additional gust size and length data are given by Sinclair et al [4-4] for three Florida storms. They report at 18 m an average gust size of 4.8 m/s and a gust length of 12.8 s, and at the height where the peak wind occurs, they report an average gust size of 6.6 m/s and a gust length of 14.8 s. The length scale based on a constant gust front speed (which was not reported) does not show the same decrease with altitude that Colmer reports. Goff [4-2] finds the change in the horizontal wind component normal to the gust front to have a value between 4 and 20 m/s with an

average of 12.8 m/s which shows good agreement with Colmer's average value above 50 m.

The track of the maximum gust tends to coincide with the track of the storm cell. The size of the gust decreases almost linearly from this maximum value having an approximate 15% decrease in gust size 5 km from the center and a 32% decrease 10 km from the center.

Frequently more than one gust is experienced during the passage of a thunderstorm. Ward and Arnett [4-8] report multiple cold air surges for a single thunderstorm which they attribute to storm pulsation. Goff's [2-2] data also shows secondary surges. There appears to be no reduction of the data which allows a quantitative statement about these multiple surges to be made. Goff [4-9] in a recent paper discusses secondary surges of high momentum air which appeared in the outflow air mass from the thunderstorm on June 7, 1971. Two surges observed were both characterized by a strong shear zone in the W_x-component and large variations in the vertical wind speed. In one surge, a downdraft in excess of 11 m/s was observed at the 177 m level.

4.3.6 Wind Speed Fields

The most useful data for simulation of aircraft flights through gust fronts is the three-dimensional velocity field in the vicinity of the gust front as a function of position

and time. A step toward providing these data is the height-time plots given by [4-2, 4, 5]. Often these plots are converted to height-distance plots by assuming Taylor's hypothesis. Taylor's hypothesis allows wind speeds measured in time at a point in space to be converted to wind speed variation with position along a line in the direction of the mean wind by assuming the turbulent flow is carried past the point of measurement sufficiently rapid that the turbulence pattern is "frozen" in the air flow and does not change over the time the measurement is taken (ie position = mean velocity X time). Typical height-time plots are shown in Figure 4-9 and height-distance plots in Figure 4-10. Generally, these data are highly smoothed by filtering techniques which remove the high frequency content. Whereas, Figure 4-9 gives the wind speed and the wind direction contours in the vertical plane, Figure 4-10 expresses the data in terms of the three velocity components: W_z, vertical velocity, W_x, horizontal velocity normal to the front, and W_y, lateral wind speed parallel to the front.

The data corresponds with the schematic of the gust front shown in Figure 4-3. Inspecting the W_x component of wind speed in Figure 4-10 one observes a negative wind speed corresponding to warm air inflow toward the front which is delineated by the zero wind speed. The positive values in the height-time plots correspond to cold air from the thunder-

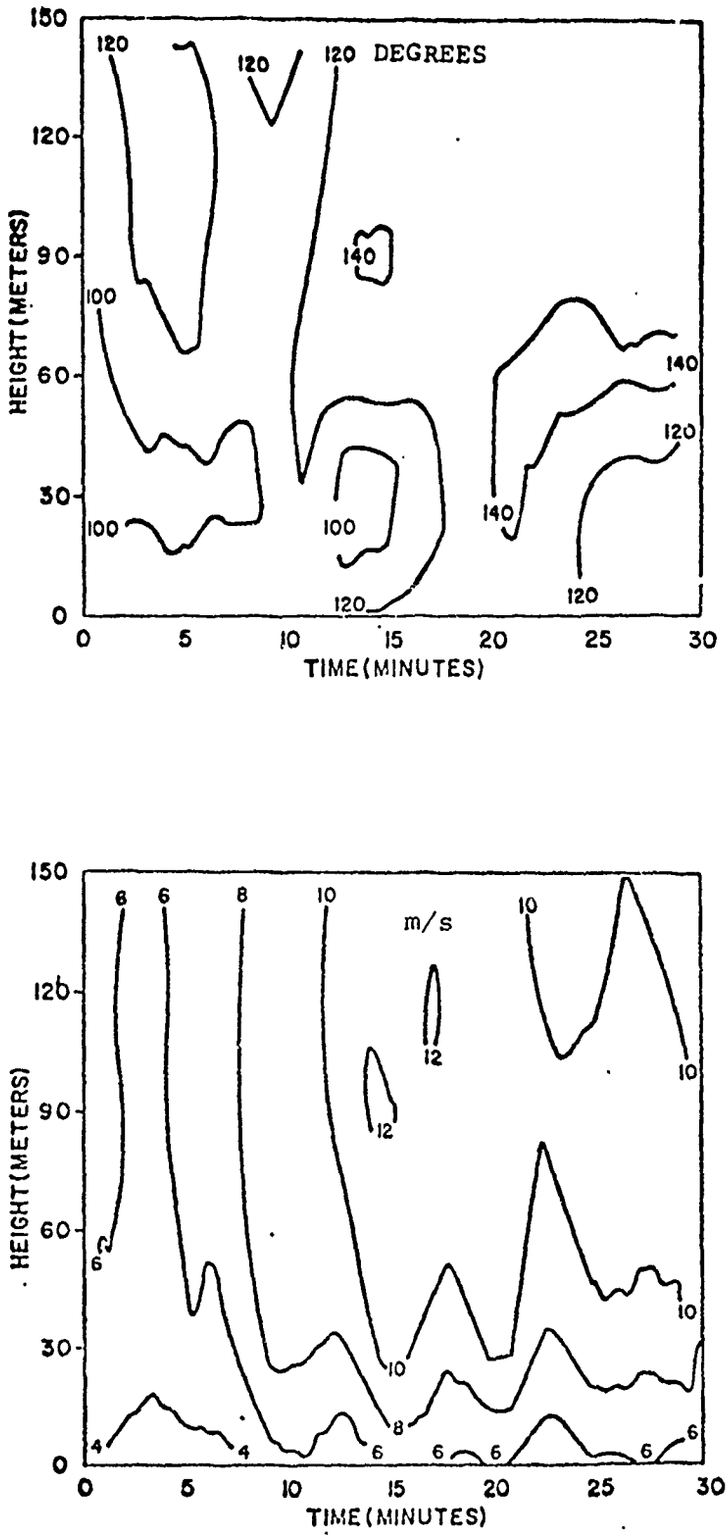

FIGURE 4-9 HEIGHT-TIME PLOTS OF GUST FRONT SPEED AND DIRECTION, [4-4]

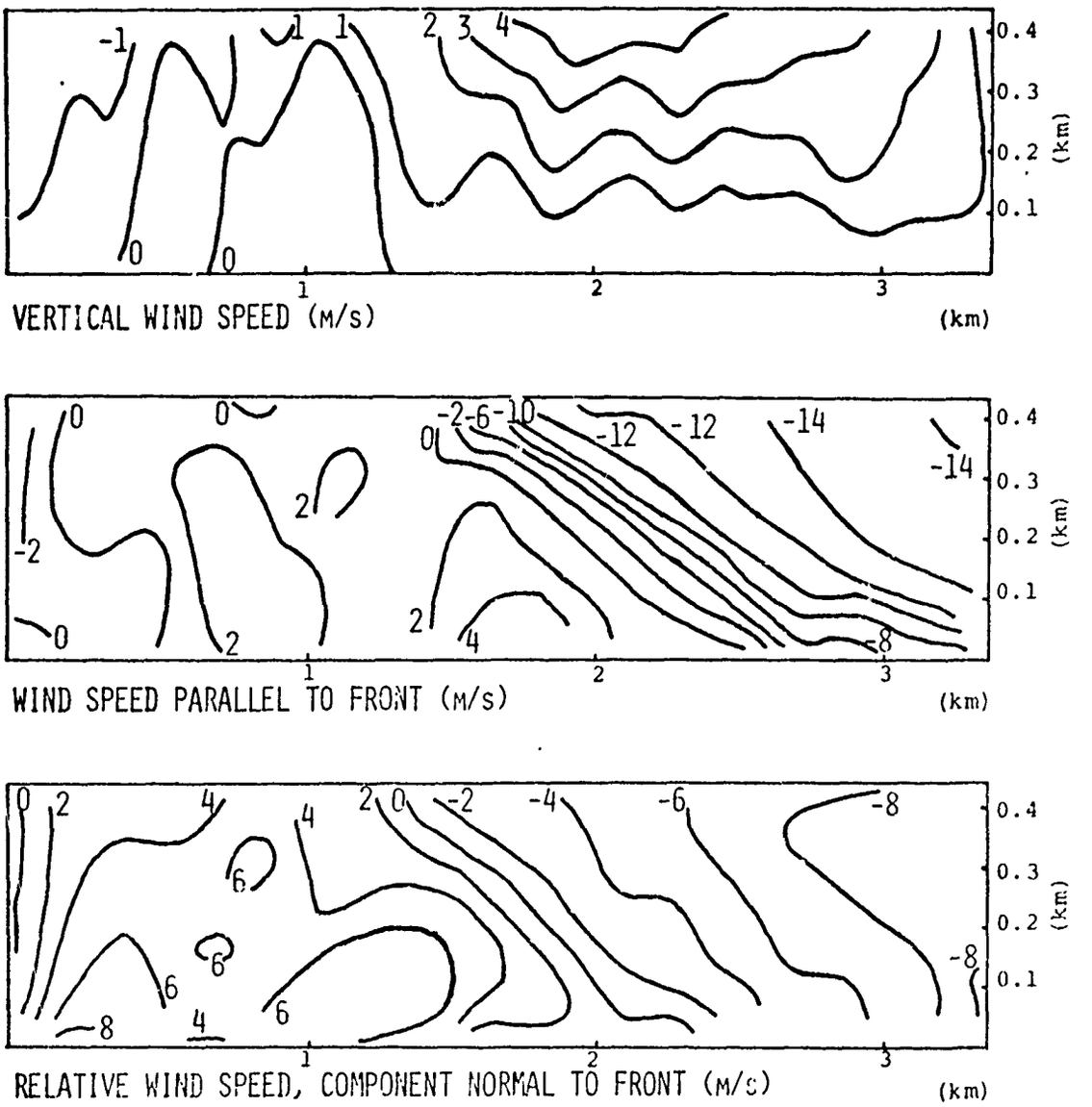

FIGURE 4-10 HEIGHT-DISTANCE PLOTS OF GUST FRONT SPEED FIELDS, [4-2]

storm flowing toward the front. Negative wind speed near the surface in the cold air zone indicates an undercurrent probably resulting from the cold air riding over a low level temperature inversion. Although filtered out of the data of Figure 4-10, a highly turbulent wake region expanding in depth with increasing distance behind the front occurs behind the elevated "head" of dense air which is characterized by strong turbulence and mixing.

Inspection of the vertical wind speed in Figure 4-10 shows a vertical updraft attributed to lifting of the less dense, warm air over the more dense forward-moving air mass. Maximum updrafts generally occur 1 km or less ahead of the gust front. The magnitude of these updrafts generally increases with frontal strength (increasing frontal slope). The value of the maximum updraft reported by Goff [4-2] is 6.7 m/s, and that by Browning and Harold [4-10] is in excess of 8 m/s and 10 m/s for two different fronts. The record from the digital flight data recorder of Eastern Air Lines Flight 66 and Eastern Air Lines 902 for the thunderstorm over J.F. Kennedy Airport gave updrafts of approximately 4.3 m/s, and 5.2 m/s, respectively. However, these values probably do not correspond to the maximum.

4.3.7 Wind Shear

Strong vertical and horizontal shears occur with all gust fronts. Vertical shear is a variation in the wind speed components with height, z, whereas horizontal shear

refers to variation with horizontal distance (in this case, with the longitudinal mean wind direction, x). Large vertical shear ($\partial()/\partial z$) occurs near the surface and at the upper boundary and large horizontal shear ($\partial()/\partial x$) occurs at the outflows leading edge. Secondary horizontal shear may occur also due to multiple outflow surges.

The maximum wind shear averaged from the 20 thunderstorm cases studied by Goff [4-2] are tabulated in Table 4-2a and Table 4-2b. The spatial derivatives were formed from the relationships $\partial/\partial x = c^{-1}\partial/\partial t$. From the table one notes that shears of horizontal wind are greatest near the ground reaching a minimum at 200 m and then increasing upward. This tends to conflict with Colmer's [4-3] conclusion that due to the increase of gust size and decrease of gust length with altitude, horizontal wind shear in the gust front between the surface and 500 m above ground doubles, i.e., the average (of 11 cases) surface shear is 0.0063 s^{-1} while the 500 m level shear is 0.016 s^{-1}. It should be noted that reported wind shear values are based on a very sparse grid system and on highly smoothed data and are, therefore, at best gross approximations.

4.4 Wind Shear Prediction Techniques

4.4.1 Raw Data

Despite the filtering and course grid space used to obtain the spatial distribution of wind speeds and wind shears given in the previous section, the results are ex-

TABLE 4-2a

Maximum Absolute Shear (m s^{-1} 100 m^{-1}) [4-2]

*Grid level or layer of gradient:

	1	2	3	4	5	6	7	8	9	10
$\partial W_x / \partial x$	11.1	5.0	4.9	5.4	4.7	4.1	4.8	5.3	4.5	4.6
$\partial W_y / \partial x$	7.0	3.2	3.4	3.8	3.4	3.7	4.0	4.8	4.8	7.8
$\partial W_z / \partial x$	0.0	1.2	2.2	3.4	3.8	3.4	2.6	2.8	3.3	3.8
$\partial W_x / \partial z$	16.2	8.4	8.7	9.6	9.4	8.6	10.8	6.5	10.6	---
$\partial W_y / \partial z$	26.1	10.2	6.9	5.6	8.2	6.4	6.4	6.3	9.7	---
$\partial W_z / \partial z$	3.8	2.1	2.3	2.0	2.6	3.1	3.1	3.1	3.1	---

TABLE 4-2b

Average Maximum Absolute Shear (m s^{-1} 100 m^{-1}) [4-2]

*Grid level or layer of gradient:

	1	2	3	4	5	6	7	8	9	10
$\partial W_x / \partial x$	4.3	2.0	2.3	2.3	2.3	2.4	2.6	2.9	2.9	3.2
$\partial W_y / \partial x$	4.0	1.5	1.5	1.7	1.9	1.9	1.9	2.2	2.2	2.6
$\partial W_z / \partial x$	0.0	0.6	0.9	1.2	1.3	1.2	1.1	1.5	1.9	2.4
$\partial W_x / \partial z$	11.6	5.8	4.7	4.6	4.1	4.7	5.0	4.1	5.1	---
$\partial W_y / \partial z$	10.6	5.3	4.1	3.6	3.9	3.6	3.4	3.2	4.3	---
$\partial W_z / \partial z$	2.1	1.6	1.7	1.3	1.7	1.9	1.9	1.9	1.9	---

* Levels 1 through 10 are 50 meters apart.

tremely useful for estimating the influence of gust fronts on aircraft flights. Two ways of using the data are to store them in the computer on an appropriate grid system and use linear interpolation with a table look-up scheme to give the wind input values to the computerized airplane equations of motion; or to superimpose geometrically scaled flight paths on to the contour plots and pick off the winds "seen" by an aircraft traversing that flight path. The latter method is more restrictive in that the aerodynamic forcing functions computed from the input winds assume the airplane remains on or in close proximity to the selected flight path.

4.4.2 Mathematical Models

Mathematical schemes for computing wind fields associated with thunderstorm gust fronts are still in the formative stages. The most direct mathematical approach is probably that of Mitchell [4-11] who solved the finite difference equation for the two-dimensional, time dependent primitive equation of fluid motion. Surface friction is modeled with a bulk aerodynamic drag function applied at the lower levels of the computation grid. Vertical diffusion of momentum is modelled with linear diffusion terms, and velocity-slip is permitted at the surface.

This model appears to capture much of the essential physics of the flow and provides a computational technique

which might be incorporated into a computer code for simultaneous solution of the fluid mechanics with the airplane dynamics. Unfortunately, however, the computer solution is costly and this prohibits any extensive flight simulation.

A less sophisticated approach to modelling two-dimensional flow fields about a gust front is proposed by Sinclair et al [4-4]. They scaled the three Florida thunderstorms with the scaling parameters; time, Δt, which characterizes gust length; velocity ΔV, which characterizes gust size and; height, Δz, which is the height of maximum velocity. Figure 4-11 shows scaled velocity contours which Sinclair et al [4-4] conclude are quite similar to all other scaled gust profiles and, hence, if ΔV, Δt, and Δz are known, at least part of the structure of the wind front can be determined. Because of the difficulty in evaluating Δz, this approach was abandoned and a simple hypothesis to find the wind structure was adopted.

We will not pursue this approach further since the effort of reference [4-4] was toward forecasting gust fronts, whereas our goal is to provide realistic wind models for use in parametric simulation and design studies. The scaled gust fronts of Figure 4-11 provides such a model in that it allows us to conduct design analysis and simulation studies with

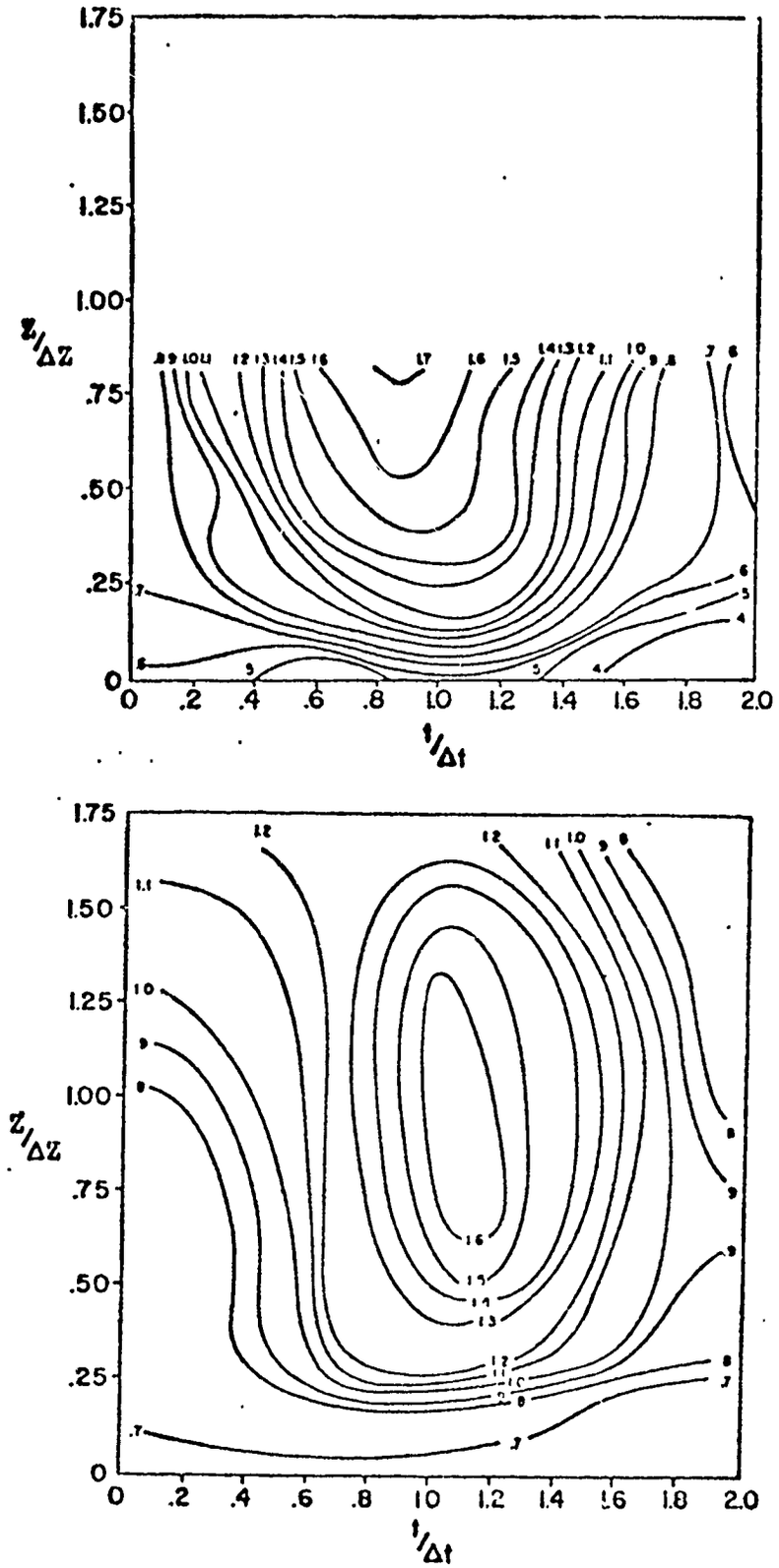

FIGURE 4-11 NONDIMENSIONAL WIND SPEED CONTOURS DISPLAYING SIMILARITY PROPOSED BY SINCLAIR ET AL , [4-4].

parametric variation of gust length, gust size and height of maximum velocity. Since we wish to establish design envelopes or limits rather than forecast gust fronts, we are at liberty to select any values of Δz, ΔV, and Δt within the confines of good engineering judgement. More will be described of this approach in the final report.

Updrafts and downdrafts associated with gust fronts along a given approach path have been correlated by Fichtl and Camp [4-10]. They scaled vertical wind speeds along a 3° glide slope from the gust front data of Goff [4-2] and also incorporated the vertical wind speeds reconstructed from the digital flight data record of Eastern 66. Their mathematical representation of the sequence of vertical wind speeds encountered by an aircraft during landing is given by the following:

Major Downdraft:

$$w = -p_1 A \sin[\pi \frac{x-x_r}{q_1}]; \quad z_D \geq z > z_r \qquad 4.4$$

Major Updraft:

$$w = A \frac{(1-2q_o)(x-x_r)^3 + (1-3q_o^2)(x-x_r)^2 + (2q_o-3q_o^2)(x-x_r)}{-q_o^2(q_o-1)^2};$$

$$z_r \geq z \geq z_r - L \qquad 4.5$$

Minor Downdraft:

$$w = -p_2 A \sin[\pi \frac{x_r - 1 - x}{q_2}]; \; z_r - L > z \geq z_r - (1 + q_2)L \qquad 4.6$$

Minor Updraft:

$$w = +p_2 A \sin[\pi \frac{x_r - 1 - x}{q_2}]; \; z_r - (1 + q_2) L > z \geq z_r - (1 + 2q_2)L \qquad 4.7$$

where

$$x_r = \frac{z_r}{L}, \quad x = \frac{z}{L} \qquad 4.8$$

The various quantities in the above equations are defined as following:

w = thunderstorm cold air outflow vertical velocity

z = altitude of airplane above surface

z_D = altitude of the top of the major downdraft

z_r = altitude of the top of the major updraft

z_B = altitude of the bottom of the minor downdraft

z_m = altitude of maximum updraft velocity in the major updraft*

A = amplitude of major vertical velocity updraft

L = vertical extent of major vertical velocity updraft relative to the flight path

p_1 = ratio of major downdraft to major updraft velocities

p_2 = ratio of minor downdraft or minor updraft to major updraft velocity

$q_0 = (z_r - z_m)/L$

---

*This parameter is not required in the calculation but serves to physically define q_0.

$$q_1 = (z_r - z_D)/L$$

$$q_2 = (z_r - z_B - L)/L$$

Values for the cold air outflow parameters are given in Tables 4-3 and 4-4. A schematic is given in Figure 4-12. Table 4-3 provides cold air outflow parameters for typical vertical wind speeds as derived from data provided by the NOAA/NSSL. Table 4-4 provides cold air outflow parameters which encompass the worst case (Eastern 66).

To apply the model, one enters the model with the parameters:

$$z_r,\ z_D,\ z_B,\ L,\ A,\ p_1,\ p_2$$

consistent with the range of parameters in Tables 4-3 and 4-4. It is recommended that a family of profiles which encompass the full range of variation of the model as implied in Tables 4-3 and 4-4 be used. This will insure that certain conditions will not be overlooked.

Wind speed as a function of height from combined tower and rawinsonde data near the time of the wind speed maximum was correlated by Frank [4-5] with the expression

$$W_x = W_o + \Delta W \tan\left((z - z_o)/\Delta H \right)(1 - e^{-z/z_m}) \qquad 4.9$$

where

z_m= 94.72m

ΔH= 889 m

z_o= 402 m

W_o= 25.0 m/s

ΔW= -23.5 m/s

Figure 4-13 shows the results. Also Frank [4-5] notes that in the surface boundary layer regions the wind profile obeys a power law

$$W_x = W_{xr}(z/z_r)^n \qquad 4.10$$

where W_x is the wind speed normal to the front at height z, z_r is a reference level, and $W_{xr} = W_x(z_r)$. Just behind the front n was found equal to 0.39 from tower data and equal to 0.35 from Doppler radar data. The power law was reported to give good agreement with gust front data up to 350 m.

Sinclair et al [4-4] demonstrated that a logarithmic wind law is valid from the surface to approximately 100 m. Therefore, the ratio of wind speed at two different levels becomes simply a function of surface roughness, i.e.,

$$\frac{V_2}{V_1} = \frac{\ln(z_2/z_o)}{\ln(z_1/z_o)} \qquad 4.11$$

TABLE 4-3

Typical Values of Cold Air Outflow Parameters (Based on NOAA/NSSL Data) [4-10]

Parameters	Units
$64 + 0.223z_r \leq L \leq 183 + z_r$	ft
$0 \leq A \leq 1 + 0.011z_r$	ft sec^{-1}
$0.3 \leq p_1 \leq 1.2$	Nondimensional
$0 < p_2 \leq 0.35$	Nondimensional
$q_0 = 0.36$	Nondimensional
$0.25\ q_1 \leq 1$	Nondimensional
$0 \leq q_2 \leq 2.3$	Nondimensional
$L \leq z_r \leq 1500$	ft
$z_D = z_r - q_1 L$	ft
$z_B = z_r - (1 + q_2)L$	ft

TABLE 4-4

Worst Case Values of Cold Air Outflow Parameters (Based on Eastern 66 and NOAA/NSSL Data) [4-11]

Parameters	Units
$64 + 0.223\ z_r \leq L \leq 183 + z_r$	ft
$0 < A \leq 10 + 0.011z_r$	ft sec^{-1}
$0.3 \leq p_1 \leq 1.2$	Nondimensional
$0 \leq p_2 \leq 0.35$	Nondimensional
$q_0 = 0.36$	Nondimensional
$0 \leq q_1 \leq 2$	Nondimensional
$0 \leq q_2 \leq 2.3$	Nondimensional
$L \leq z_r \leq 1500$	ft
$z_D = z_r - q_1 L$	ft
$z_B = z_r - (1 + q_2)\ L$	ft

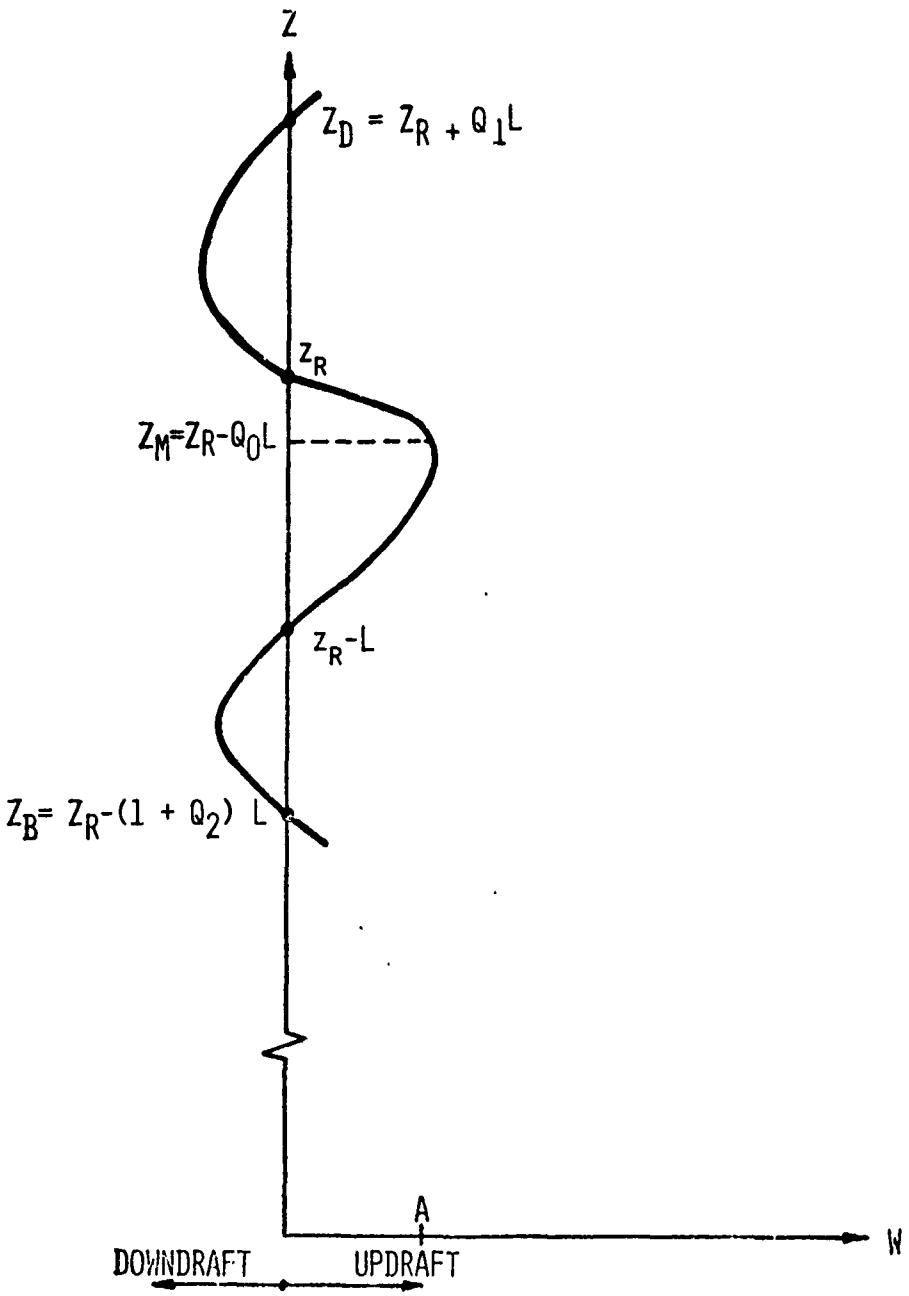

FIGURE 4-12 VERTICAL WIND SPEED ALONG A 3° GLIDE SLOPE THROUGH GUST FRONTS AS CORRELATED BY FICHTL AND CAMP, [4-10].

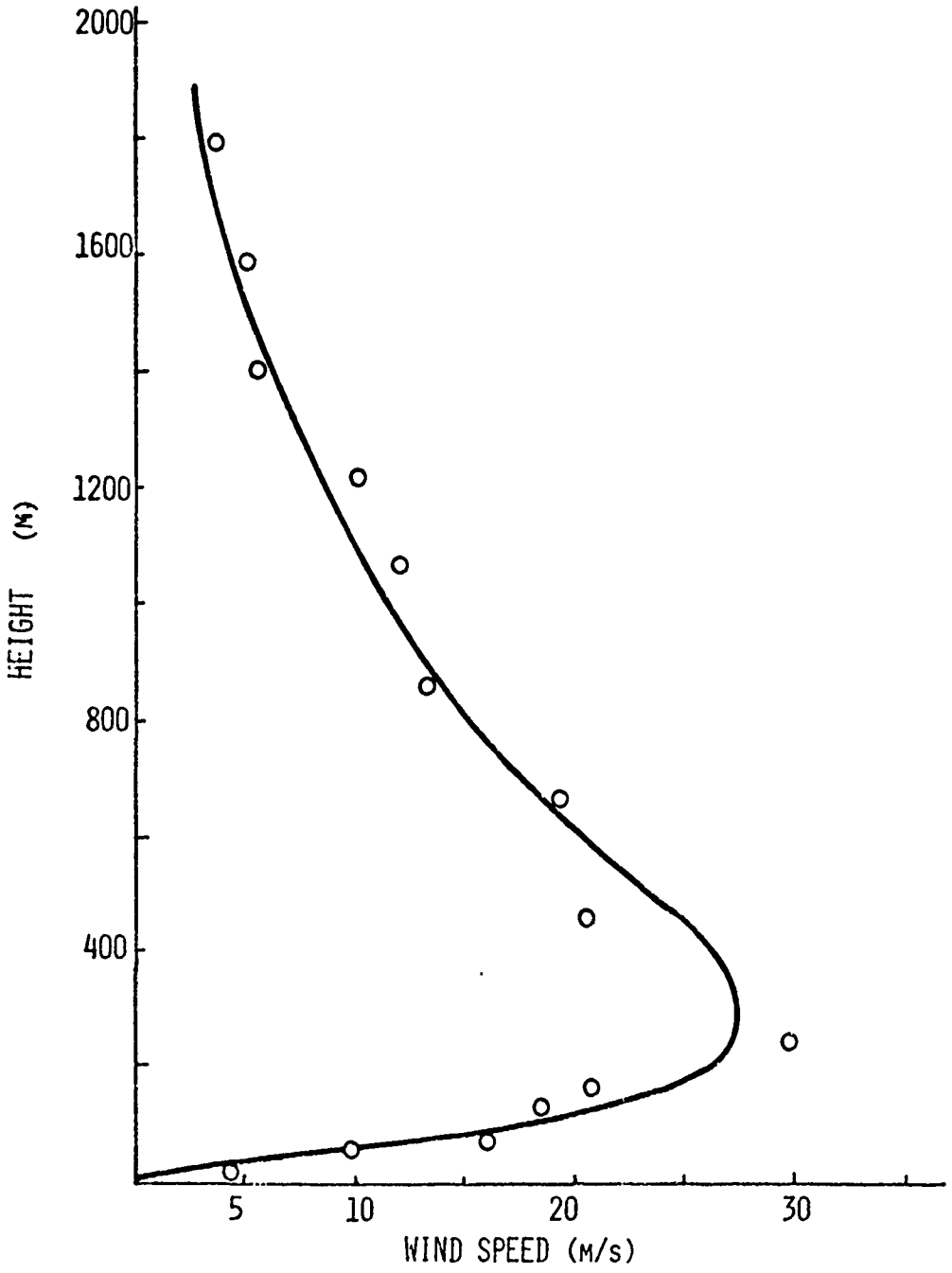

FIGURE 4-13 WIND SPEED FROM COMBINED TOWER AND RAWINSONDE DATA NEAR THE TIME OF MAXIMUM WIND SPEED DURING THE PASSAGE OF A GUST FRONT, [4-5].

5.0 BOUNDARY LAYER OVER FLAT TERRAIN

5.1 Introduction

Considerable information on the behavior of the atmospheric boundary layer at specific locations has been obtained with individual meteorological towers up to altitudes of typically 150 m with some data up to 500 m. These data are normally assumed valid over flat, horizontally homogeneous terrain and are transferred to spatial coordinates with Taylor's hypothesis which requires that the boundary layer be satistically stationary. Above the altitude which can be reached with towers; aircraft, rawinsonde and jimsphere data provide insight into the turning layers of the atmosphere but these data are not as precise as tower data.

5.2 Mean Flow in the Lower Surface Layers

Below 150 m the mean wind direction has, in general, little variation with height, and over flat terrain is considered to be steady plane-parallel flow of a horizontally homogeneous and statistically stationary surface layer. Numerous reviews of the atmospheric boundary layer are available [5-1, 2, 3, 4, 5] and it is only necessary to summarize these here.

In the surface boundary layer, the mean wind is considered to be influenced by surface conditions, atmospheric stability, and elevations. Mean wind models receiving the

greatest acceptance are expressed in terms of nondimensional wind shear as:

$$\frac{zk}{u_*}\frac{dW_x}{dz} = \phi(z/L) \qquad 5.1$$

The wind speed is then given by

$$W_x(z) = \frac{u_*}{k}\int_{z_o}^{z+z_o} \frac{\phi(z/L)}{z}\, dz \qquad 5.2$$

$$W_y(z) = 0 \qquad 5.3$$

$$W_z(z) = 0 \qquad 5.4$$

where $W_x(z)$, $W_y(z)$ and $W_z(z)$ are the wind speed in the x, y, and z directions respectively; the x axis is aligned with the mean wind direction, the y axis is perpendicular to x and the z axis is vertical to the horizontal plane. The constant k is the von Karman constant having a numerical value of approximately 0.4 and z_o is a length scale that characterizes the surface roughness. Typical values of z_o are given in Figure 5-1.

The surface friction velocity u_* is normally assumed constant which is experimentally verified only in the lower 30 meters, however, its variations to 150 m is generally negligible.

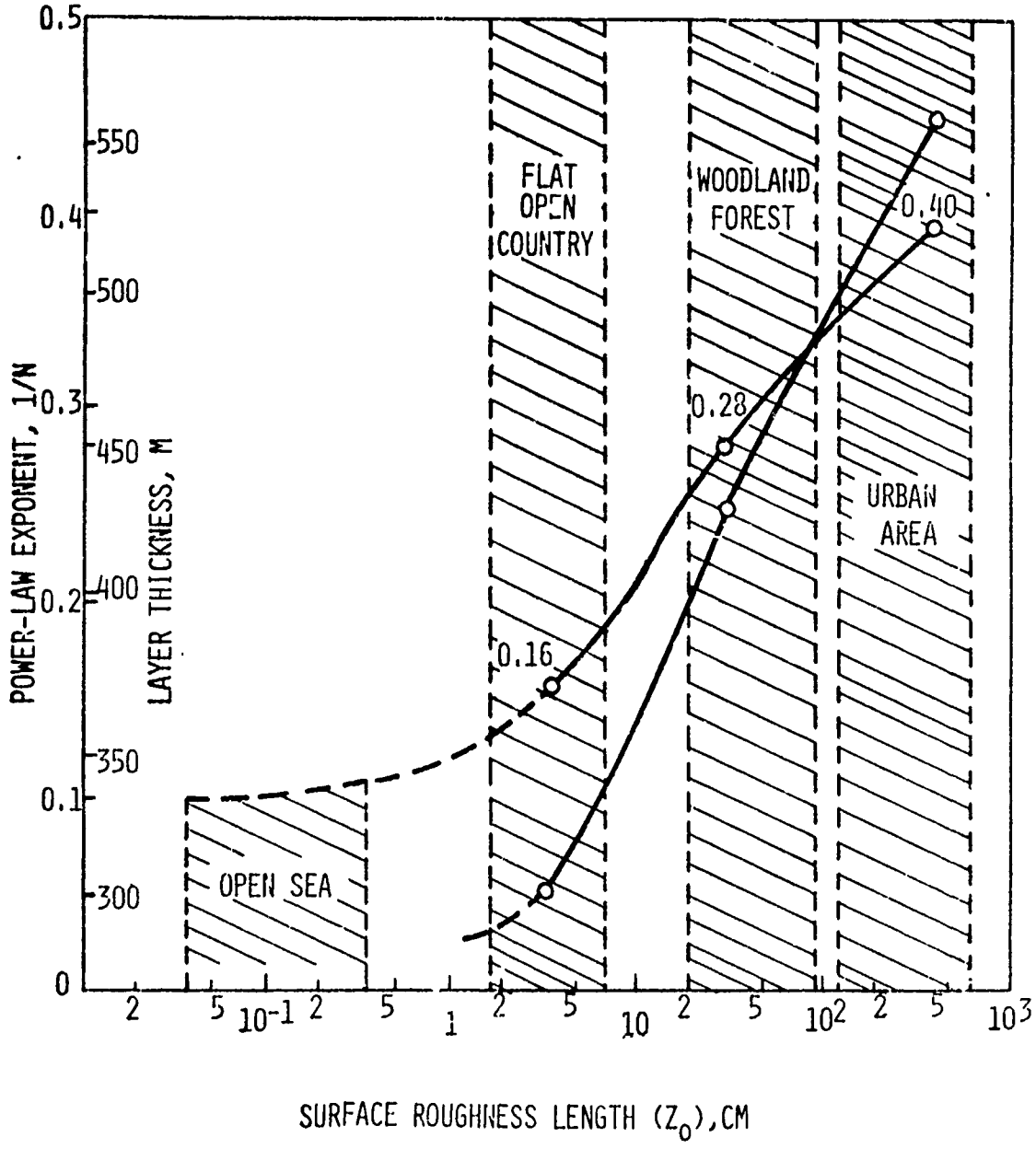

FIGURE 5-1 SURFACE ROUGHNESS LENGTH, Z_0, VERSUS THE POWER-LAW EXPONENT 1/N; WHERE $W_X/W_{X\ REF}=(Z/Z_{REF})^{1/N}$ [5-23].

The quantity L is the Monin-Obukhov stability parameter

$$L = -\frac{u_*^3 \, c_p \rho T}{kg \, H} \qquad 5.5$$

Since the heat flux, H, appearing in this expression is difficult to measure, an alternate scaling length L' is frequently used:

$$L' = -\frac{u_* T \, \frac{\partial W_x}{\partial z}}{kg\left[\frac{\partial T}{\partial z} + \frac{g}{c_p}\right]} \qquad 5.6$$

The relationship between L and L' is given by

$$L = \frac{K_H}{K_M} \, L' \qquad 5.7$$

where K_H and K_M are the eddy conductivity and the eddy viscosity, respectively. L' in turn is related to a more conventional stability parameter, Ri, called the gradient Richardson's number:

$$Ri = \frac{\frac{g}{T}\left[\frac{\partial T}{\partial z} + \frac{g}{c_p}\right]}{\left[\frac{\partial W_x}{\partial z}\right]^2} \qquad 5.8$$

hence

$$\frac{z}{L'} = \frac{\frac{g}{T}\left[\frac{\partial T}{\partial z} + \frac{g}{c_p}\right]}{\left[\frac{\partial W_x}{\partial z}\right]^2} = Ri \; \phi(z/L') \qquad 5.9$$

Richardson's number is a nondimensional ratio between the mechanical wind shear that tends to displace air and the buoyancy force, which may damp or amplify this tendency. The atmosphere is said to be stable if Ri, $z/L'>0$ corresponding to $\partial T/\partial z<-g/c_p$ indicating a stable lapse rate or inversion; neutral if Ri, $z/L'=0$ giving $\partial T/\partial z = -g/c_p$ indicating an adiabatic lapse rate; and unstable if Ri, $z/L'<0$ giving $\partial T/\partial z>-g/c_p$ indicating an unstable lapse rate.

The empirically derived expressions for $\phi(z/L')$ for different conditions of stability are given by a number of investigators. Barr et al [5-5] recommends the following forms for $\phi(z/L')$.

Neutral case:

$$\phi(z/L') = 1; \quad z/L' = 0 \qquad 5.10$$

Stable case:

$$\phi(z/L') = 1 + \alpha' \frac{z}{L'}, \quad ; \quad 1 > z/L' > 0 \qquad 5.11$$

Very stable case:

$$\phi(z/L') = 1 + \alpha'; \quad z/L' > 1 \qquad 5.12$$

where

$$\frac{z}{L'} = 1 + \alpha' \, Ri$$

Unstable case:

$$\phi(z/L') = \frac{1}{(1 - \gamma' \, Ri)^{\frac{1}{4}}}; \quad 0 > z/L' \qquad 5.13$$

where

$$\frac{z}{L'} = \frac{Ri}{(1 + \gamma' \, Ri)^{\frac{1}{4}}}$$

The nondimensional wind shear has the form shown in Figure 5-2 where $\alpha = 4.5$ and $\gamma = 4\alpha = 18$. Details of the development of Equations 5.10 to 5.13 are given in [5-5,6].

The integrated form of Equations 5.10 to 5.13 is

$$W_x = \frac{u_{*o}}{k} \left[\ln \frac{z + z_o}{z_o} + \psi(z/L') \right] \qquad 5.14$$

where

$$\psi(z/L') = \int_o^{z/L'} \frac{\phi(z/L') - 1}{z/L'} \, d(z/L') \qquad 5.15$$

Before considering the result of the integration, it is noted that the above expressions for nondimensional shear become increasingly less accurate at altitudes above $z > 90$ m. This is due to the fact that their development assumes a constant shear stress which does not hold at high altitudes. Barr et al [5-5] propose an extension of the model to altitudes on the order of 350 m by allowing the friction velocity to vary linearly as

$$u_* = u_{*o} (1 - z/\delta) \qquad 5.16$$

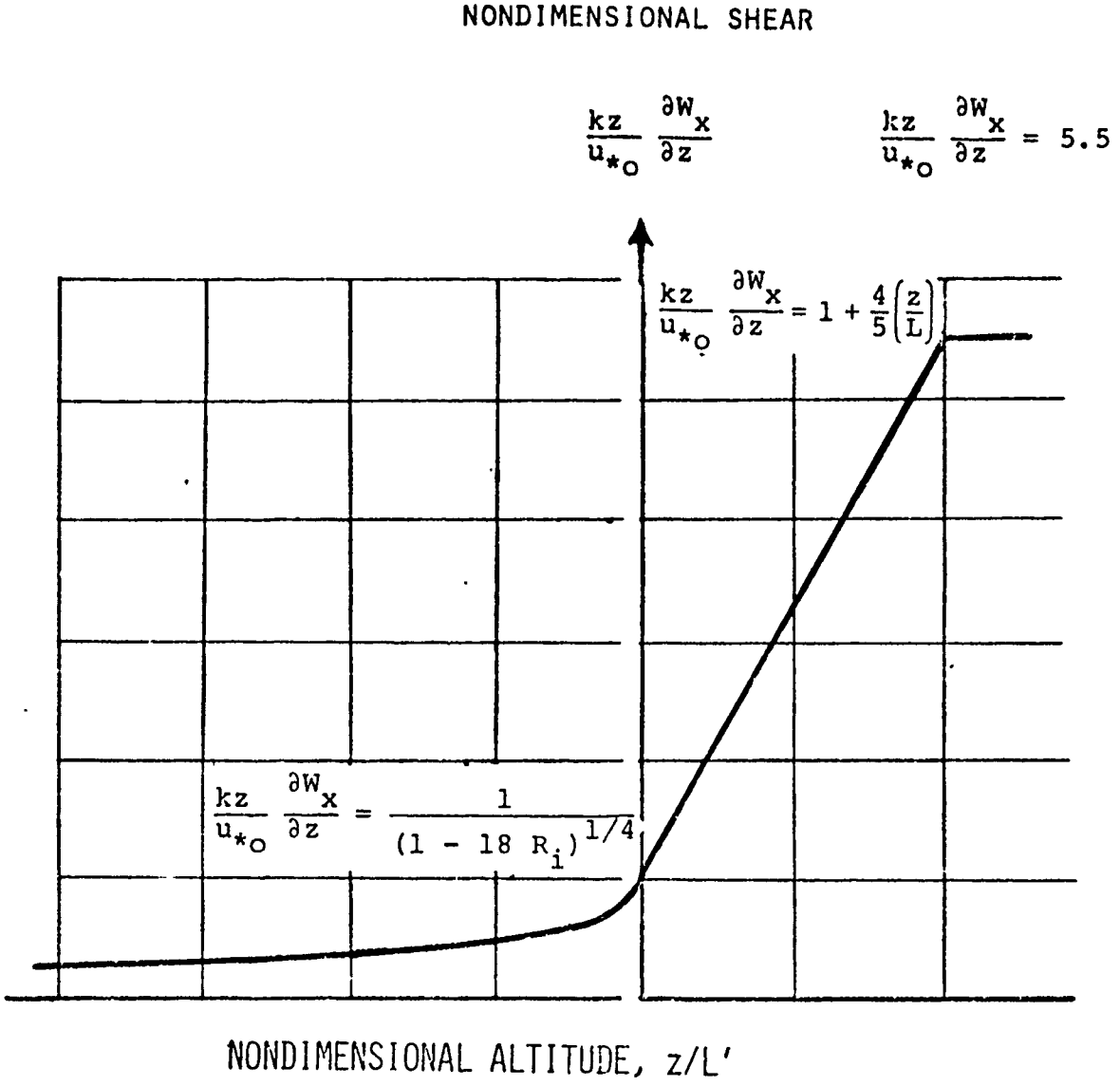

FIGURE 5-2 NONDIMENSIONAL WIND SHEAR AS A FUNCTION OF HEIGHT, Z, OVER MONIN-OBUKHOV STABILITY LENGTH, L', [5-5].

where δ is the atmospheric boundary layer thickness given by

$$\delta = u_{*o} / 10.7f \qquad 5.17$$

The parameter f is the Coriolis parameter. The nondimensional wind shear is then given by

$$\frac{kz}{u_{*o}} \frac{\partial W_x}{\partial z} = (1 - z/\delta)\ \phi(z/L') \qquad 5.18$$

Integration of the shear gives

$$W_x = \frac{u_{*o}}{k} \left[\ln \frac{z + z_o}{z_o} - \frac{z}{\delta} + \psi_1\left(\frac{z}{L'}, \frac{z}{\delta}\right)\right] \qquad 5.19$$

The wind profile for the given stability cases then becomes;

Neutral case:

$$W_x = \frac{u_{*o}}{k} \left[\ln \frac{z + z_o}{z_o} - \frac{z}{\delta}\right] \quad ; \quad z/L' = 0 \qquad 5.20$$

Stable case:

$$W_x = \frac{u_{*o}}{k}\left[\ln\frac{z+z_o}{z_o} - \frac{z}{\delta} + \alpha'\frac{z}{L'}(1-z/2\delta)\right]; \qquad 5.21$$

$$0<z/L'\leq 1$$

Unstable case:

$$W_x = \frac{u_{*o}}{k}\left[\ln\frac{z+z_o}{z_o} - \frac{z}{\delta} + \psi_1\left(\frac{z}{L'}, \frac{z}{\delta}\right)\right] \qquad 5.22$$

where

$$\psi_1\left(\frac{z}{L'}, \frac{z}{\delta}\right) = \psi\left(\frac{z}{L'}\right)\left(1-\frac{z}{\delta}\right) + \frac{z/\delta}{z/L'}\int_0^{-z/L'}\psi(\xi)\,d\xi \qquad 5.23$$

where

$\xi = z/L'$ and $z/L' < 0$

Numerical integration of Equation 5.23 is carried out in [5-5].

Very stable case:

$$W_x = \frac{u_{*o}}{k}\left[\ln\frac{z+z_o}{z_o} + \alpha'\left(1+\ln\frac{z}{L'}\right) + \frac{z}{\delta}\left[1+\alpha'-\frac{1}{2(z/L')}\right]\right]$$

$$z/L' > 1 \qquad 5.24$$

The very stable wind profile is applied above the altitude z_1 where $z_1/L' = 1$.

Equation 5.24 must be used with discretion since it is based primarily on conjecture. Little is actually known about the very stable wind profile, the shape of which is largely determined by the absence of turbulence above $z/L'>1$. Very near the ground where z/L' is less than unity a turbulent layer can exist. As height increases beyond $z/L'=1$ a non-turbulent layer can occur which is decoupled from the lower layer. Change in wind direction in excess of 45° is not uncommon between these uncoupled layers. Leurs [5-4] suggests a discontinuous wind profile for very stable conditions. Below a given level z_1 he assumes either a calm $W_x(z) = 0$ or a logarithmic profile. Above z_1 he considers various constant values of $W_x(z)$. The wind speed change across z_1 is taken as discrete which is probably not physically meaningful but represents a limiting case.

The application of the mean wind profiles is most frequently based on a reference wind speed at a specified height. Present efforts to standardize tower heights at airports to 20 ft suggests 20 ft might serve as a meaningful reference height. Given a reference wind and height, u_{*o} can be determined from

$$u_{*o} = \frac{W_x(z_{ref})}{\ln \frac{z_{ref} + z_o}{z_o} + \psi_1\left(\frac{z_{ref}}{L'}, \frac{z_{ref}}{\delta}\right) - \frac{z_{ref}}{\delta}} \qquad 5.25$$

In view of the fact that δ is a function of u_{*_o} an iteration procedure is required if the z/δ function proposed by Barr et al [5-5] is retained. The effects of altitude variation of shear stress, ie $u_* = u_{*_o}\ (1-z/\delta)$, is negligible for unstable conditions but can be appreciable for stable conditions. The Richardson number or L' must also be known at the reference height; or a parametric study of variation with Ri may be carried out depending on the design problem.

The roughness length, z_o, should be specified for each particular airport and may be a function of wind direction (see [5-7] for an example of a surface roughness wind direction rose), wind speed (for instance tall grass and water have changing roughness characteristics with wind speed), season, etc.

A comparison of the various equations given above (see [5-5]) indicates that stable conditions result in more severe and higher winds above a certain level for the same reference wind speed. However, since this wind is propagated from the geostrophic wind, it might be expected that greater stability at the reference height will be associated with lower mean wind speeds at the same height, and consequently the differences in the shears between stable and unstable conditions may not be so great.

5.3 Turning Layer

5.3.1 Introduction

Above the constant stress layer the presence of mean flow synoptic scale horizontal pressure gradients and the action of the Coriolis force tend to produce vertical variation in the vertical transport of horizontal momentum and clockwise turning of the mean flow, looking toward the earth, in the northern hemisphere and counterclockwise turning in the southern hemisphere. As indicated earlier, however, experimental evidence [5-8,9] appears to show that in the height interval 30 m $\leq z \leq$ 150 m the vertical variation of the wind direction is approximately 2° - 4°, which is negligible for most design analyses. Additionally, by allowing u_* to vary linearly with altitude, Barr et al [5-5] argues that Equations 5.20 to 5.24 reliably predict $W_x(z)$ to an elevation of approximately 300 m. This may be true under barotropic conditions, but if baroclinicity exists, the turning of the wind may become important as low as 150 m and should be considered in analyses of aircraft flight characteristics and control system design.

Most solutions for the wind profile in the turning layer treat the barotropic case which assumes that the large-scale synoptic horizontal pressure gradients which are related to the geostrophic wind $\vec{W}_G$ by

$$W_{xG} = -\frac{1}{\rho f}\frac{\partial P}{\partial y} \; ; \quad W_{yG} = \frac{1}{\rho f}\frac{\partial P}{\partial x} \qquad 5.26$$

do not vary in the vertical direction. Surveys of such solutions are given in [5-1, 3, 10, 11 and 12] . Reference [5-12] summarizes as well, analytical solutions which discard the barotropic assumption and consider specified height variation of the geostrophic wind, i.e., the baroclinic case. The results of these solutions will be summarized below, for further details the reader should see the stated references.

5.3.2 Barotropic Turning Layer

According to similarity theory, if a variable wind is appropriately scaled then its profile is given by an empirically determined universal function. For flow far from the surface, similarity gives:

$$\frac{\vec{W} - \vec{W}_{ref}}{u_{*o}} \equiv F\left(\frac{z}{h}, \frac{h}{L}\right) \qquad 5.27$$

where W_{ref} is the appropriate wind scale to be discussed later and F is the outer profile function.

For flow in the surface layer

$$\frac{\vec{W}}{u_*} = \frac{1}{k}\left[\ln \frac{z}{z_o} - \psi\left(\frac{z}{L}\right) \vec{i}\right] \qquad 5.28$$

where $\vec{i}$ is the unit vector in the x direction. It is commonly assumed that there exists a layer where Equations 5.27 and 5.28 can be asymptotically matched [5-13, 14] to give

$$\frac{1}{k} \ln \frac{h}{z_o} \vec{i} - \frac{\vec{W}_{ref}}{u_*} = A\left(\frac{h}{L}\right) \vec{i} + B\left(\frac{h}{L}\right) \vec{j} \qquad 5.29$$

Equating components of the vector:

$$A(h/L) = \ln \frac{h}{z_o} - \frac{k\, W_{xref}}{u_*} \qquad 5.30$$

and

$$B(h/L) = - \frac{kW_{yref}}{u_*} \frac{f}{|f|} \qquad 5.31$$

The functions A(h/L) and B(h/L) are determined from empirical data.

Under neutral conditions A(0) and B(0) have a range of values as shown in Table 5-1.

The geostrophic drag $u_*/|W_{ref}|$ is found from Equation 5.30 as

$$C_D = u_*/|W_{ref}| = k \left[[\ln h/z_o - A(h/L)]^2 + [B(h/L)]^2 \right]^{-\frac{1}{2}} \qquad 5.32$$

TABLE 5-1

Values of A(h/L) and B(h/L) Under Neutral Conditions h/L ≈ 0

Reference	A(0)	B(0)
Yamada [5-15]	1.855	3.020
Fichtl [5-1]	1.6	4.7
Tennekes [5-10]	2	5
Monin [5-3]	1 to 2	4.2 to 4.7
Clarke and Hess [5-16]	1.1 ± 0.5	4.3 ± 0.7

and the angle between the direction of the surface wind and that of the reference wind vector W_{ref} is obtained from

$$\sin \alpha = -\frac{u_*}{k|W_{ref}|} B(h/L) \frac{f}{|f|} \qquad 5.33$$

For the barotropic atmosphere the appropriate scale for wind is

$$\vec{W}_{ref} = \vec{W}_G \qquad 5.34$$

where the geostrophic wind, W_G, is constant.

The appropriate height scale for neutral stability is $h = c_1 u_*/|f|$ where $c_1 \approx 0.3$. Departures from neutral stability cause some controversy over the appropriate form of h. Yamada [5-15] found the relationship between h/L and $u_*/|f|L$ shown in Figure 5-3. The expression $h/L = 0.3\ u_*/|f|L$

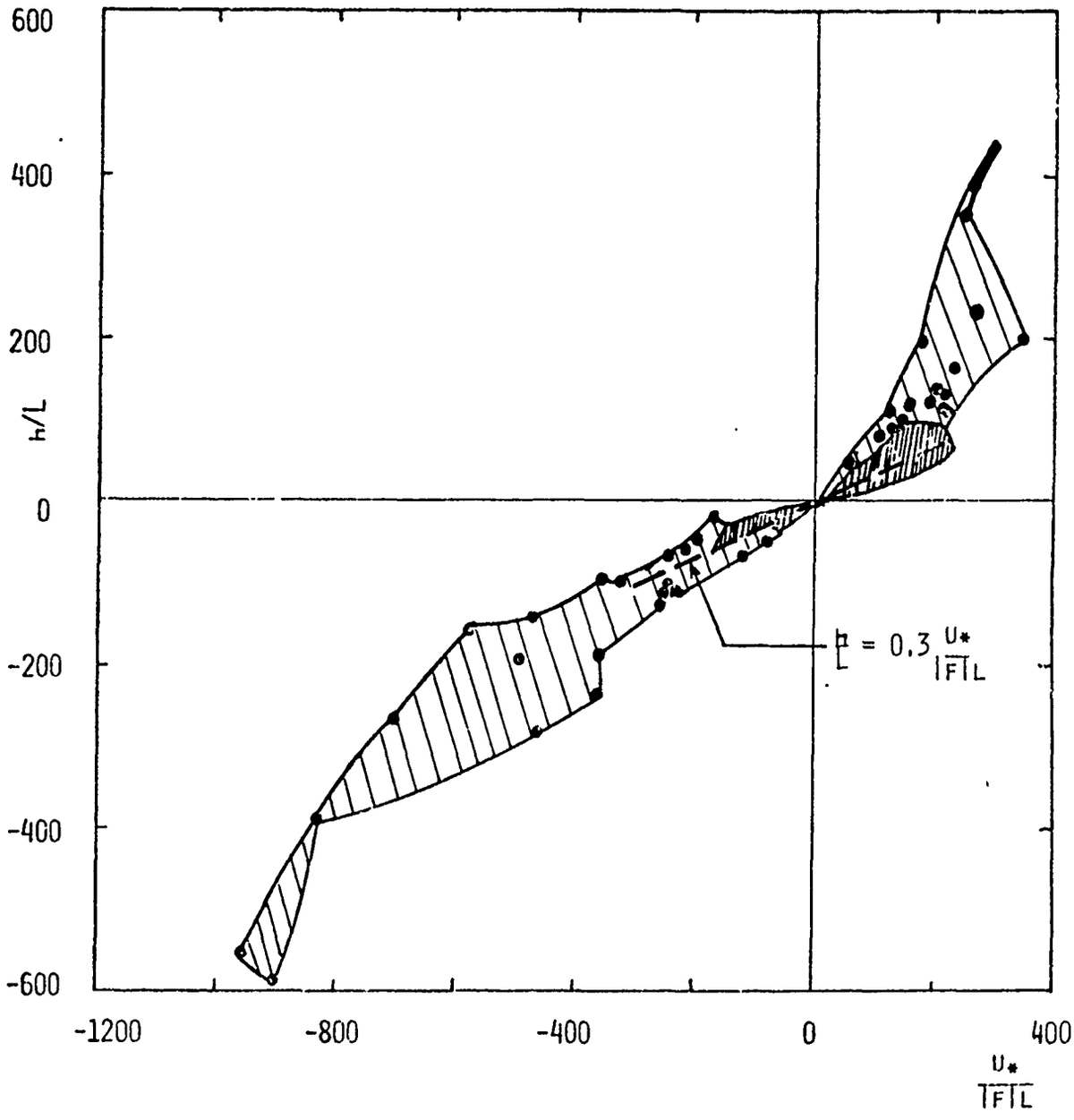

FIGURE 5-3 HEIGHT SCALE FOR THE PLANETARY BOUNDARY LAYER [5-15].

holds reasonably well for $u_*/|f|L < 200$ but it underestimates h/L considerably for $u_*/|f|L > 200$. Other workers [5-17] find the height of the inversion layer z_i during nighttime and the mixing layer during daytime to be the correct scaling height.

The foregoing analysis does not permit computation of the wind profile variation with altitude. It does express the geostrophic drag coefficient $u_*/|W_G|$ and the cross isobaric wind angle as a function of the surface Rossby number $Ro = |W_G|/fz_o$ for given values of h/L. Note, if h can be written u_{*o}/f, Equation 5.33 can be rewritten

$$\ln Ro = B(h/L) + \ln \frac{|W_G|}{u_{*o}} + \left[\frac{k^2|W_G|^2}{u_{*o}} - A(h/L)^2\right]^{\frac{1}{2}} \qquad 5.35$$

A meaningful wind profile variation with elevation can not be expressed in a simple mathematical form. Most all solutions to the wind spiral with height have been carried out numerically. The equations solved are

$$\frac{1}{\rho}\frac{\partial \tau_x}{\partial z} = -f(W_{xG} - W_x(z)) \qquad 5.36$$

and

$$\frac{1}{\rho}\frac{\partial \tau_y}{\partial z} = f(W_{yG} + W_y(z)) \qquad 5.37$$

where

$$\tau_x = \rho K \frac{dW_x}{dz} \; ; \; \tau_y = \rho K \frac{dW_y}{dz} \qquad 5.38$$

The eddy momentum K must be modeled to close the set of equations. The expression

$$K = \ell^2 \left[\left(\frac{\partial W_x}{\partial z} \right)^2 + \left(\frac{\partial W_y}{\partial z} \right)^2 \right]^{\frac{1}{2}} \qquad 5.39$$

where

$$\ell = \frac{k(z + z_o)}{1 + 4 \, (z/z_m)^{5/4}} \qquad 5.40$$

was proposed by Lettau as reported by Hanna [5-11]. Other authors [5-18, 19] have used similar forms for K and ℓ and obtain essentially the same solutions for $W_x(z)$ and $W_y(z)$. Figure 5-4 shows Lettau's solution in dimensionless form. This solution is valid for all neutral wind spirals, the only variation being the length of the straight line extension along the left asymptote.

To construct the neutral barotropic wind profiles from Figure 5-4, first locate the required value of $fz_o/(0.185 \, u_{*o})$. The geostrophic wind is the vector from this point to the central point of the wind spiral. Any other vector drawn from this point to any point on the curve represents the wind velocity at the height indicated by the end point.

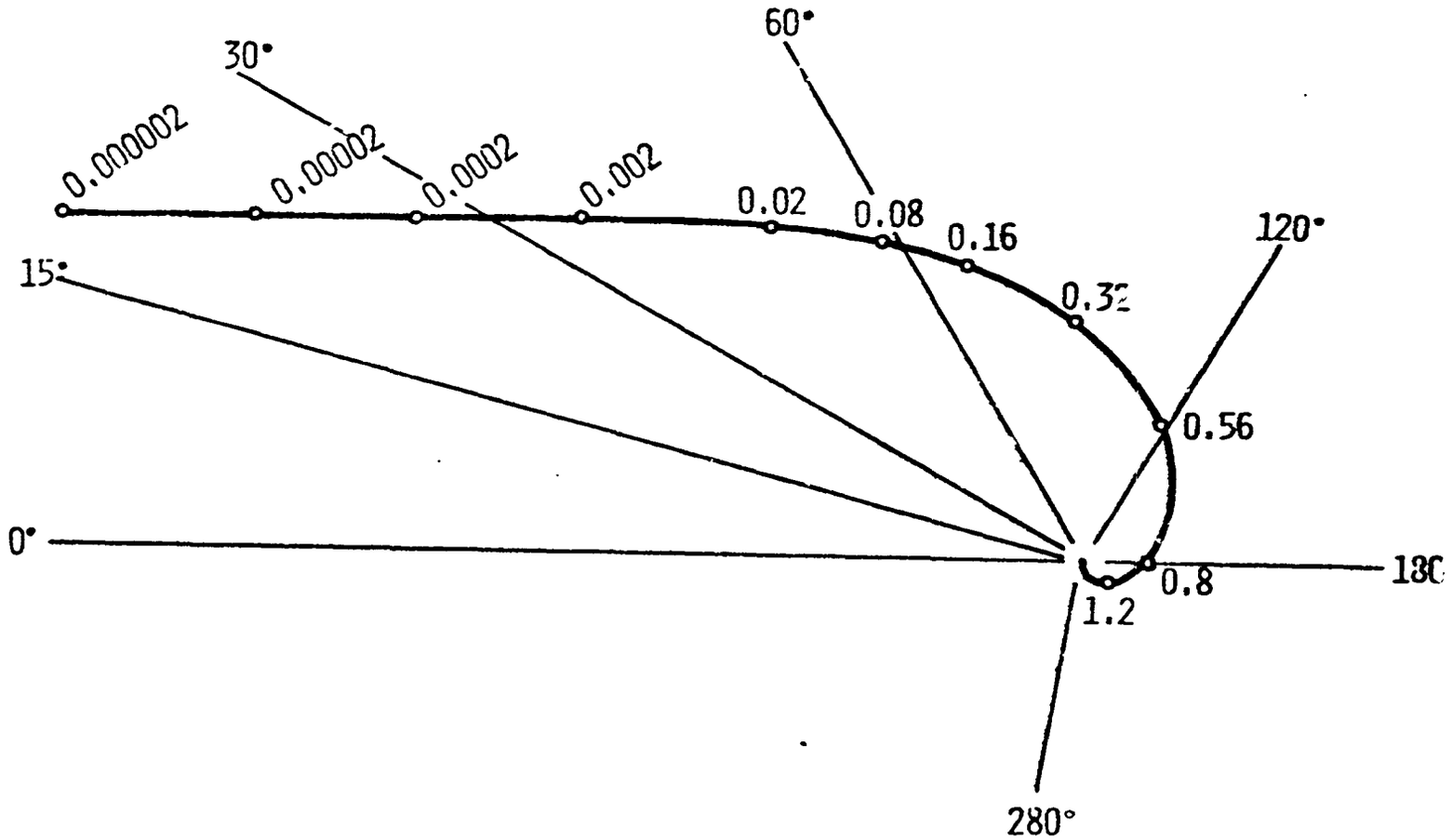

FIGURE 5-4 HODOGRAPH OF DIMENSIONLESS VELOCITY FOR THE NEUTRAL BAROTROPIC TURNING LAYER [5-11].

As an example, suppose z_o = 0.01m, f = 0.84×10^{-4} s^{-1} and u_{*o} = 0.22 m/s, the geostrophic wind is given by

$$W_g = \sqrt{W_{xg}^2 + W_{yg}^2}$$

where W_{xg} and W_{yg} are determined from Equations 5.30 and 5.31 with $h = 0.3u_*/|f|$. Thus, W_{xg} = 5.11 m/s, W_{yg} = 1.63 m/s and W_g = 5.36 m/s. The wind speed and direction at z = 162 m is obtained by scaling from Figure 5-4 which gives

$$W = \text{Scaled Distance (0.32-0.00002) } W_g/\text{Scaled Distance (center - 0.00002)}$$

$$= (4.75)(5.36 \text{ m/s})/5.16 = 4.93 \text{ m/s}$$

and $\alpha = 7°$.

Solutions for the diabatic barotropic wind profiles have been numerically computed [5-20, 21] but are not expressible in a non-dimensional form such as Figure 5-4.

The experimental results of Clarke and Hess [5-16] provide a method of estimating the wind profile for conditions departing from those of neutral stability. Figures 5-5 and 5-6 give the departure of the nondimensional wind components parallel, $W_x(\hat{z})/u_{*o}$, and perpendicular, $W_y(\hat{z})/u_{*o}$, to the surface wind respectively from the reference wind defined at $\hat{z} = zf/u_{*o} = 0.15$ as a function of nondimensional height, $\hat{z}$. Using the values of $A_1(\mu)$ and $B_1(\mu)$ where $\mu = ku_*/|f|L$, given in Figure 5-7 and 5-8 which are based on $\hat{z} = 0.15$ and Equations 5.30 and 5.31 with $h = |f|/u_{*o}$ the values of $W_{xref} = W_x(\hat{z} = 0.15)$ and $W_{yref} = W_y(\hat{z} = 0.15)$ can be determined. For a given

stability condition μ the values of $\Delta W_x = (W_x(\hat{z} = 0.15) - W_x(\hat{z}))/u_{*o}$ and $\Delta \hat{W}_y = (W_y(\hat{z} = 0.15) - W_y(\hat{z}))/u_{*o}$ can be scaled from Figures 5-5 and 5-6 at any height $\hat{z}$ up to a value of 0.15.

Figure 5-9 shows a plot of the wind spiral for a stable atmosphere of L = 11m determined in the above manner. One observes that the turning of the wind begins at approximately 20m indicating that the turning layer can become very significant under stable nighttime inversion. Figure 5-10 compares the log-linear wind profile Equation 5.14 and Equation 5.11 with the horizontal component of the turning layer. The log-linear law begins to depart appreciably at 20m.

5.3.3 Baroclinic Turning Layer

The baroclinic turning layer has been solved numerically by Blackadar [5-22] for the assumption of a linearly varying geostrophic wind.

$$\vec{W}_G = \vec{W}_{Go} + \vec{A}z \qquad 5.41$$

where $\vec{W}_{Go}$ is the surface value of the geostrophic wind and $\vec{A}$ is the vectorial rate of increase with height. The results of calculations for four different directions of $\vec{A}$ are shown in Figure 5-11. The curves are calculated for $|A| = 42 \times 10^5 f$, $|W_g| = 84 \times 10^5 f$, $z_o = 0.01$m, and the indicated heights are expressed in meters. The baroclinic

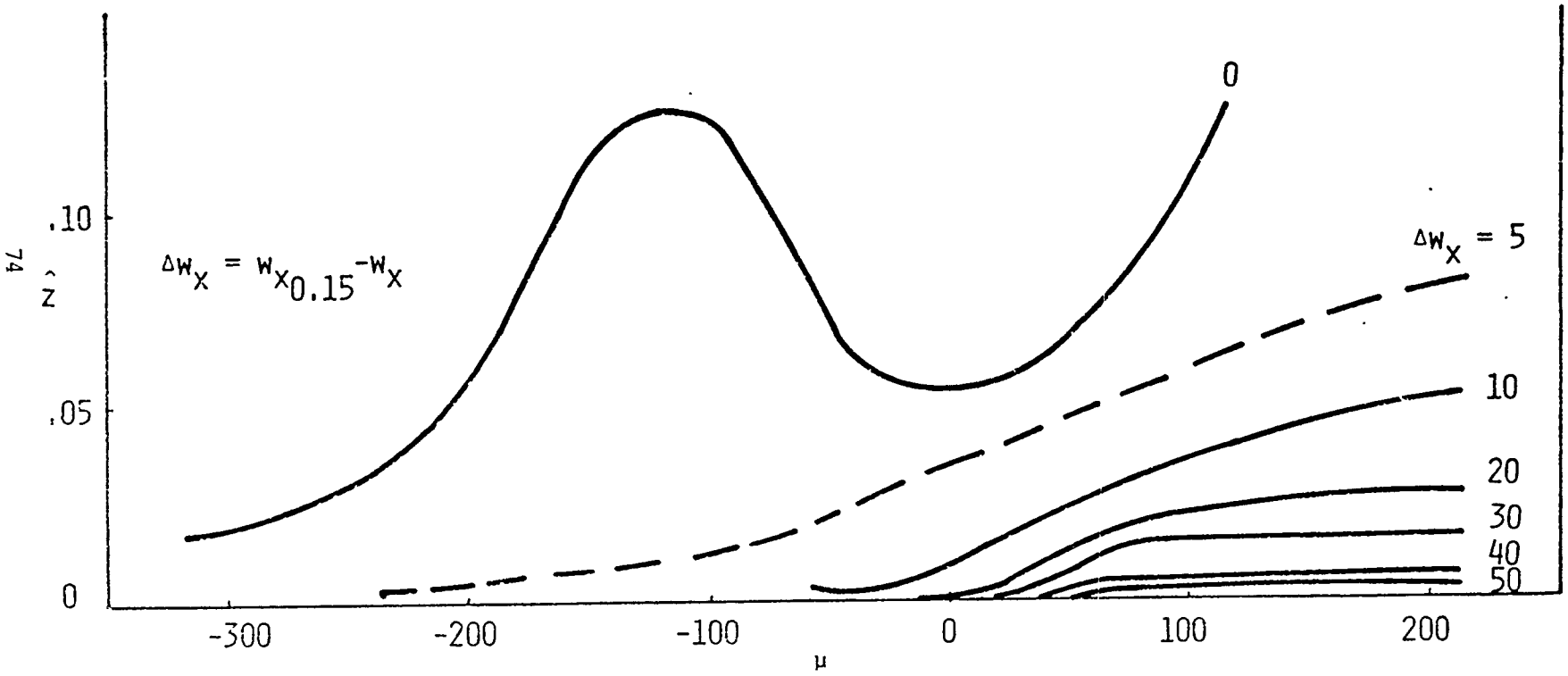

FIGURE 5-5 DEPARTURE OF THE NONDIMENSIONAL WIND COMPONENT PARALLEL TO THE SURFACE WIND FROM THE WIND AT $\hat{z}$=0.15, [5-16].

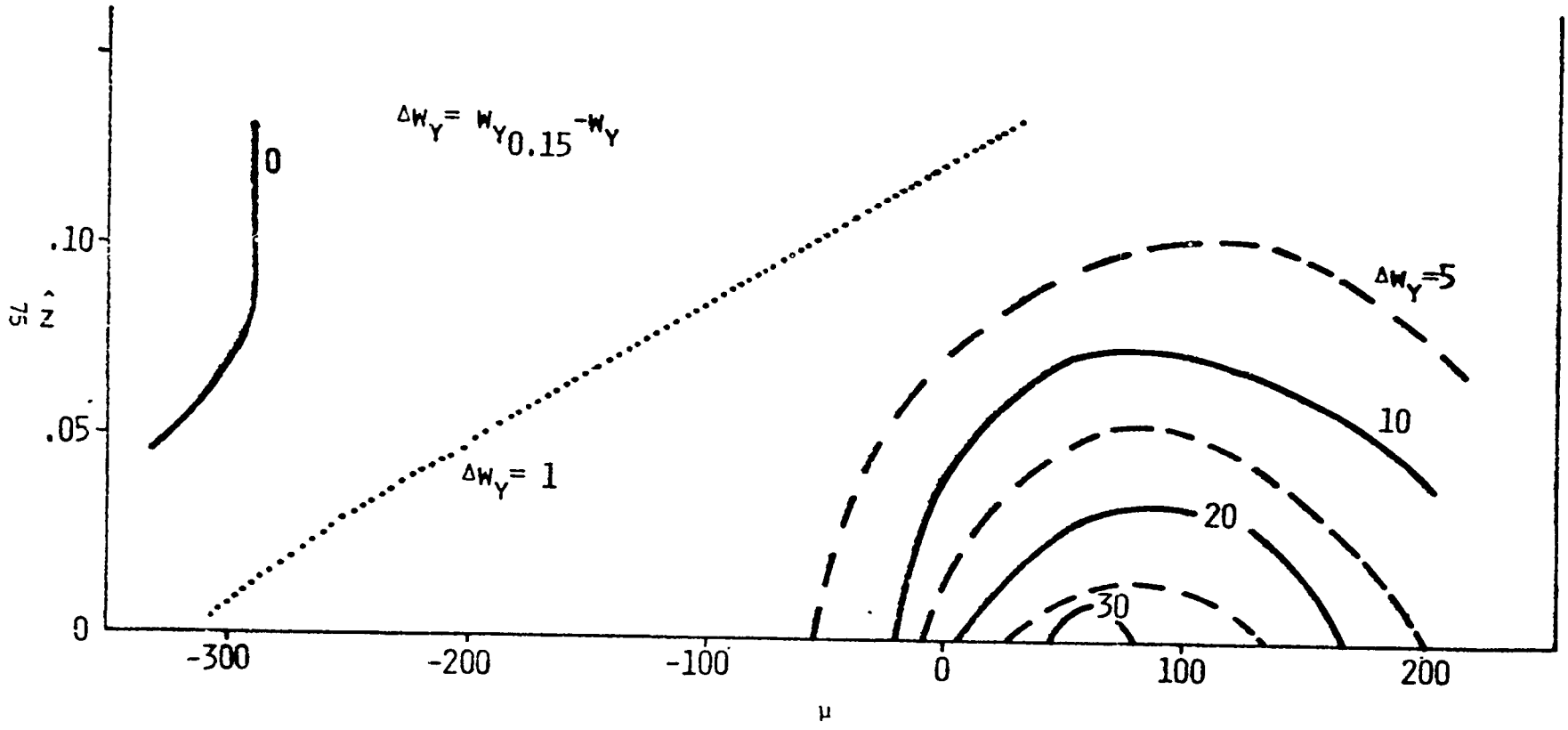

FIGURE 5-6 DEPARTURE OF THE NONDIMENSIONAL WIND COMPONENT PERPENDICULAR TO THE SURFACE WIND FROM THE WIND AT $\hat{z}$=0.15, [5-16].

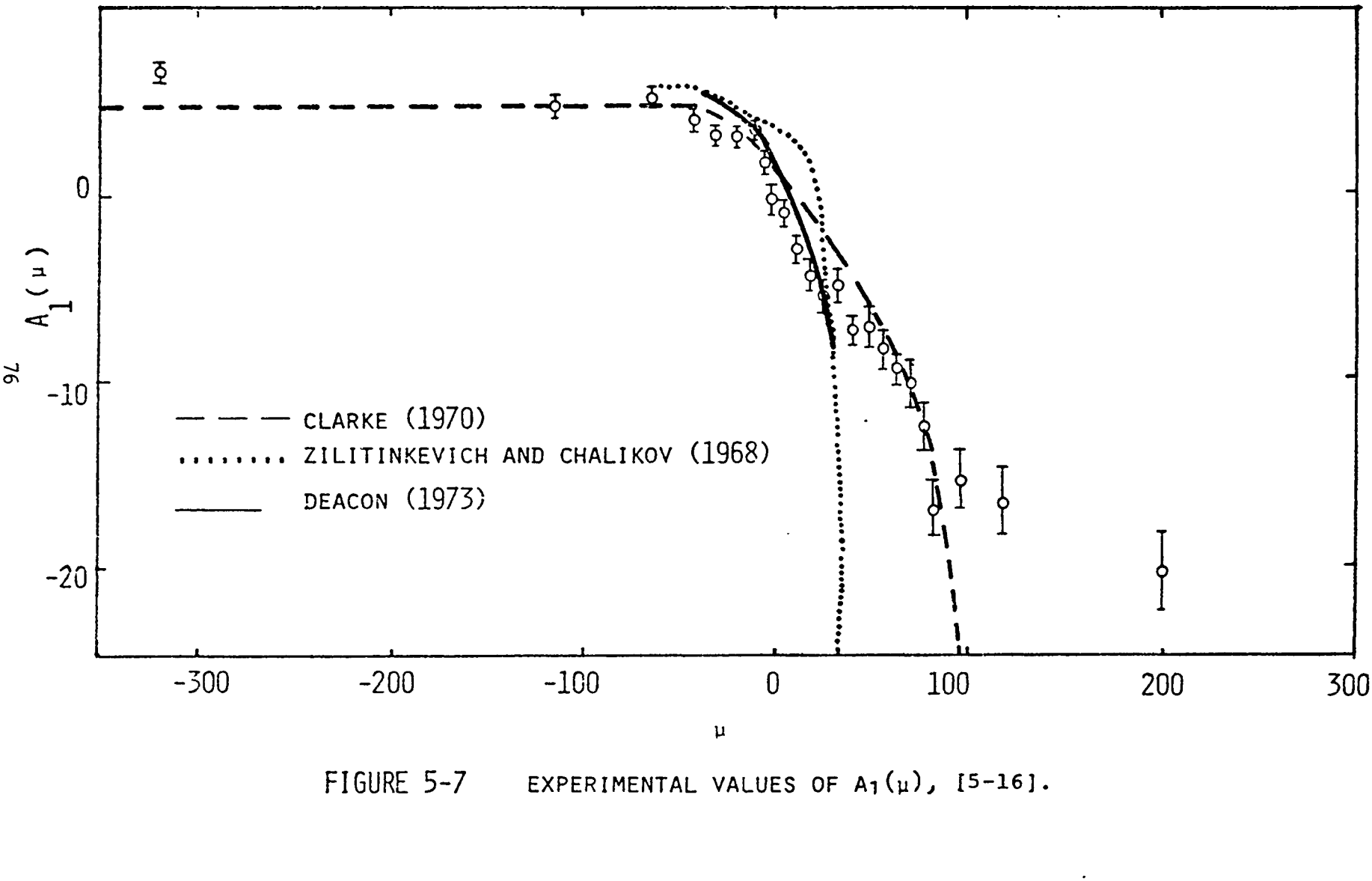

FIGURE 5-7 EXPERIMENTAL VALUES OF $A_1(\mu)$, [5-16].

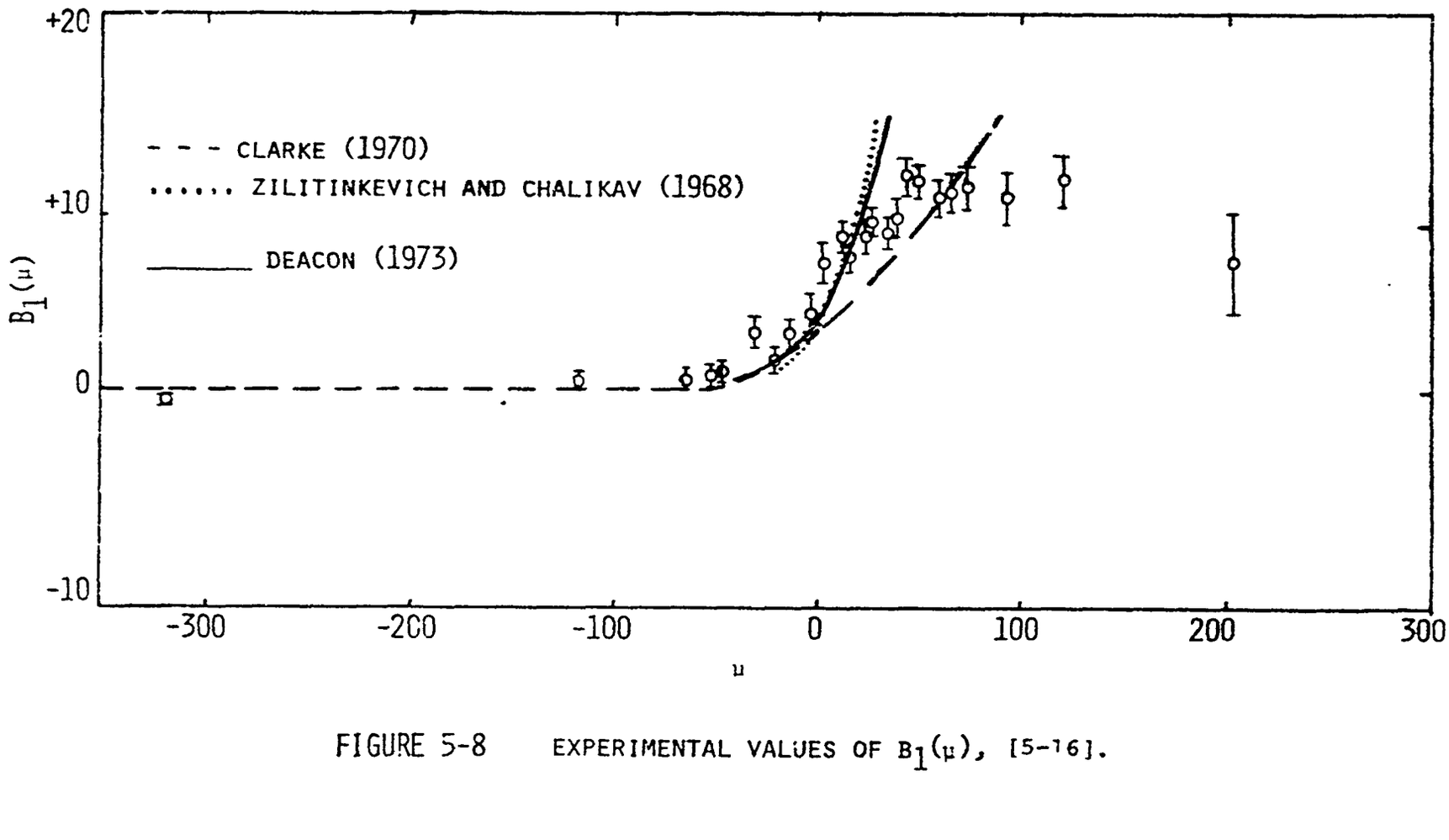

FIGURE 5-8 EXPERIMENTAL VALUES OF $B_1(\mu)$, [5-16].

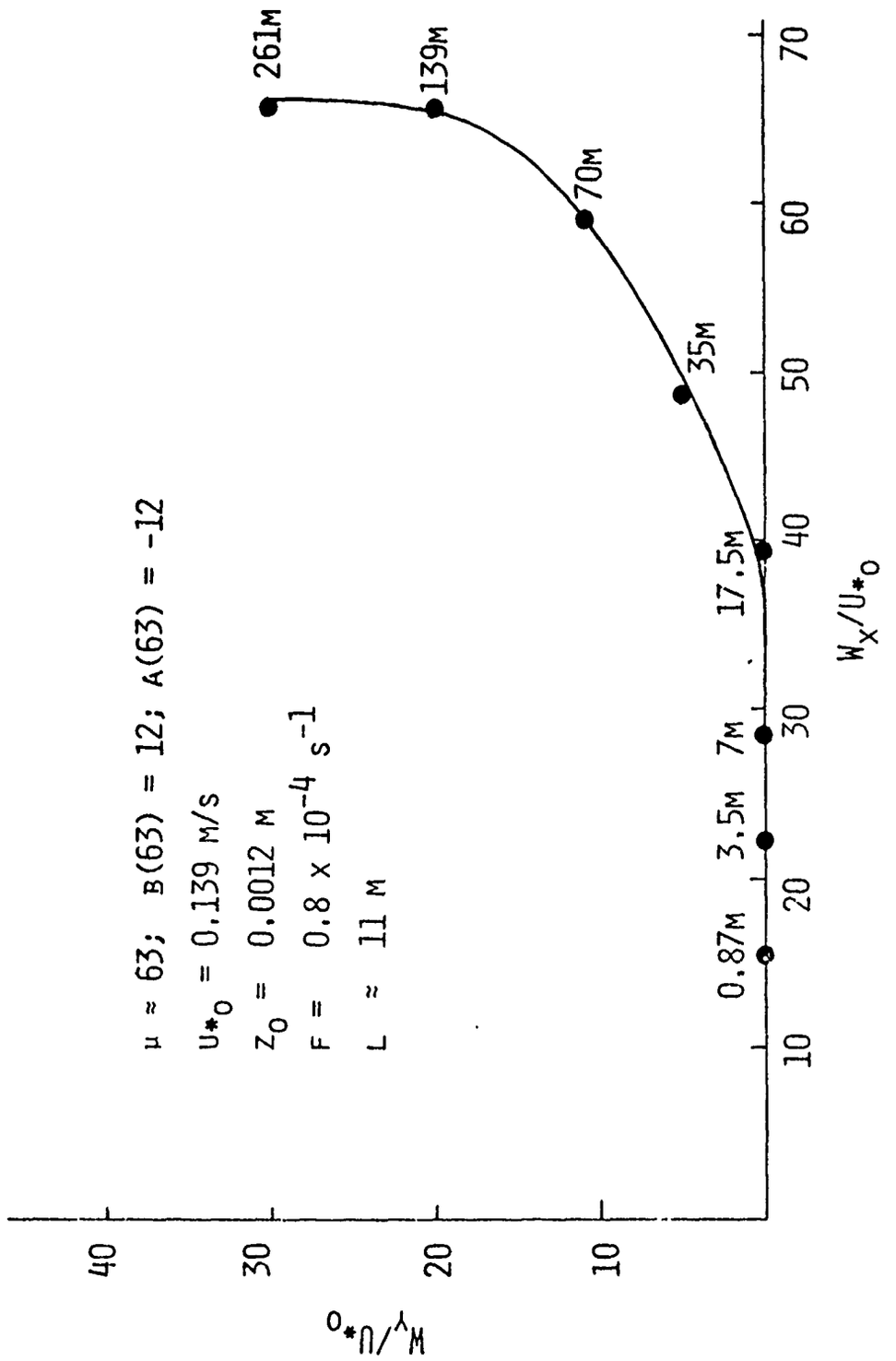

FIGURE 5-9 CALCULATED WIND SPIRAL FOR A STABLE ATMOSPHERE, L=11M.

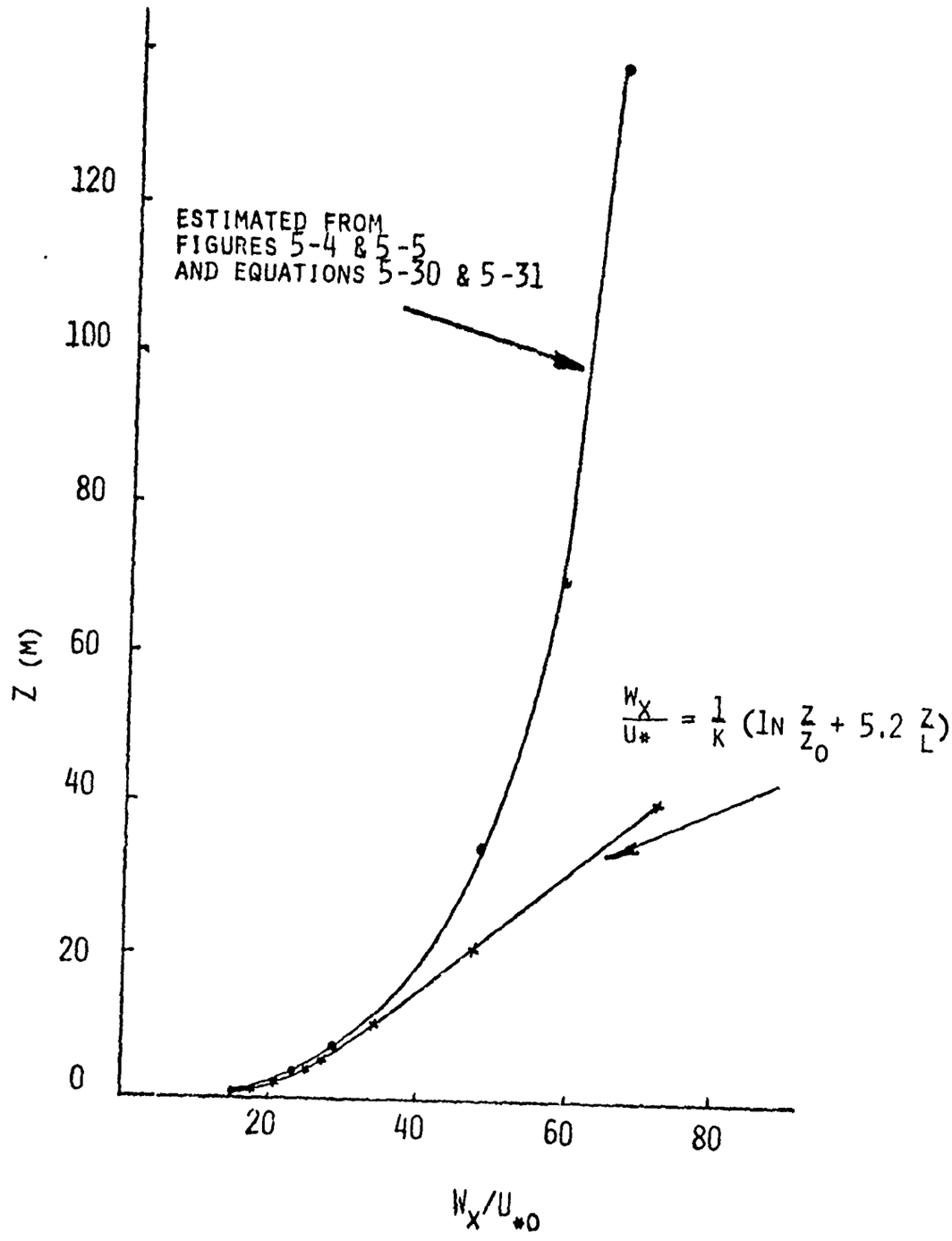

FIGURE 5-10 COMPARISON OF THE LOG-LINEAR VELOCITY PROFILE WITH THE WIND COMPONENT PARALLEL TO THE SURFACE WIND AS DETERMINED FROM FIGURE 5-9.

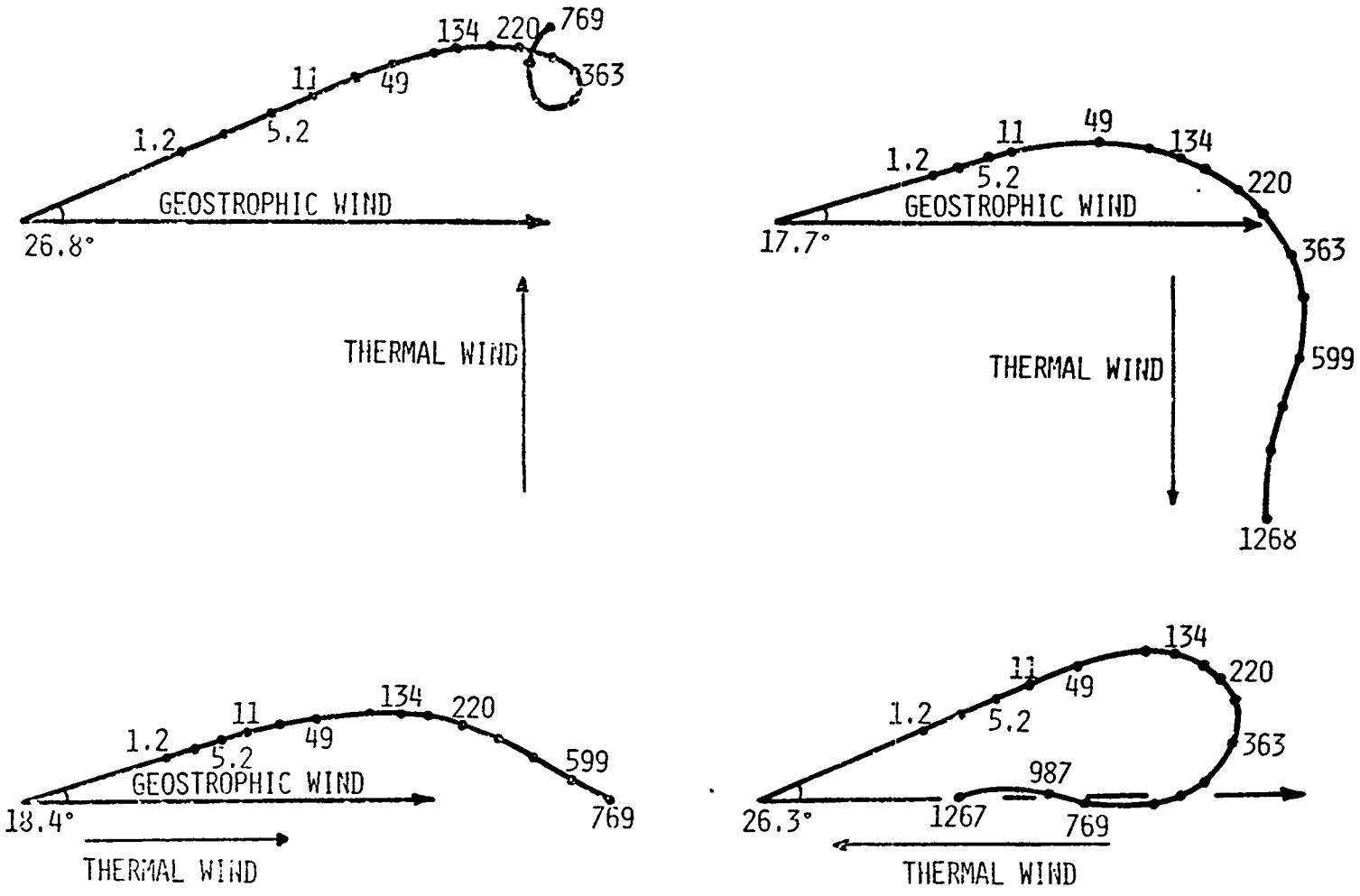

FIGURE 5-11 NUMERICALLY COMPUTED BAROCLINIC WIND HODOGRAPHS FOR FOUR DIFFERENT DIRECTIONS OF THE THERMAL WIND, [5-12].

wind profile can be scaled from these curves only for the specific conditions stated.

Application of Equations 5.30, 5.31, 5.36 and 5.37 requires a different scaling velocity than W_G. Yamanda [5-15] uses a vertically averaged geostrophic wind

$$\vec{W}_{ref} = \langle \vec{W}_G \rangle = \frac{1}{h} \int_0^h W_G(z)\, dz \qquad 5.42$$

Scaling velocities used by other investigators are also reported in [5-15].

5.4 Boundary Layer Over Non-Homogeneous Terrain

5.4.1 Surface Roughness Transition

An internal boundary layer occurs within the atmospheric boundary layer when the moving air mass passes over a change in surface roughness. Typically the internal boundary layer will develop as shown in Figure 5-12. When a change from surface roughness z_{o1} to surface roughness z_{o2} occurs at location x = 0, a transition zone grows upward and spreads outward from the discontinuity in surface roughness. Above region II shown in Figure 5-12 the wind profile is undisturbed from the upstream profile which, depending on stability conditions, is described by Equations 5.20 through 5.24. Below region II, the wind speed profile may be taken as logarithmic

$$W_x = \frac{u_{*o2}(x)}{k} \ln \frac{z + z_{o2}}{z_{o2}} \qquad 5.43$$

Further from the discontinuity, where z/L within region I becomes large, the wind speed profile may more adequately be described for the existing diabatic conditions by the appropriate equations given in Section 5.2. Within region II the wind blends gradually from the velocity profile in region I to that in region III. At large distances from either side of the discontinuity in roughness, the shear stress at the surface adjusts to values consistent with those expected of the flow had it developed over uniform terrain.

Numerous mathematical model and numerical solutions of the internal boundary layer have been proposed. Surveys of these are given in [5-23, 24, 25]. The experimental data to confirm these models are somewhat limited, however. Reported data from measurements in the laboratory and in the atmosphere are given in [5-26, 27, 28, 29]. These data tend to corroborate the mathematics, but are generally not measured over sufficient distances to verify the character of the boundary layer at elevations where encounters with airplanes occur. In the absence of such experimental data, mathematical models are used to extend the data to heights of interest for this report.

It is generally agreed both experimentally and analytically that the height of the internal boundary layer, essentially δ_m in Figure 5-12, grows as:

$$\frac{\delta(x)}{z_{o2}} = c_1 \left(\frac{x}{z_{o2}}\right)^n \qquad 5.44$$

For neutral conditions, values of n range from 0.70 to 0.80 and values for c_1 are given as: $0.75 - 0.03 \ln (z_{o2}/z_{o1})$ by Elliott [5-30] and unity by Munro and Oke [5-27].

Rao [5-31] numerically computes for unstable flow that δ grows as $x^{0.88}$ for L =-20m and as $x^{1.39}$ for L =-2m. For neutral conditions he reports n = 0.77.

Figure 5-13 illustrates the approximate growth of the internal boundary layer, based on Equation 5.44 relative to a 3° glide slope for some typical roughness changes near airports. Wind shear may be expected as aircraft pass through the internal boundary layer and knowledge of the shape of the wind profile is required to assess the magnitude of this shear.

Solutions of the two-dimensional flow field over a change in surface roughness by numerical solution of either the boundary layer or Navier-Stokes equations using various turbulence models are given in [5-12, 32, and 34]. Typical horizontal velocity profiles at various stations in the windward direction from the surface roughness change are shown in Figure 5-14, and a characteristic vertical

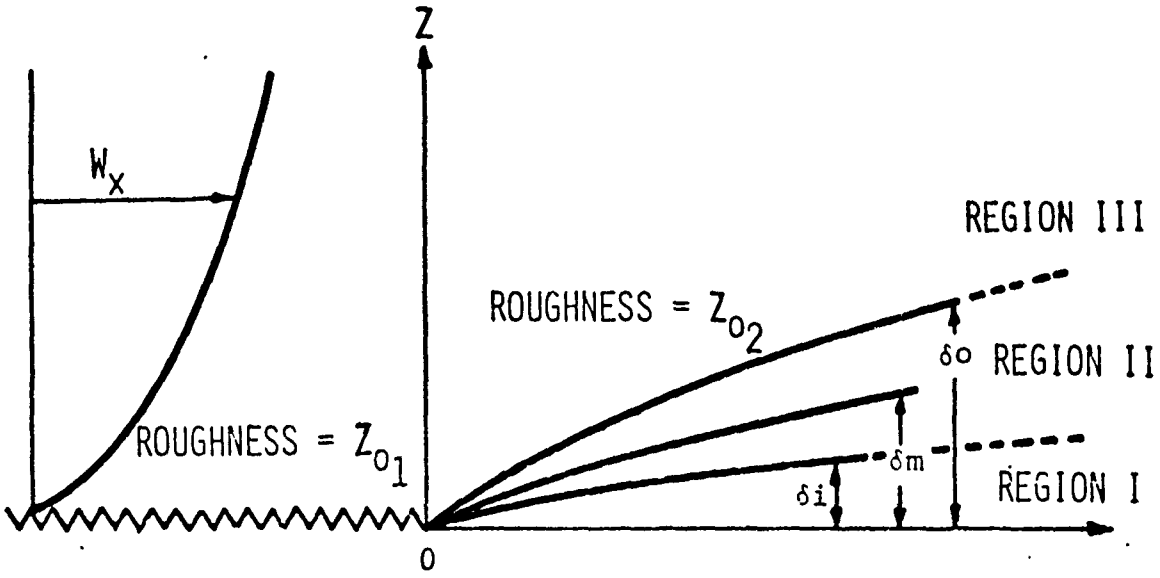

FIGURE 5-12 SCHEMATIC ILLUSTRATION OF THE DEVELOPING INTERNAL BOUNDARY LAYER [5-35].

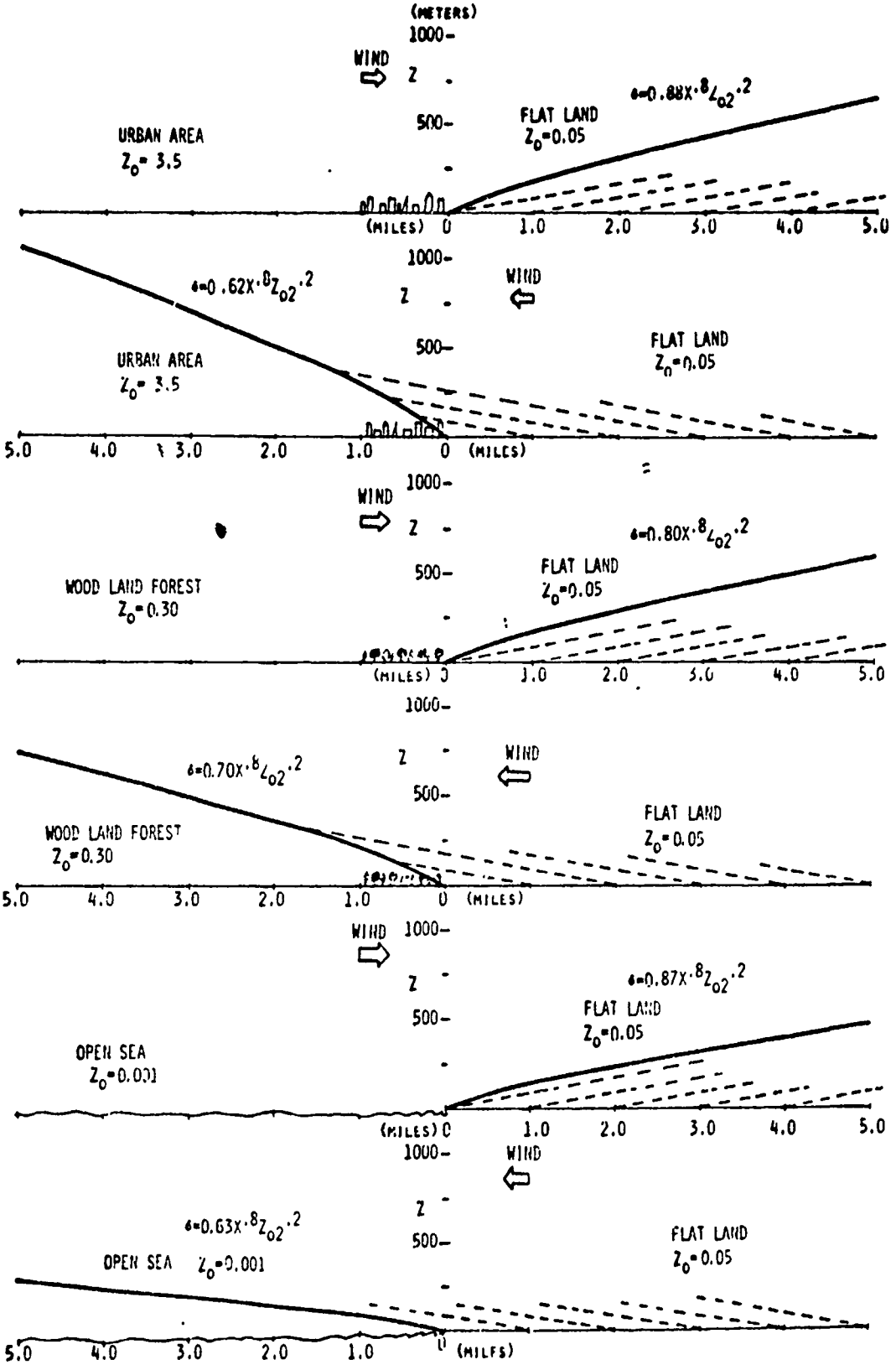

Figure 5-13 COMPUTED GROWTH OF THE INTERNAL BOUNDARY LAYER RELATIVE TO A 3° GLIDE SLOPE (DASHED LINES) FOR SOME TYPICAL ROUGHNESS CHANGES NEAR AIRPORTS.

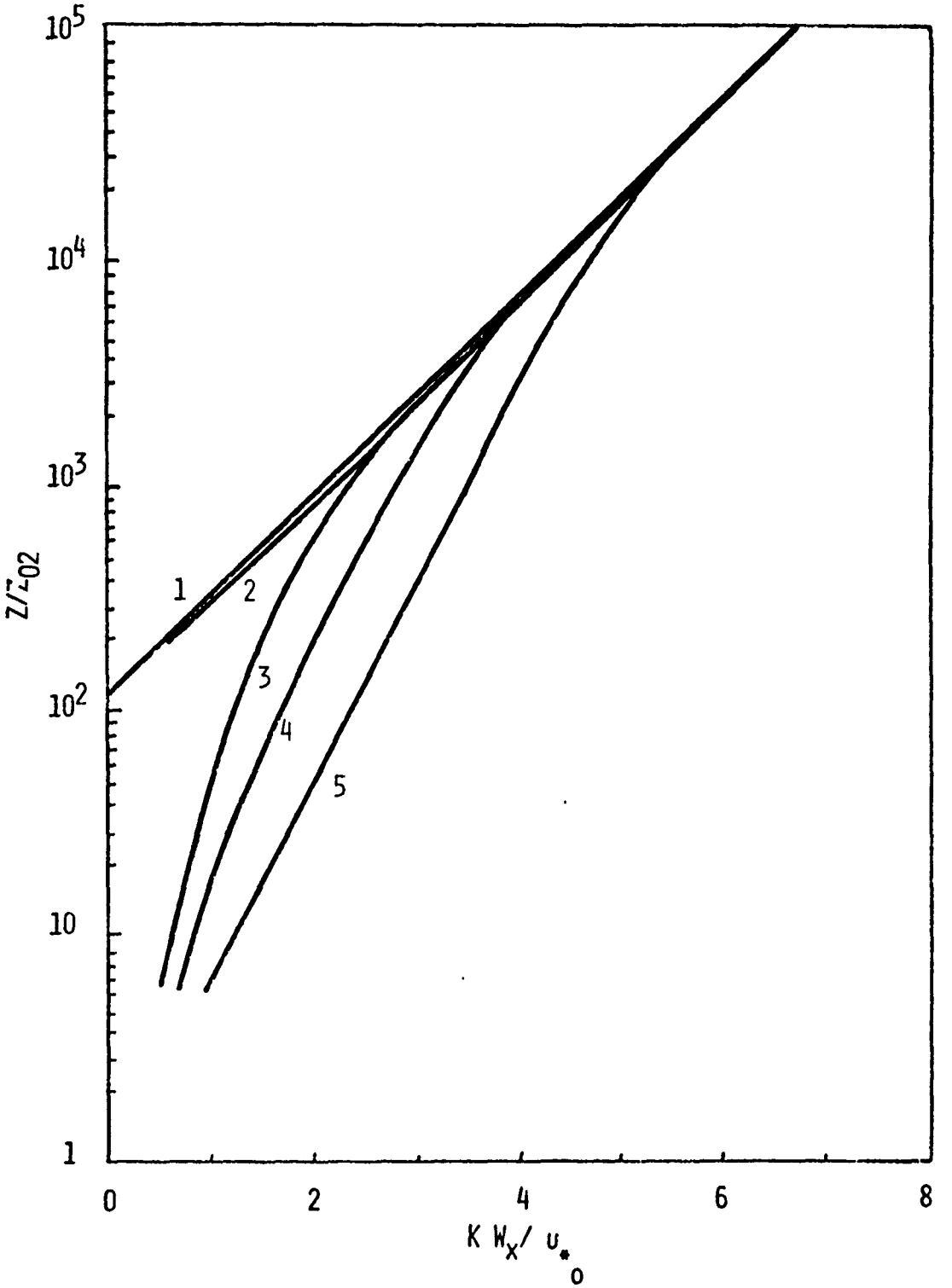

FIGURE 5-14 TYPICAL HORIZONTAL VELOCITY PROFILES AT GIVEN X STATIONS DOWNWIND OF A CHANGE IN SURFACE ROUGHNESS [5-24].

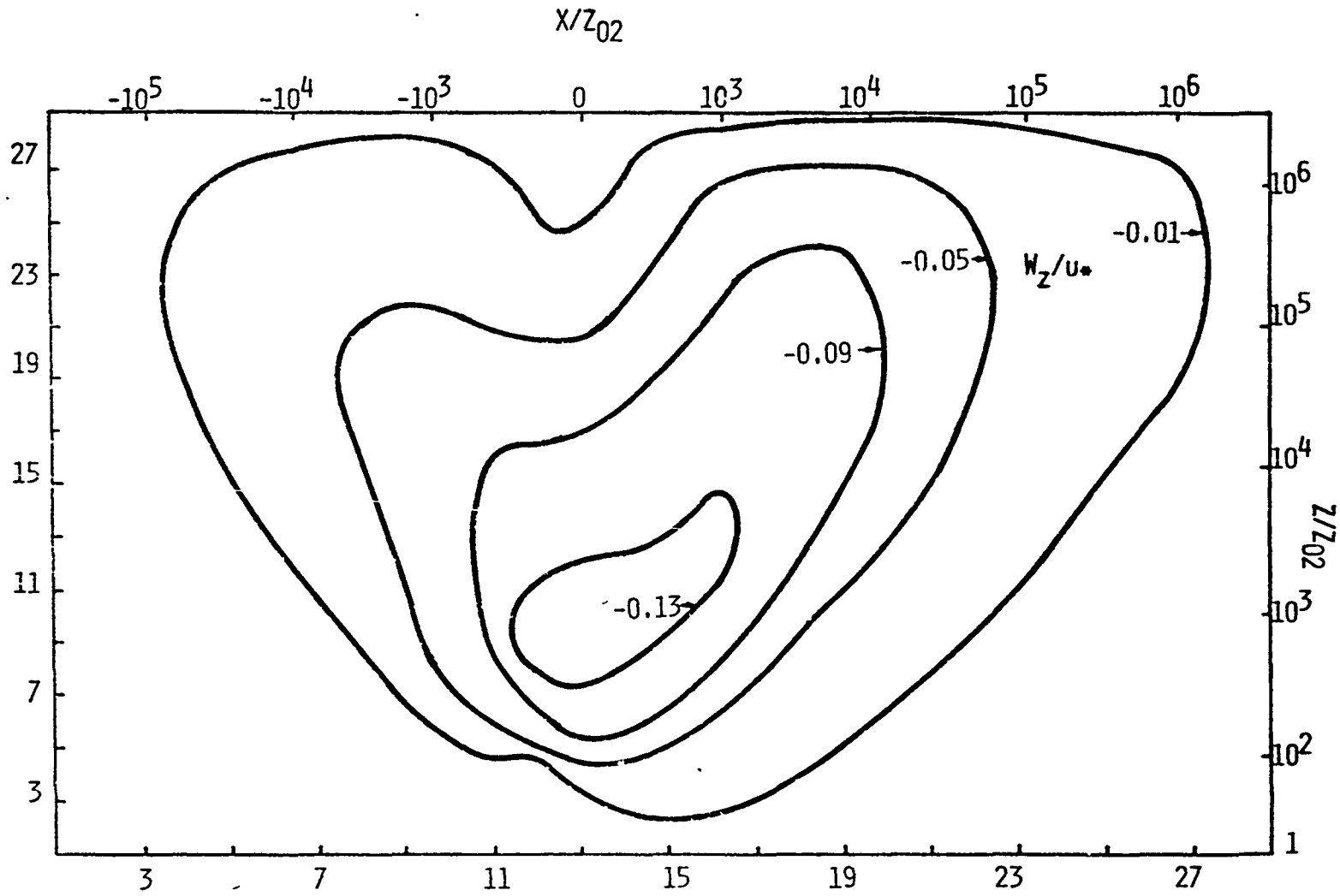

FIGURE 5-15 CHARACTERISTIC VERTICAL VELOCITY FIELD OVER A CHANGE IN SURFACE ROUGHNESS [5-24].

velocity field is shown in Figure 5-15. The velocity information given in the two figures are for a rough to smooth transition of $\ln z_{o1}/z_{o2}=5$. Similar results are obtained for smooth to rough transitions and some results for the unstable case have also been reported. One observes a downward motion of the air as it passes over the change of surface roughness. This suggests an unexpected downdraft may be encountered by aircraft approaching, say over a forested area breaking into a cleared airfield.

The application of the above numerical solutions to computer simulation of airplane flight over transitions in surface roughness requires either on-line solution of the complete ser of equations, which is extremely costly in computer time, or a table look-up scheme with the wind field data stored on tapes or cards. The latter approach is readily carried out. However, for quick preliminary analyses, a simple mathematical expression for the wind profile through the internal boundary layer would be valuable.

Logan and Fichtl [5-35] have recently proposed such a model for neutrally stable conditions consisting of two bounding logarithmic layers and an intermediate velocity defect layer. Velocities and stress distribution functions within region II, Figure 5-12, which meet all boundary and matching conditions of regions I and III are given by:

$$u(z) = u_*(z,x)\ F(\eta) + u_i \qquad 5.45$$

$$u_*^2\ (z,x) = (u_{*o2}^2 - u_{*o1}^2)\ G(\eta) + u_{*o1}^2 \qquad 5.46$$

where $\eta = z/\delta_o$ and δ_o is the outer boundary of region II. The velocity u_i is given by:

$$\frac{u_i}{u_{*o1}} = \frac{1}{k} \ln \frac{\delta_m}{z_{o1}} \qquad 5.47$$

where $\delta_m < z < \delta_o$ defines a region in which the flow has decelerated relative to the original equilibrium logarithmic profile:

$$\frac{W_x}{u_{*o1}} = \frac{1}{k} \ln \frac{z}{z_{o1}} \qquad 5.48$$

and $\delta_i < z < \delta_m$ defines a region in which the flow has accelerated relative to the logarithmic velocity profile:

$$\frac{W_x}{u_{*o2}} = \frac{1}{k} \ln \frac{z}{z_{o2}} \qquad 5.49$$

By appropriate matching techniques the relationships given below can be found:

$$\delta_o = \delta_m \quad (1 + \frac{1}{\psi}) \qquad 5.50$$

$$\psi = \frac{\sqrt{2\pi}}{2} \frac{z_{o2}}{k^2 x} [r(\ln r - (1+M)) + e^m] \qquad 5.51$$

$$M = \ln(z_{o1}/z_{o2}) \ ; \quad r = \delta_m/z_{o2} \qquad 5.52$$

$$u_{*o2} = u_{*o1} \frac{1}{\frac{M}{\ln(\delta_m/z_{o1})} + 1} \qquad 5.53$$

$$u_i = \frac{u_{*o1}}{k} \ln \frac{\delta_m}{z_{o1}} \qquad 5.54$$

These relationships are based on the functions

$$G(\eta) = \text{erf}\left[\frac{4(\delta_o+\delta_L-2z)}{(\delta_o-\delta_L)}\right] \qquad 5.55$$

where

$$\text{erf}(\xi) = \frac{1}{\sqrt{2\pi}} \int_{-\infty}^{\xi} e^{-\xi^2} d\xi \qquad 5.56$$

and

$$F(\eta) = \frac{1}{k} \ln \frac{z}{\delta_m} \qquad 5.57$$

The expression relating δ_i, δ_m and δ_o is:

$$\delta_m = (\delta_o + \delta_i) / 2 \qquad 5.58$$

The model is thus complete except that δ_i must be determined from experiment. In Reference [5-35] the data of Bradley [5-26] was used to determine δ_m. The authors of [5-35] point out that δ_m must be determined separately

for each analysis from experimental data having the required value of z_{o1}/z_{o2}.

To circumvent the requirement of individual experimental results for each analysis, it is proposed that δ_m simply be related to x by

$$\delta_m = x^{0.8} z_{o2}^{0.2} \qquad 5.59$$

(see Equation 5.44)

A linear expansion around δ_m is assumed which gives

$$\delta_o = (1 + c_2)\delta_m \qquad 5.60$$

$$\delta_i = c_2 \delta_m \qquad 5.61$$

The solution for the velocity profile within the internal boundary layer is then straight forward. With $c_2 = 0.5$ the computed velocity profiles using Equations 5.52, 5.54, 5.55 and 5.57 were evaluated and are compared with Bradley's data in Table 5-2.

Table 5-2

Comparison of Modified Logan and Fichtl[5-35] solution with Bradley's Data [5-26].

x = 1220 cm

z (cm)	MODEL $u(z)/u_{ref}$	BRADLEY $u(z)/u_{ref}$
100	0.96	0.97
60	0.90	0.895
42	0.87	0.86

x = 210 cm

z (cm)	MODEL $u(z)/u_{ref}$	BRADLEY $u(z)/u_{ref}$
31.2	0.79	0.79
20	0.72	0.72
10	0.67	0.64

The agreement is seen to be very good. Thus, the modified approach to the solution technique of Logan and Fichtl [5-35] provides an easily programmable mathematical model for computing internal boundary layer wind profiles. Figure 5-16 illustrates computed wind profiles at various stations downstream of a discontinuity in surface roughness. It appears from inspection that the wind shear is probably negligible, however, this will be confirmed by introducing the model into the flight dynamic computer code in a later section.

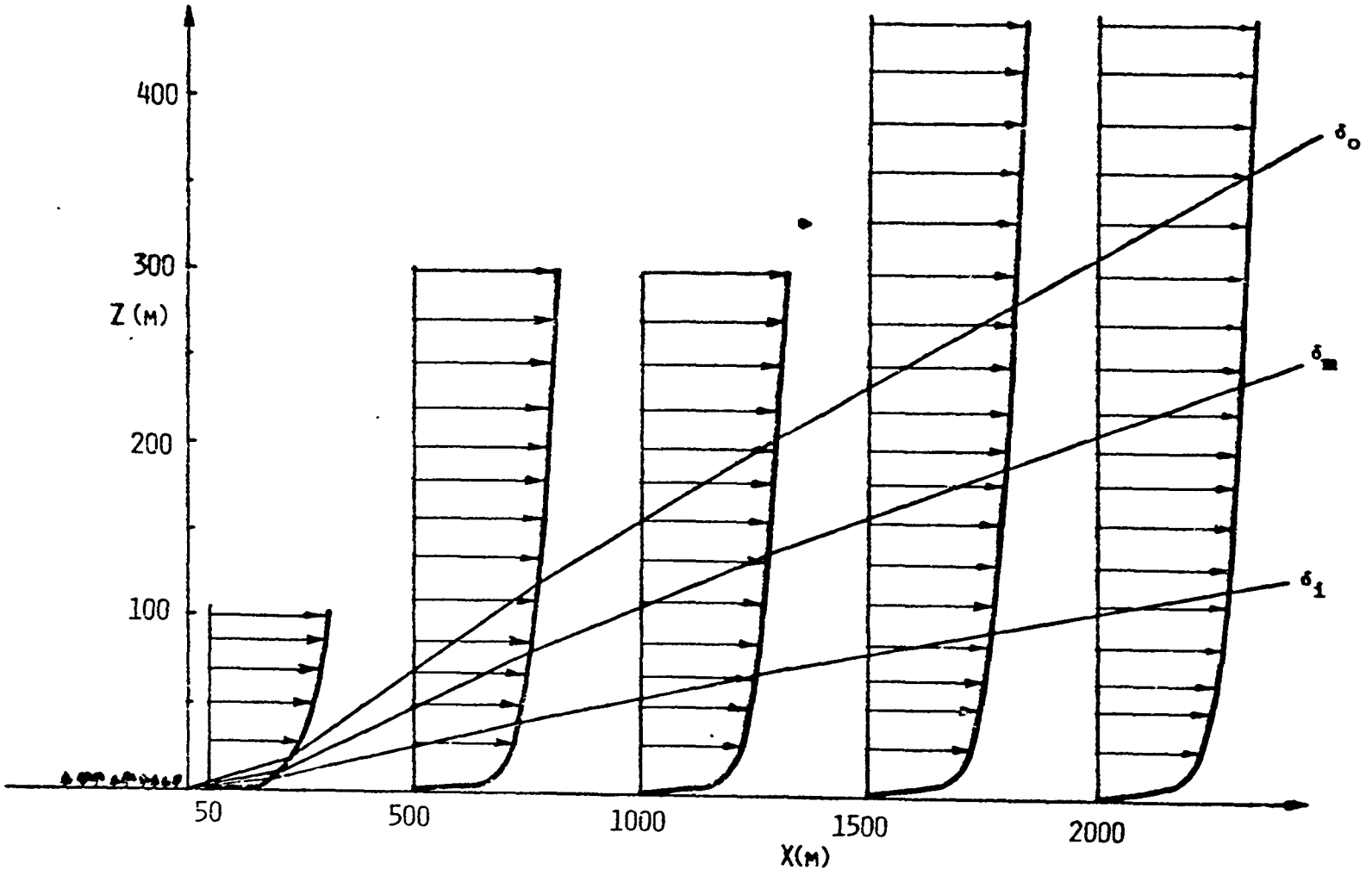

FIGURE 5-16 COMPUTED WIND PROFILES AT VARIOUS STATIONS DOWNSTREAM OF A DISCONTINUITY IN SURFACE ROUGHNESS.

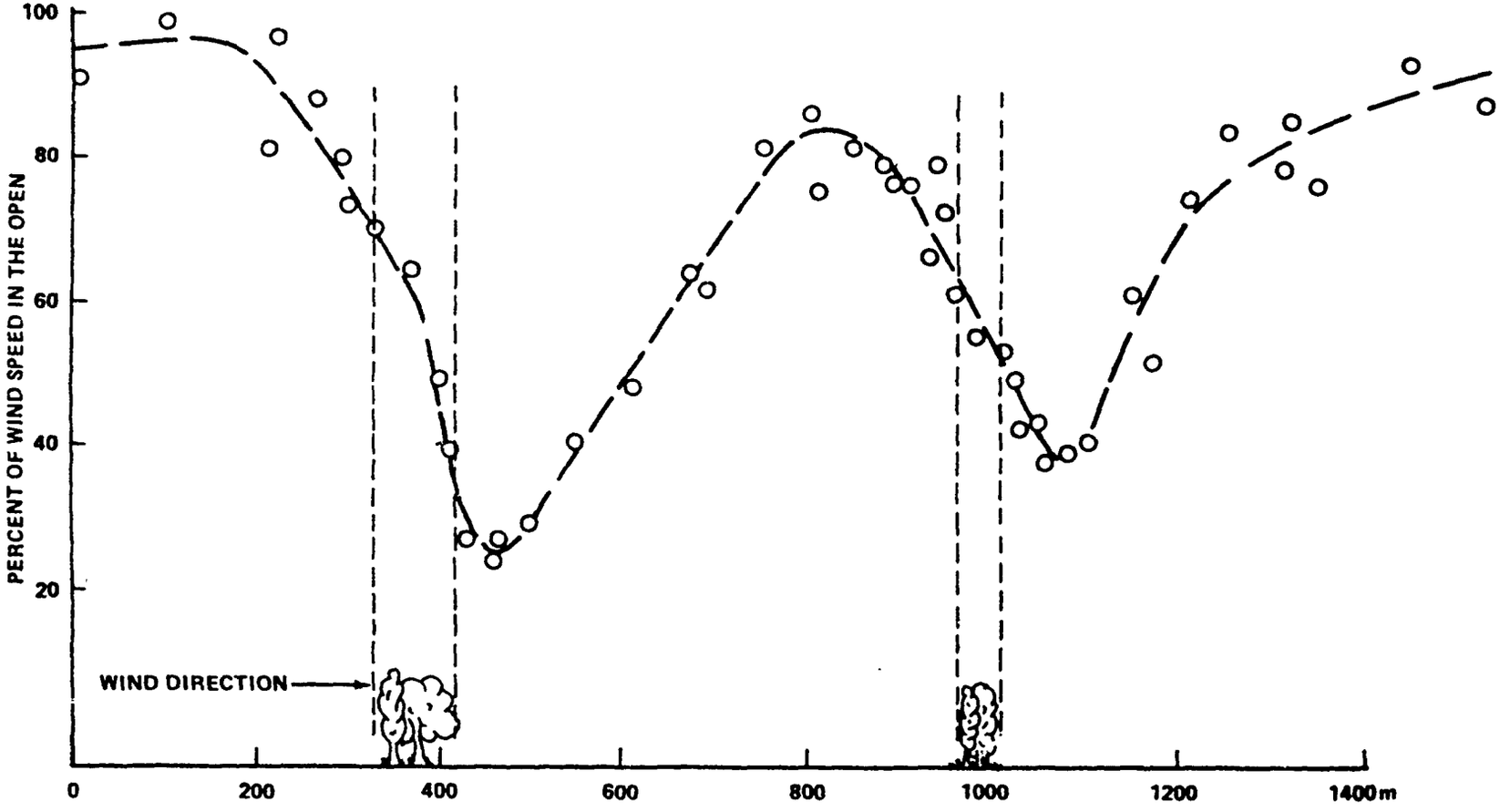

FIGURE 5-17 VELOCITY VARIATION OVER PATCHES OF TREES [5-36].

5.4.2 Other Surface Variations

The preceeding discussion considers only winds over changes in surface roughness where the wind approaches over a large uniform plane and re-establishes itself over an equally large uniform plane. More complex boundary layers may develop over irregularly spaced patches of roughness such as illustrated in Figure 5-17, see [5-36]. These types of wind fields may best be analyzed as wind barriers for which an extensive review is given in [5-37].

When the surfaces of different roughness are also at different temperature, recirculation can occur as in sea breezes [5-38, 39, 40]. Sea breezes have been reported to cause difficult landing conditions [1-9]. Since many airfields are located near the sea or near other large bodies of water, a model of sea breezes for use in flight simulation studies should be developed.

The atmospheric boundary layer over "heat islands", that is, surfaces of different heat flux, temperature and roughness such as a large metropolitan area surrounded by flat grass land, are currently being studied [5-24, 40, 41]. In view of the fact that many approach and departure flight paths are over expansive cities, wind shear over heat islands is another area which requires investigation.

6.0 SUMMARY

6.1 Introduction

Physical models of wind shear environments potentially encounterable by aircraft in the terminal area have been reviewed. Numerous mathematical models and data sources describing wind shear conditions as reported in the literature are surveyed. Table 6-1 summarizes the result of the survey. Sections 6.2, 6.3 and 6.4 discuss the tentative conclusions and recommendation for the three major areas of wind shear; fronts, thunderstorms and neutral and stable boundary layers, respectively. Section 6.5 describes the turbulence models to be used in establishing the primitive turbulent wind shear profiles and Section 6.6 discusses application of the models to simulator operations.

6.2 Fronts

The search for data sources from which mathematical models of wind shear can be established for synoptic scale warm and cold fronts is still being carried out. Data from the 500 m tower at NSSL/NOAA Laboratories in Norman, Oklahoma have been measured and these measurements are currently being reduced to a format similar to that given by Goff [4-2] for thunderstorm gust fronts, see Figure 4-10. It is expected that these data will be available by April, 1977 and they will be tabulated and used with a computer lookup routine as described in Section 6.3 for thunderstorm gust front data.

TABLE 6-1

SUMMARY OF LITERATURE SURVEY

Fronts

(a) 2- and 3-dimensional wind shear or data models are unavailable at this time.
(b) 1-dimensional profiles of wind speed variation with height are available from rawinsonde and jimsphere measurements, but these lack the necessary detail, below 500 m, to develop mathematical expressions for computer simulations.

Thunderstorm Gust Fronts

(a) 3-dimensional wind speed models or data are unavailable.
(b) (i) 2-dimensional, spatial cross sections of isotach measured from high towers (preferably 500 m) and converted to spatial coordinates by Taylor's hypothesis provide the most useful data currently available for wind shear modelling, see Figures 4-10 and 4-11.
(ii) 2-dimensional numerical models, see Reference 4-11, require too much computational time for simulation purposes and have not been validated.
(c) (i) 1-dimensional wind speed profiles, i.e., wind speed variation with altitude only, Equations 4-9 and 4-11 do not allow horizontal wind shear to be simulated. Current evidence suggests that horizontal wind shear excites the phugoid mode and can create instability, thus 1-dimensional equations cannot be used for meaningful simulation.
(ii) 1-dimensional equations of wind speed as a function of position along a specified glide slope (Equations 4.4 through 4.7) give erroneous results when aircraft depart from the glide slope. These equations are useful for determining control inputs required to maintain glide slope position but are not meaningful for simulation purposes.

Atmospheric Boundary Layers

(a) 3-dimensional models of the atmospheric boundary layer near the ground are dependent on terrain features and are indigenous to the terminal area. No complete model or source of wind shear data is available at this time to formulate 3-dimensional mathematical expressions for simulation purposes of even simple terrain features, such as buildings, hills, patches of trees, etc.
(b) 2-dimensional wind speed models which include horizontal or lateral shear are also indigenous to the terminal area. Approximate formulation of wind speed distribution for certain individual terrain features such as discontinuities in surface roughness, see Figures 5-13, 14 and 15 and Equation 5.45, irregularly spaced patches of different terrain features, see Figure 5-17 and Reference [5-37], sea breezes, see References [5-38, 39, 40], and heat islands, see References [5-24, 40, 41] can be estimated at this time.
(c) (i) 1-dimensional models of wind speed variation with height are numerous. Figures 5-5 and 5-6 which are averaged plots of approximate 1,000 measured wind speeds and which include stable, neutral and unstable conditions appear as the most complete data set for formulating wind speed profiles for simulation purposes. These data encompass the barotropic turning layer, i.e. variations with height of both the longitudinal wind component, W_x, and the lateral wind component, W_y.
(ii) 1-dimensional models of wind speed as a function of height for the baroclinic turning layer have been numerically modeled, see Figure 5-11 and Reference [5-12, 22]. The strongest directional shears occur under baroclinic conditions but further research is required to establish which profiles, such as those shown in Figure 5-11, are realistic.
(iii) 1-dimensional model of wind speed variation with height to 150 m (492 ft), without turning, i.e., longitudinal wind component, W_x, only, are given for:
(1) very stable conditions by Equation 5.24
(2) stable conditions by Equation 5.21
(3) neutral conditions by Equation 5.20
(4) unstable conditions by Equation 5.22

6.3 Thunderstorm Gust Front

The most extensive thunderstorm gust front data for formulating detailed wind speed profiles are those measured by Goff [4-2] in the form of cross sections of lines of constant vertical, W_z, longitudinal, W_x, and lateral, W_y, wind speed components through the thunderstorm parallel to its mean motion. Tabulating these data on a grid and utilizing a computer lookup routine allows the wind speed to be predicted at any horizontal and vertical position called for by the simulator control program.

The range of data is 500 m in vertical and 3,321 m-11,685 m in horizontal extent, depending on the data set considered. Twenty data sets are available and have been punched on computer cards for the table-lookup routine. Figure 6-1 illustrates the grid system superimposed on the wind field. Tabulated values of wind speed for the 20 thunderstorm gust front cases are given in the appendix in Tables A-1 to A-20.

The vertical grid spacing is the same for all tables, however, the horizontal grid spacing varies according to the length of record available. The vertical grid spacing DZ and horizontal grid spacing DX are listed in meters at the upper right=hand corner of the table. Each data set has 11 nodes in the vertical and 41 nodes in the horizontal; not all nodes are shown on Figure 6-1. Thus for example, the horizontal spatial extent of the record in Table A-1 is 40 x 100 m = 4000 m whereas in Table A-7 it is 40 x 196 m = 7840 m.

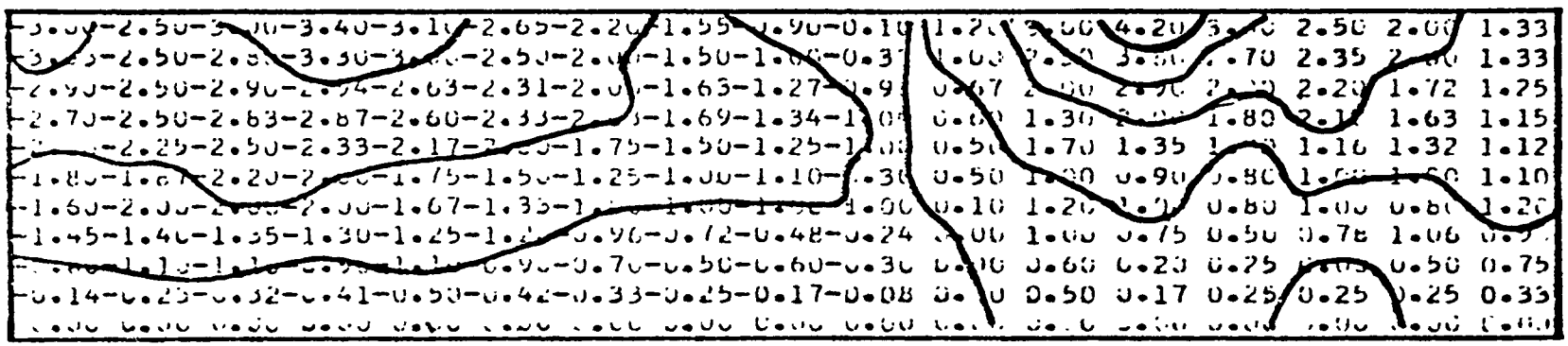

FIGURE 6-1 VERTICAL VELOCITY CONTOUR GIVEN BY GOFF [4-2] COMPARED WITH TABULATED VALUES FOR COMPUTER LOOK-UP GRID SYSTEM.

Figure 6-2 shows the flight path of an airplane characteristic of a DC-8 landing with fixed controls through the thunderstorm. Figure 6-3 gives the wind speed encountered by the airplane during descent. The wind speeds encountered are seen to have a very complex profile indicating that mathematical formulations of gust fronts which express the wind speed only as a function of elevation, such as Equations 4.9, 4.10, and 4.4 through 4.7 cannot provide realistic simulations.

In principle, three-dimensional wind fields are required to give meaningful simulations, but these data are not available. Thus, simulation of flight across the direction of travel of the storm is not at this time possible. Note that all cross section given by Goff [4-2] are in planes parallel to the direction of travel of the storm and any simulation employing these data assumes the aircraft is flying either toward or away from the storm along the direction of its mean motion. Work is continuing to provide estimates of three-dimensional gust fronts from Goff's data [4-2].

Developing the statistics to provide risk of exceedance criteria promises considerable difficulty. The approach envisioned at this time will first attempt to establish a common point on all 20 storm cases such as the location of the gust front. Second, the mean wind speed for all 20 cases will be computed at corresponding grid points relative to the common point. Third, the standard deviation about

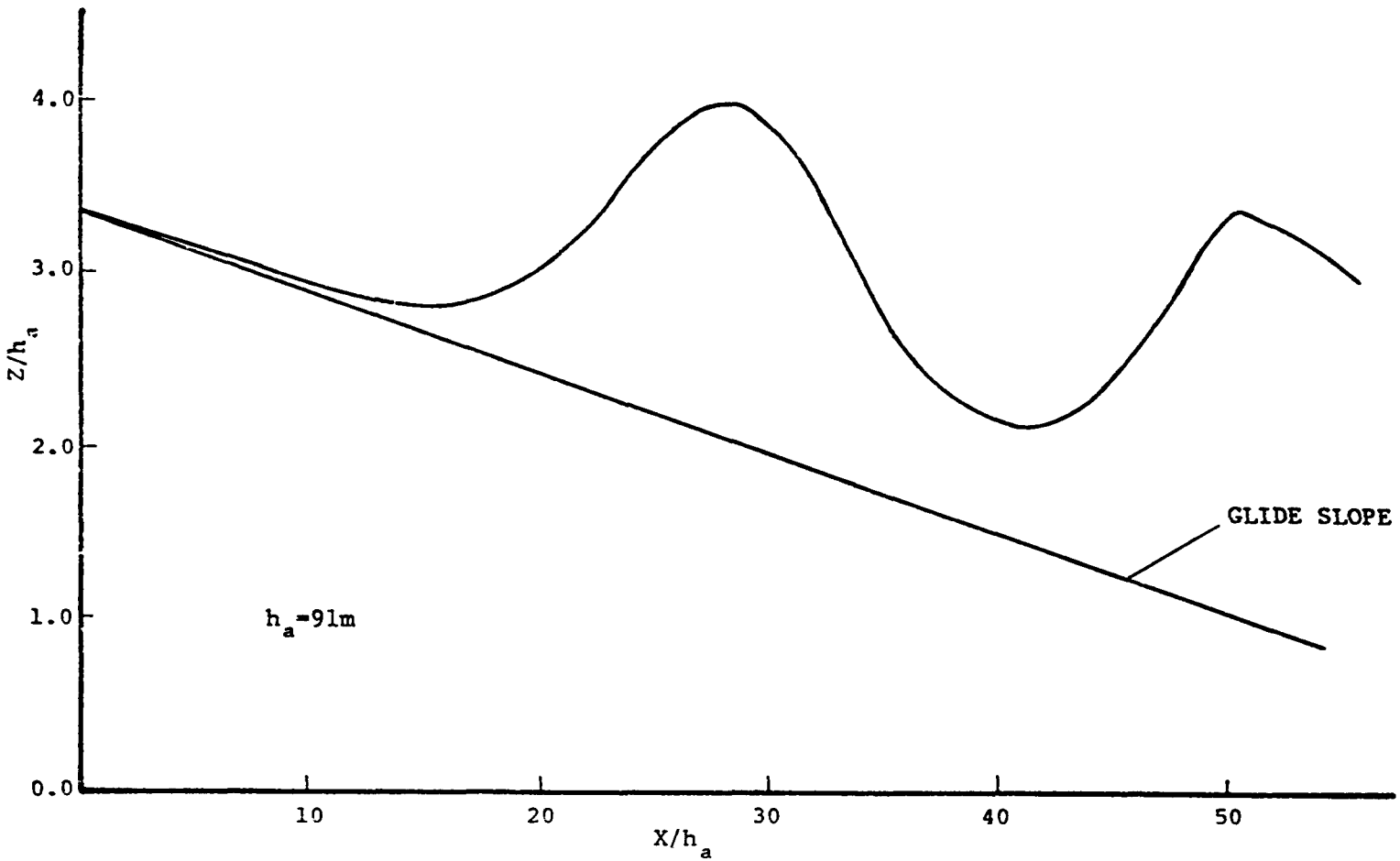

FIGURE 6-2 COMPUTERIZED FLIGHT PATH OF AIRCRAFT CHARACTERISTIC OF D C 8 THROUGH CASE 9 THUNDERSTORM

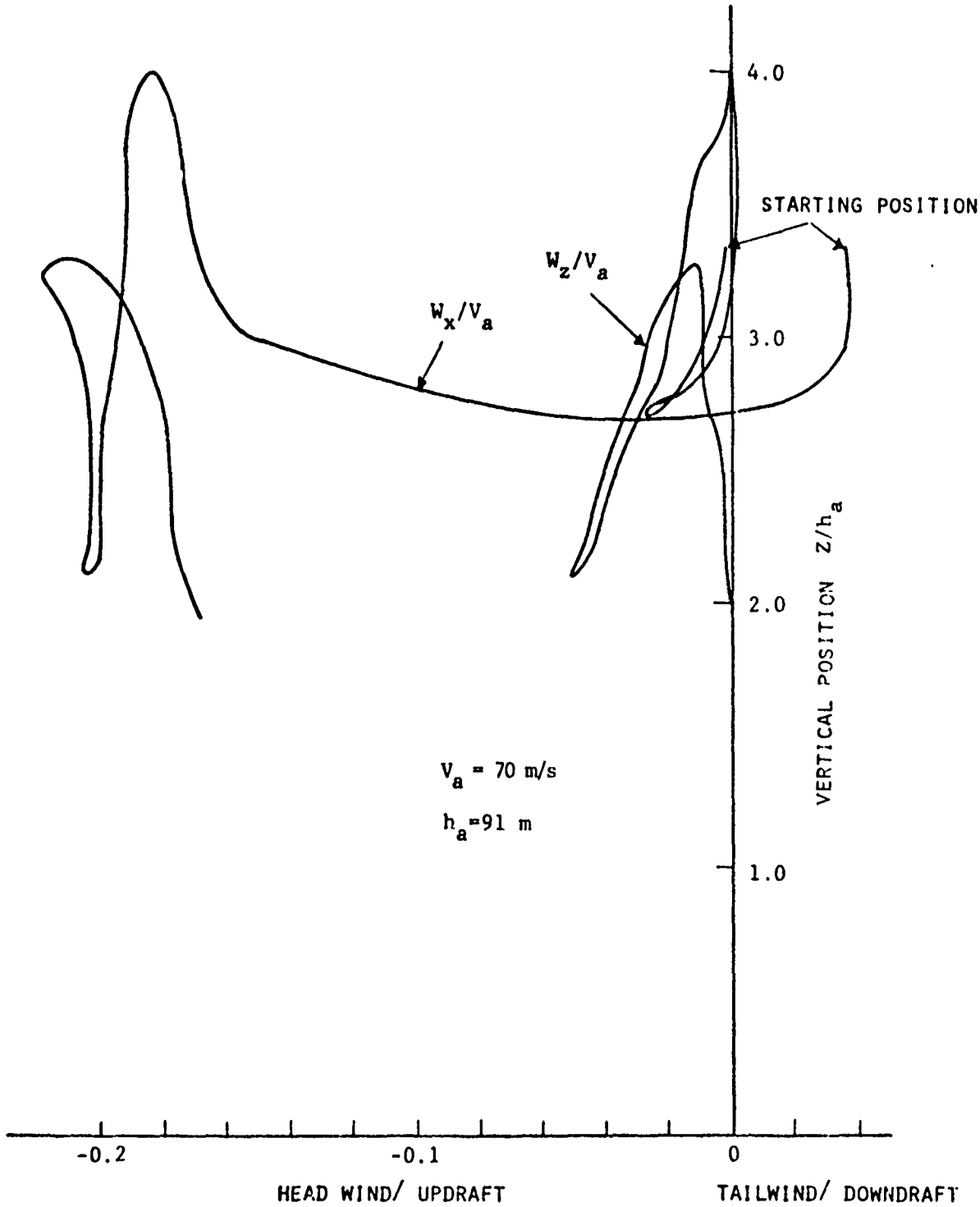

FIGURE 6-3 WIND "SEEN" BY DC-8 LANDING WITH FIXED CONTROLS IN CASE 9 THUNDERSTORM

the mean with the assumption of normality will be used to estimate the probability of exceeding a prescribed wind speed or wind shear at each grid point.

6.4 Atmospheric Boundary Layer

The data of Clarke and Hess [5-16] from Figures 5-5 and 5-6 have been tabulated in Table 6-2 as a function of dimensionless height $\hat{z} = fz/u_*$ and stability parameter $\mu = ku_*/fL$. Coupled with a computer lookup scheme the longitudinal, W_x, and lateral, W_y, components of wind speed can be determined for dimensionless heights of $0 \leq \hat{z} \leq 0.15$ and for given atmospheric stability conditions of $-300 \leq \mu \leq 200$. The range in physical height, z, of the data is dependent on the latitude through the Coriolis parameter, f, and the friction velocity, u_*. For typical values of $u_* \approx 10^{-4}s^{-1}$, z ranges from 0 to 750 m.

Wind speed profiles generated by the computer lookup scheme are shown in Figures 6-4 and 6-5. Note that the strongest speed shear occurs under very stable conditions, $\mu = 200$, but the strongest directional shear occurs under intermediately stable conditions, $\mu = 50$.

Actually, the strongest directional shear occurs under baroclinic conditions. A computer code for computing wind speed profiles under baroclinic conditions where the synoptic pressure gradients vary linearly with height [5-22] is programmed. Realistic magnitudes for the rates of variation, however, are being justified before meaningful wind speed profiles can be presented for simulation work.

TABLE 6-2

LONGITUDINAL AND LATERAL WIND COMPONENTS AS A FUNCTION OF DIMENSIONLESS HEIGHT Z AND STABILITY μ

W_x/u_*

$\hat{z}/\mu$	1	3	5	7	9	11	13	15	17	19	21	23	25	27	29	31	33
11	23.0	23.0	23.0	23.0	23.0	23.0	23.0	23.0	23.0	23.0	35.5	48.0	60.0	73.0	79.0	82.0	87.0
10	23.0	23.0	23.0	23.0	23.0	23.0	23.0	23.0	23.0	23.0	35.5	48.0	60.0	73.0	78.8	81.2	86.2
9	23.0	23.0	23.0	23.0	23.0	23.0	22.9	22.8	23.0	23.0	35.5	48.0	60.0	73.0	78.0	80.3	85.3
8	23.0	23.0	23.0	23.0	23.0	23.0	22.5	22.5	23.0	23.0	35.5	48.0	60.0	73.0	77.0	79.5	84.2
7	23.0	23.0	23.0	23.0	23.0	22.9	22.0	22.0	23.0	23.0	35.5	48.0	60.0	72.1	76.2	78.5	83.0
6	23.0	23.0	23.0	23.0	23.0	22.4	21.6	21.5	22.3	23.0	35.5	48.0	59.5	70.0	74.8	77.0	81.0
5	23.0	23.0	23.0	23.0	23.0	21.9	20.8	20.8	21.5	23.0	35.5	48.0	57.0	68.0	72.0	74.2	78.7
4	23.0	23.0	23.0	23.0	22.0	20.7	20.1	20.1	20.3	20.5	32.5	43.5	54.0	65.0	69.2	71.1	74.2
3	23.0	23.0	23.0	22.0	20.8	19.8	19.3	19.2	19.2	18.5	29.5	40.0	50.0	58.0	61.0	63.7	66.5
2	22.5	22.5	22.2	21.3	20.5	19.5	18.7	18.0	17.0	15.5	26.5	34.7	35.0	43.0	49.0	52.0	57.0
1	21.5	20.5	20.2	19.8	19.5	18.7	17.9	17.0	16.0	14.0	16.5	14.0	17.0	23.0	26.0	28.0	33.0

W_z/u_*

$\hat{z}/\mu$	1	3	5	7	9	11	13	15	17	19	21	23	25	27	29	31	33
11	0.8	1.2	1.5	1.8	2.3	2.8	3.3	4.0	4.7	7.8	18.0	26.5	31.0	28.0	25.0	21.0	15.0
10	0.8	1.2	1.5	2.0	2.4	3.1	3.8	4.5	5.3	8.5	18.8	27.5	32.3	29.5	26.5	22.0	16.0
9	0.8	1.2	1.6	2.0	2.6	3.2	3.9	4.7	5.5	8.6	19.0	28.8	33.6	30.8	27.7	23.5	17.2
8	0.8	1.2	1.6	2.1	2.6	3.3	4.0	4.8	5.6	9.1	20.0	30.1	35.6	33.0	29.8	25.2	18.6
7	0.8	1.2	1.6	2.1	2.8	3.4	4.1	5.0	6.2	10.3	21.5	31.5	38.0	35.5	32.0	27.0	19.5
6	0.8	1.2	1.7	2.2	2.8	3.5	4.3	5.5	7.2	11.0	23.0	34.5	41.2	38.0	34.0	29.0	20.5
5	0.8	1.3	1.8	2.4	3.0	3.8	4.9	6.5	7.7	11.8	25.5	38.5	44.0	42.0	37.0	31.0	22.8
4	0.8	1.5	2.1	2.6	3.4	4.3	5.3	7.0	8.4	12.8	28.0	41.5	48.0	45.5	40.0	33.0	25.0
3	1.1	1.7	2.4	3.3	3.8	4.8	5.9	7.2	8.7	14.8	30.6	44.0	52.0	49.5	45.0	36.0	27.5
2	1.3	2.0	2.7	3.4	4.1	5.3	6.3	7.6	9.2	15.0	33.0	48.5	56.0	53.0	47.5	39.0	29.0
1	1.6	2.3	3.0	3.7	4.5	5.5	6.7	8.0	9.3	15.5	36.0	53.0	62.0	56.0	50.0	42.0	30.0

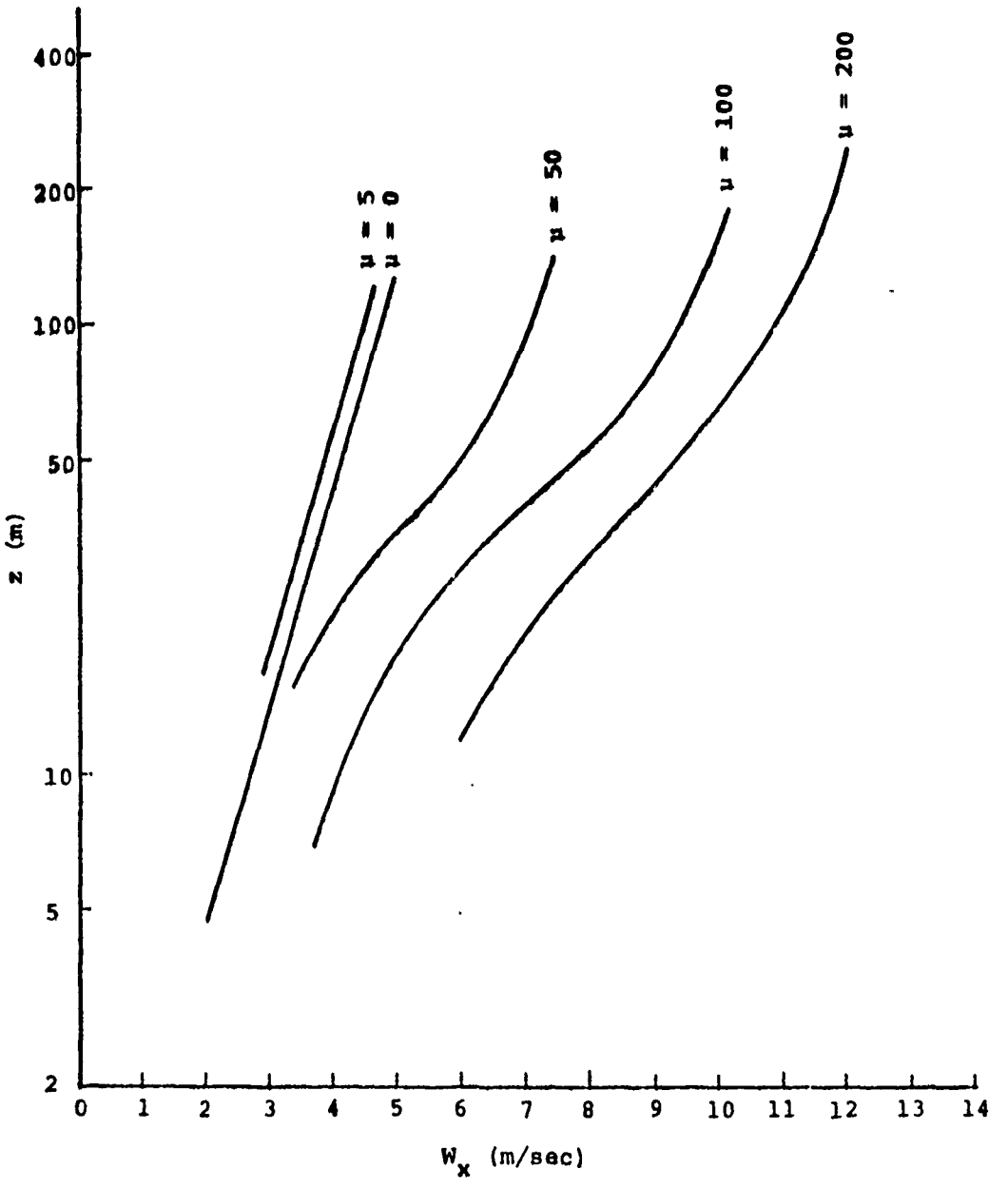

FIGURE 6.4 LONGITUDINAL WIND COMPONENT

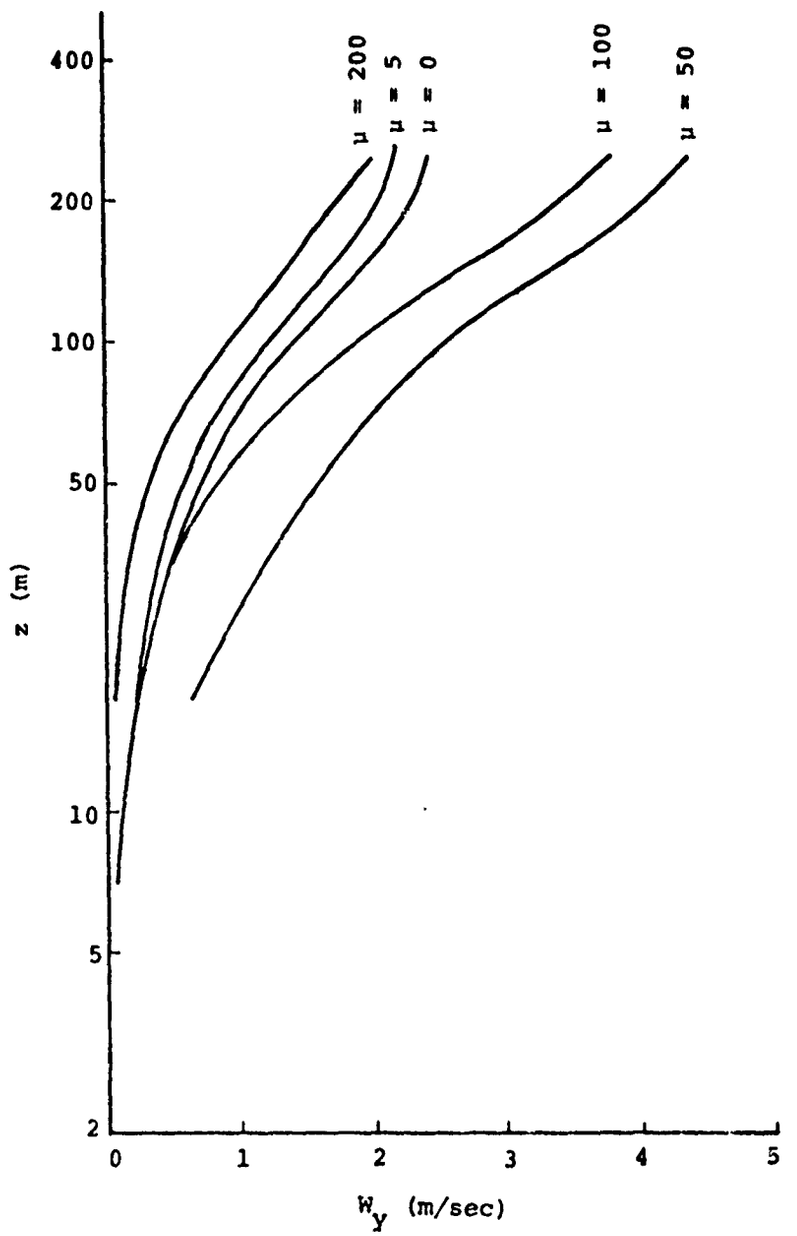

FIGURE 6.5 LATERAL WIND COMPONENT

Horizontal wind shear for the atmospheric boundary layer models is not being considered in this program. Figure 5-16 suggests that horizontal shear resulting from terrain features diffuse rather rapidly and should not cause significant effect above elevations of approximately 25 m. Under high wind conditions, however, these low level wind shears due to vortices or recirculation zones near buildings and other obstructions to the surface wind may create hazardous flight conditions. This is an area where a follow on effort to establish mathematical models of hazardous wind conditions for simulation of flight near building is needed.

Risk of exceedance predictions for the atmospheric boundary layer require establishing the probability of a given value of μ. Figure 6-6 from [5-16] provides some insight in this regard. The figure shows a 40 day average of the daily variation of μ with two standard deviation error bands. Assuming a Gaussian distribution, the probability of exceeding a given value of μ can be estimated. This curve is, of course, highly sensitive to location and further research is required to establish a more general daily variation in atmospheric stability.

6.5 Turbulence Models

The primitive turbulent wind speed profiles will be generated by superimposing a randomly generated turbulence signal on the steady-state wind speed. The review of the

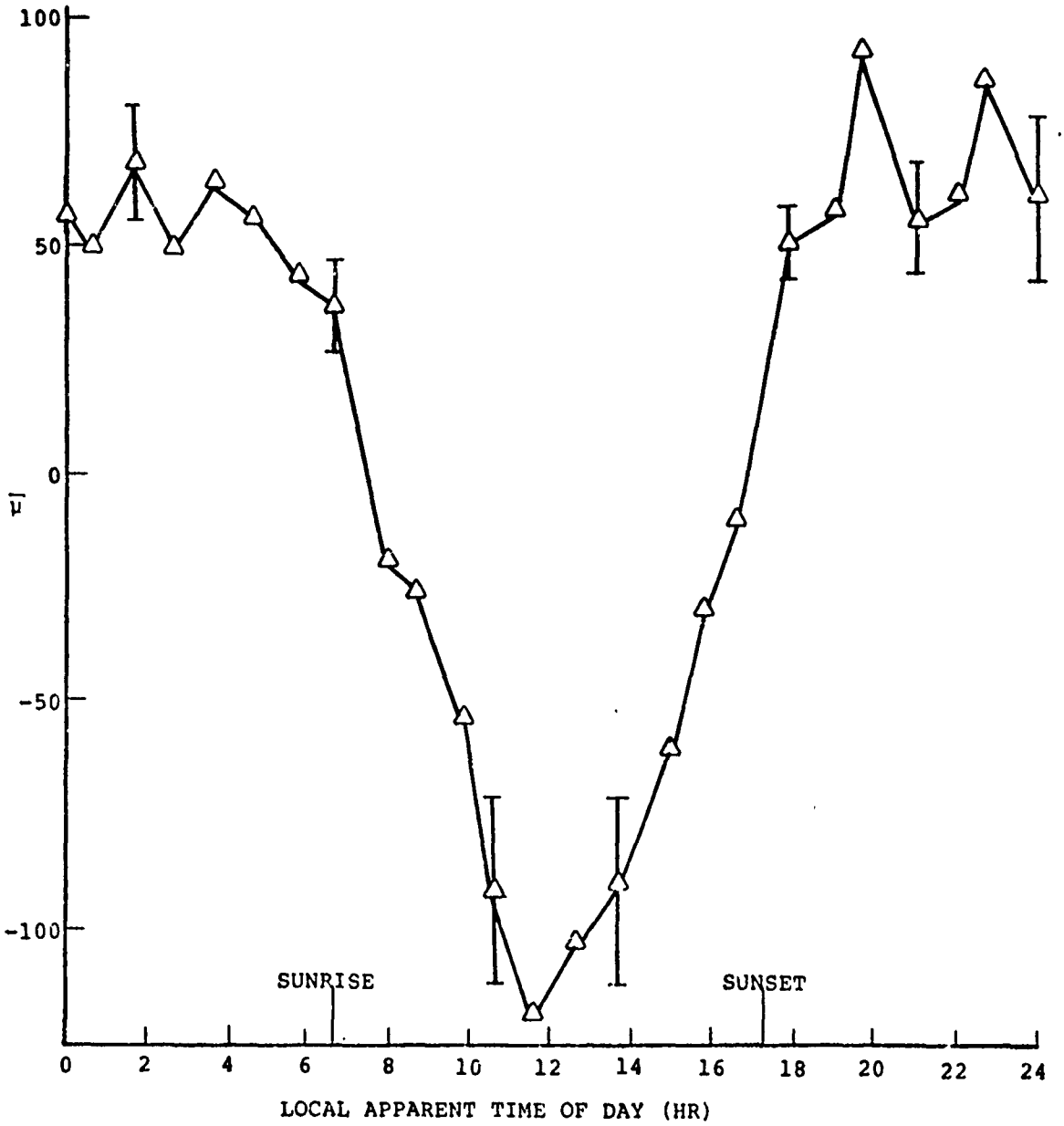

FIGURE 6-6 VARIATION OF $\bar{\mu}$ WITH TIME OF DAY [5-16].

literature pertaining to turbulence model is not included in this interim report, however, the reader is referred to [6-1 through 7] for information on current models.

The development of a realistic turbulence model depends primarily on knowledge of the appropriate turbulence energy spectra. For atmospheric boundary layers, well established turbulence spectra are given in [5-2, 5, 6 and 6-8] and turbulence simulation in these cases is straightforward. For turbulence simulation in thunderstorms, spectra are still in the development stage. In fact, thunderstorm turbulence is neither statistically stationary nor homogeneous and superimposing a turbulent component of wind on the quasi-steady state values given in Tables A-1 through A-20 may not be realistic. However, in lieu of a more reliable method, this approach will be employed until the state of the art in thunderstorm turbulence modelling is improved.

6.6 Flight Simulator Applications

Mathematical models for programming simulators to respond to fronts are not ready at this time. Models for steady-state thunderstorm gust fronts, as described in Section 6.3, and for atmospheric boundary layers, as described in Section 6.4, are available as computer lookup routines which are ready for immediate application. Additional work is required to increase the sophistication of the models to include turbulence and a statement relative to the risk of encountering a specific wind shear.

The thunderstorm gust front model consists of 20 separate data sets. The suggested application of these data to programs for evaluating visual displays, for testing avionics, for verifying operational procedures or for designing control systems where a pilot poll is taken as the evaluation criteria, is as follows. Each pilot should "fly" as many of the wind shear cases as desired, say, 10 to 20 cases, in a prescribed order. The pilots would be unable to learn the wind shear encountered as each one would be different, however, the experimental sampling would be consistent in that every member of the team would experience the exact same sequence of wind shears.

A similar procedure can be carried out with the atmospheric boundary layer model. In this case, a matrix of μ values would be established prior to the experiment and the simulator would be programmed to accept these in a specified sequence. The selection of values for μ can be guided by the data in Figure 6-6.

It should be cautioned that the present data decks are not likely to include the extreme wind shear that might be encountered once in a lifetime. The ability to simulate extremes is contingent on developing the risk of exceedance statistics which are currently under investigation.

Real time simulations are easily achieved with the computer lookup routines since interpolation between tabulated values requires only milliseconds of machine time. Moreover, data card decks are easily incorporated into

simulator program logic [6-9, 10] and thus facilitate application to existing simulator programs.

6.7 Conclusion

Efforts are continuing to develop simulation models of detailed wind shear profiles in large-scale frontal motions, to establish meaningful turbulence spectra for thunderstorms and to establish risk of exceedance criteria based on valid statistics of extreme wind shears. Models of quasi steady-state wind shear for thunderstorm gust fronts and atmospheric boundary layers are completed and ready for immediate application in wind shear hazard/flight simulation studies.

APPENDIX A

TABLE A-1

W_x (m/s) CASE 1 DX = 100.00 DZ = 50.00

Node Points	1	3	5	7	9	11	13	15	17	19	21	23	25	27	29	31	33	35	37	39	41
11	4.1	4.1	8.1	7.8	5.8	4.0	5.7	6.3	6.0	6.6	7.5	8.1	7.1	4.1	2.8	1.1	-0.9	-1.9	-1.8	-2.2	-2.1
10	5.1	4.1	8.0	8.2	5.8	4.2	5.5	6.3	6.0	6.6	7.6	8.2	8.1	5.1	3.1	1.1	-0.4	-0.8	-0.7	-1.6	-1.8
9	6.1	5.1	6.8	8.1	5.7	5.0	5.8	6.4	6.1	6.9	7.7	8.2	8.1	6.1	4.1	2.0	0.3	0.1	0.3	-1.1	-0.8
8	6.5	6.1	6.8	8.1	5.8	5.3	5.9	6.4	6.7	6.9	7.8	8.6	8.5	7.1	5.1	3.1	1.6	1.1	1.2	-0.4	-0.3
7	7.0	6.3	6.3	8.1	6.1	6.1	6.1	6.6	6.5	7.3	8.0	8.7	8.7	7.5	6.1	4.0	2.1	2.0	2.1	0.2	0.2
6	6.9	6.4	6.2	8.0	6.5	6.4	6.4	6.9	7.3	7.8	8.4	9.0	8.9	8.0	5.4	4.1	3.5	2.8	2.6	1.8	1.1
5	6.8	6.5	7.2	8.0	7.6	7.2	6.8	6.9	7.4	7.9	8.6	9.4	9.2	8.1	6.8	5.4	4.1	3.6	3.1	2.3	1.4
4	6.1	6.8	7.5	7.8	7.5	7.2	6.9	7.0	7.5	8.0	9.0	10.1	9.3	8.2	7.2	6.1	5.1	4.1	4.1	3.1	1.9
3	6.0	6.6	7.3	8.0	7.7	7.4	7.2	6.9	7.5	8.1	9.3	10.2	9.8	8.5	7.5	6.8	6.1	5.4	4.8	4.1	4.1
2	5.9	6.5	7.3	8.1	8.1	7.7	7.3	6.9	7.6	8.2	9.5	10.2	10.1	8.3	7.7	7.2	6.6	6.1	5.1	4.1	3.1
1	5.8	6.1	7.1	8.1	8.2	7.9	7.4	7.0	7.7	8.7	10.1	10.3	10.1	8.6	7.7	7.2	6.8	6.3	5.7	4.9	4.1

W_z (m/s)

Node Points	1	3	5	7	9	11	13	15	17	19	21	23	25	27	29	31	33	35	37	39	41
11	-0.5	-2.4	-3.0	-2.5	-3.0	-3.4	-3.1	-2.6	-2.2	-1.5	-0.9	-0.1	1.2	3.0	4.2	3.0	2.5	2.0	1.3	0.8	0.3
10	-0.5	-2.4	-3.0	-2.5	-2.8	-3.3	-3.0	-2.5	-2.0	-1.5	-1.0	-0.3	1.0	2.5	3.8	2.7	2.3	2.0	1.3	0.8	0.3
9	-0.5	-2.2	-2.9	-2.5	-2.9	-2.9	-2.6	-2.3	-2.0	-1.6	-1.3	-0.9	0.7	2.0	2.9	2.0	2.2	1.7	1.3	0.8	0.3
8	-0.5	-2.0	-2.7	-2.5	-2.8	-2.9	-2.6	-2.3	-2.0	-1.7	-1.3	-1.0	0.6	1.3	2.0	1.8	2.1	1.6	1.1	0.7	0.2
7	0.0	-2.3	-2.0	-2.3	-2.5	-2.3	-2.2	-2.0	-1.8	-1.5	-1.3	-1.0	0.5	1.7	1.3	1.0	1.2	1.3	1.1	0.5	0.0
6	0.0	-2.0	-1.8	-1.9	-2.2	-2.0	-1.8	-1.5	-1.3	-1.0	-1.1	-0.3	0.5	1.0	0.9	0.8	1.0	1.0	1.1	0.5	0.0
5	0.0	-1.2	-1.6	-2.0	-2.0	-2.0	-1.7	-1.3	-1.0	-1.0	-1.0	-1.0	0.1	1.2	1.0	0.8	1.0	0.8	1.2	0.6	0.0
4	0.0	-1.5	-1.4	-1.4	-1.3	-1.3	-1.3	-1.2	-1.0	-0.7	-0.5	-0.2	0.0	1.0	0.8	0.5	0.8	1.1	0.9	0.3	0.0
3	0.5	-0.9	-0.8	-1.1	-1.1	-0.9	-1.1	-0.9	-0.7	-0.5	-0.6	-0.3	0.0	0.6	0.2	0.3	0.0	0.5	0.8	0.3	0.0
2	0.5	-0.0	-0.1	-0.2	-0.3	-0.4	-0.5	-0.4	-0.3	-0.3	-0.2	-0.1	0.0	0.5	0.2	0.3	0.3	0.3	0.3	0.0	0.0
1	0.0	0.0	0.0	0.0	0.0	0.0	0.0	0.0	0.0	0.0	0.0	0.0	0.0	0.0	0.0	0.0	0.0	0.0	0.0	0.0	0.0

TABLE A-2

W_x (m/s) CASE 2 DX = 81.97 DZ = 90.00

Node Points	1	3	5	7	9	11	13	15	17	19	21	23	25	27	29	31	33	35	37	39	41
11	4.5	7.3	8.0	8.4	9.1	10.0	8.8	7.1	5.0	2.7	2.0	1.0	0.4	-0.2	-1.1	-1.9	-2.8	-2.9	-3.0	-3.3	-3.7
10	4.6	7.3	8.3	8.8	9.0	9.5	9.0	7.6	5.8	3.0	2.2	1.4	0.7	0.0	-1.0	-1.8	-2.4	-2.9	-3.3	-3.4	-3.5
9	4.6	7.3	8.6	9.0	9.7	11.0	8.8	7.8	7.0	5.0	3.0	1.9	1.0	0.0	-0.9	-1.8	-3.1	-3.2	-3.3	-3.3	-3.4
8	4.6	7.4	9.1	9.3	10.1	10.5	9.3	7.9	7.5	5.5	5.0	2.5	1.0	0.3	-0.6	-1.7	-3.0	-3.1	-3.3	-3.4	-3.5
7	4.7	7.8	9.5	9.8	10.1	11.0	9.0	9.0	9.0	9.0	6.5	3.0	1.8	1.0	0.2	-1.0	-2.0	-3.0	-3.5	-4.0	-3.4
6	4.7	8.0	10.0	10.6	10.3	10.2	10.1	10.1	10.2	9.8	8.0	5.0	2.2	1.7	0.7	-0.5	-1.5	-2.3	-3.0	-3.1	-3.3
5	4.9	9.0	10.5	11.0	11.0	11.6	11.4	11.1	11.1	11.0	9.0	6.0	3.0	2.1	1.0	0.2	-2.0	-2.3	-2.6	-2.8	-3.0
4	5.0	9.0	11.3	11.3	11.0	12.0	11.3	11.1	11.4	10.5	9.0	7.0	4.5	2.6	1.9	0.6	-0.4	-1.3	-2.2	-3.2	-2.9
3	5.5	10.5	11.6	11.0	10.0	10.7	11.2	11.5	11.3	11.0	9.0	7.3	5.4	3.7	2.8	1.3	-0.2	-0.8	-1.8	-3.2	-2.2
2	6.4	12.0	12.5	11.3	9.5	11.0	11.4	11.2	11.1	9.5	7.0	7.2	5.8	5.0	4.6	2.0	0.5	-0.5	-1.7	-3.2	-2.4
1	7.0	13.2	13.0	11.3	9.4	9.8	11.5	11.0	8.8	6.5	7.5	7.3	6.0	6.2	6.4	3.0	0.2	-0.4	-1.6	-3.3	-2.5

W_z (m/s)

Node Points	1	3	5	7	9	11	13	15	17	19	21	23	25	27	29	31	33	35	37	39	41
11	-1.8	-1.5	-1.2	-0.8	-0.3	0.6	1.0	1.0	1.5	2.8	4.0	4.1	4.3	4.2	4.1	3.8	3.5	3.2	2.7	2.0	0.6
10	-1.8	-1.5	-1.2	-0.9	-0.8	0.9	0.6	0.7	1.3	2.4	3.3	4.0	4.0	4.0	4.0	3.6	3.3	2.9	2.6	2.0	0.6
9	-1.6	-1.2	-1.1	0.0	-1.0	0.6	0.0	0.2	1.3	2.0	2.5	3.0	3.5	3.3	3.2	3.0	2.8	2.6	2.4	1.5	0.7
8	-1.5	-1.2	-1.1	0.1	0.0	0.1	0.1	-0.0	1.0	1.8	2.1	2.3	2.6	2.8	3.0	2.8	2.6	2.2	2.1	1.6	0.8
7	-1.5	-1.0	-1.0	0.3	0.3	0.2	-0.0	-0.1	1.1	1.5	1.8	2.1	2.4	2.8	2.8	2.6	2.4	2.2	2.0	1.6	0.8
6	-1.5	-1.0	-0.4	-0.1	-0.0	-0.1	-0.2	-0.1	0.5	1.4	1.6	1.8	2.0	1.9	1.8	1.7	1.7	1.6	1.5	1.4	0.8
5	-1.3	-0.9	-0.3	0.5	0.5	-0.1	-0.3	-0.1	1.0	1.2	1.4	1.5	1.7	1.9	2.0	2.0	2.0	2.0	1.6	1.2	0.8
4	-1.1	-0.8	-0.3	0.5	0.4	-0.2	-0.5	-0.2	0.5	1.0	1.0	1.0	1.0	1.0	1.0	1.0	1.0	1.0	1.1	1.1	0.7
3	-1.0	-0.7	-0.2	0.1	0.0	-0.3	-0.6	-0.2	0.4	0.9	0.9	0.9	0.9	0.9	0.9	1.0	1.0	1.0	1.0	1.0	0.8
2	-0.9	-0.7	-0.2	0.3	0.1	-0.7	-0.8	-0.3	0.3	0.4	0.4	0.4	0.5	0.5	0.5	0.5	0.5	0.4	0.4	0.4	0.2
1	0.0	0.0	0.0	0.0	0.0	0.0	0.0	0.0	0.0	0.0	0.0	0.0	0.0	0.0	0.0	0.0	0.0	0.0	0.0	0.0	0.0

TABLE A-3

W_x (m/s) CASE 3 DX = 142.86 DZ = 50.00

Node Points	1	3	5	7	9	11	13	15	17	19	21	23	25	27	29	31	33	35	37	39	41
11	12.1	12.6	12.8	13.0	12.9	12.8	12.8	12.9	13.1	12.7	11.5	9.4	5.6	2.7	2.4	2.2	1.9	1.4	0.9	0.8	0.6
10	12.2	12.7	12.8	12.9	12.7	12.6	12.6	12.7	12.9	12.8	11.8	10.2	6.4	3.4	2.5	2.3	1.8	1.4	0.9	0.7	0.5
9	12.3	12.9	12.9	12.7	12.4	12.1	11.9	12.4	12.9	12.5	12.1	10.6	6.6	4.1	3.1	2.4	2.1	1.5	0.9	0.5	0.3
8	12.4	12.9	12.7	12.6	12.0	11.5	12.0	12.5	12.6	12.8	11.9	10.7	7.8	4.4	3.3	2.6	2.0	1.4	0.7	0.3	0.2
7	12.3	12.7	12.8	12.1	11.4	11.3	11.3	11.9	12.6	12.7	12.2	11.0	8.6	5.5	3.9	2.9	2.2	1.9	0.8	0.4	0.1
6	12.0	12.6	12.6	11.7	11.0	10.7	10.9	11.5	12.0	12.4	12.2	11.3	9.5	6.4	4.4	3.3	2.4	1.8	1.1	0.6	0.1
5	11.3	11.5	11.4	11.0	10.6	10.6	10.9	11.5	11.6	11.8	11.9	11.2	10.6	7.6	5.2	3.7	2.6	1.8	1.2	0.7	0.2
4	10.8	11.2	11.0	10.5	9.8	10.3	10.8	11.2	11.4	11.3	11.3	11.0	10.8	8.6	5.6	3.9	2.8	1.8	0.8	0.6	0.3
3	8.8	10.1	10.6	9.9	9.3	10.2	10.6	10.7	10.9	11.2	11.2	10.8	10.5	9.0	6.2	4.2	3.1	2.1	1.1	0.5	0.4
2	7.6	8.6	7.8	8.2	8.6	10.0	10.7	10.6	10.5	10.4	10.5	10.6	10.5	9.0	6.6	4.3	3.0	2.1	1.4	0.8	0.5
1	7.3	7.8	7.3	6.9	7.4	9.9	10.8	10.3	10.4	10.6	10.6	10.4	10.2	9.1	7.0	4.6	3.1	2.0	1.6	1.2	0.8

W_z (m/s)

Node Points	1	3	5	7	9	11	13	15	17	19	21	23	25	27	29	31	33	35	37	39	41
11	-1.2	-1.3	-1.3	-1.3	-1.5	-1.9	-2.0	-2.2	-1.8	-1.0	-0.6	0.1	3.0	4.0	3.0	1.7	1.0	0.8	0.7	0.5	0.3
10	-1.0	-1.1	-1.2	-1.3	-1.5	-1.8	-2.1	-2.0	-1.6	-0.9	-0.4	0.1	2.0	4.0	2.4	1.5	1.0	0.8	0.6	0.4	0.3
9	-1.0	-1.0	-1.1	-1.0	-1.2	-1.5	-1.9	-1.4	-1.0	-0.8	-0.5	0.0	1.2	3.4	2.3	1.3	0.9	0.7	0.5	0.4	0.2
8	-0.9	-1.1	-1.0	-0.9	-0.9	-1.2	-1.3	-1.1	-0.8	-0.5	-0.4	-0.2	1.0	3.0	2.1	1.1	0.9	0.7	0.5	0.3	0.1
7	-0.8	-0.9	-0.9	-0.8	-0.9	-1.0	-1.1	-0.8	-0.5	-0.5	-0.5	-0.2	0.5	2.4	2.9	0.9	0.8	0.6	0.4	0.3	0.1
6	-0.8	-0.8	-0.8	-0.7	-0.6	-0.8	-0.9	-0.6	-0.3	0.0	-0.4	-0.4	0.0	2.0	1.4	1.0	0.8	0.6	0.4	0.7	1.0
5	-0.6	-0.6	-0.7	-0.5	-0.5	-0.6	-0.7	-0.4	-0.0	-0.2	-0.4	-0.3	0.2	1.2	1.5	0.9	0.7	0.5	0.4	0.2	-0.0
4	-0.6	-0.6	-0.4	-0.3	-0.3	-0.5	-0.6	-0.3	0.0	-0.0	-0.2	-0.4	0.3	1.0	1.1	0.9	0.7	0.5	0.3	0.1	-0.1
3	-0.6	-0.4	-0.3	-0.2	-0.0	-0.3	-0.5	-0.3	0.0	0.0	-0.3	-0.5	-0.2	0.5	0.9	0.8	0.6	0.5	0.3	0.1	-0.1
2	-0.5	-0.4	-0.3	-0.1	-0.1	-0.2	-0.4	-0.3	-0.1	0.0	-0.3	-0.5	-0.2	0.1	0.2	0.3	0.4	0.4	0.3	0.1	-0.1
1	0.0	0.0	0.0	0.0	0.0	0.0	0.0	0.0	0.0	0.0	0.0	0.0	0.0	0.0	0.0	0.0	0.0	0.0	0.0	0.0	0.0

TABLE A-4

W_x (m/s) CASE 4 DX = 192.31 DZ = 50.00

Node Points	1	3	5	7	9	11	13	15	17	19	21	23	25	27	29	31	33	35	37	39	41
11	14.1	15.1	15.6	15.6	15.6	15.4	15.1	14.9	14.7	14.4	14.2	13.9	13.7	9.7	1.8	0.3	-0.7	-1.3	-1.8	-2.4	-2.6
10	13.8	14.5	15.2	15.2	15.2	15.5	15.3	15.0	14.8	14.5	14.2	13.9	13.6	10.4	4.6	0.9	-0.5	-1.1	-1.6	-2.2	-2.6
9	13.7	14.6	15.5	15.5	15.6	15.5	15.4	15.3	15.2	14.8	14.5	14.1	13.9	10.3	3.6	1.6	-0.3	-0.9	-1.5	-2.1	-2.5
8	13.7	14.5	15.4	15.1	15.2	15.6	15.3	15.1	15.4	14.9	14.5	14.0	13.6	9.6	4.9	1.6	0.3	-0.7	-1.4	-2.1	-2.5
7	13.7	14.9	15.5	15.4	15.1	15.4	15.4	15.1	15.6	15.0	14.5	13.9	12.6	10.6	5.3	1.8	0.5	-0.6	-1.6	-2.2	-2.6
6	13.8	15.0	15.4	15.5	15.2	15.3	15.6	15.1	15.7	15.1	14.0	13.5	12.2	10.1	6.5	2.9	0.9	-0.4	-1.4	-2.3	-2.7
5	14.0	15.6	15.0	15.6	15.3	15.4	15.6	15.1	15.8	14.6	13.6	12.6	11.3	10.2	7.6	3.5	1.2	-0.3	-1.3	-2.3	-2.7
4	14.1	15.3	14.7	15.3	15.4	15.5	15.4	15.0	15.7	14.2	11.9	11.7	11.0	9.9	7.9	5.0	2.3	0.2	-1.1	-1.4	-2.7
3	15.8	12.7	13.8	14.1	15.4	13.6	13.6	13.6	14.5	12.6	11.3	11.6	9.8	9.6	8.3	5.6	3.6	1.6	-0.6	-1.5	-2.4
2	15.5	12.2	13.4	13.6	14.1	11.6	11.7	11.9	10.8	8.6	8.6	9.6	9.5	8.6	7.6	6.6	5.6	3.6	0.1	-0.7	-1.5
1	15.1	11.6	11.6	11.6	13.6	10.6	9.6	11.7	9.6	7.6	7.5	8.0	8.6	7.6	7.5	7.6	7.6	5.6	1.6	0.6	-0.4

W_z (m/s)

Node Points	1	3	5	7	9	11	13	15	17	19	21	23	25	27	29	31	33	35	37	39	41
11	1.1	1.2	1.1	1.0	0.9	1.2	1.0	0.9	1.1	1.2	1.4	1.2	1.0	1.9	5.1	5.0	3.3	2.0	1.5	1.0	0.6
10	1.1	1.2	1.2	1.1	0.9	1.1	1.0	0.9	1.1	1.2	1.3	1.2	1.1	1.5	4.5	4.4	3.0	2.2	1.4	0.8	0.5
9	1.0	1.3	1.3	1.1	0.9	1.1	1.0	0.8	1.1	1.2	1.1	1.1	1.0	1.3	4.1	3.9	2.9	1.8	1.2	0.8	0.5
8	0.9	1.3	1.3	1.1	0.8	1.1	1.0	0.8	1.1	1.2	1.1	1.0	1.0	1.4	2.8	3.3	2.5	1.7	1.0	0.8	0.5
7	0.8	1.2	1.2	1.1	0.8	0.9	1.0	0.8	0.9	1.1	1.0	0.9	1.1	1.0	2.6	3.0	2.2	1.4	0.9	0.6	0.4
6	0.7	1.1	1.2	1.1	1.0	0.9	0.9	0.8	0.8	1.0	1.0	0.9	0.9	1.1	2.0	2.5	2.0	1.3	0.8	0.5	0.3
5	0.6	1.0	1.1	0.9	0.8	0.7	0.7	0.8	0.8	0.9	0.9	0.7	0.9	1.0	1.3	2.0	1.9	1.5	1.1	0.7	0.3
4	0.5	0.8	0.9	0.8	0.7	0.6	0.5	0.4	0.3	0.5	0.6	0.6	0.7	0.8	1.0	1.3	1.3	0.9	0.7	0.4	0.2
3	0.4	0.6	0.7	0.6	0.6	0.5	0.4	0.2	0.0	0.1	0.2	0.3	0.4	0.3	0.2	0.1	0.0	0.1	0.1	0.2	0.2
2	0.3	0.4	0.5	0.4	0.4	0.3	0.2	0.1	-0.1	0.1	0.2	0.3	0.4	0.5	0.6	0.7	0.7	0.6	0.4	0.3	0.1
1	0.0	0.0	0.0	0.0	0.0	0.0	0.0	0.0	0.0	0.0	0.0	0.0	0.0	0.0	0.0	0.0	0.0	0.0	0.0	0.0	0.0

TABLE A-5

W_x (m/s) CASE 9 DX = 285.71 DZ = 50.00

Node Points	1	3	5	7	9	11	13	15	17	19	21	23	25	27	29	31	33	35	37	39	41
11	25.4	25.8	26.3	26.7	26.7	25.6	24.6	24.1	23.6	23.1	22.9	22.8	20.7	12.7	7.7	6.0	4.7	2.2	1.2	0.4	0.6
10	25.1	24.9	24.8	25.5	25.6	25.2	24.6	23.8	23.2	22.7	22.5	22.9	21.0	13.7	9.1	6.5	4.9	2.8	1.7	0.6	0.7
9	24.7	24.2	23.7	25.0	24.9	24.9	24.3	23.7	23.1	21.8	21.4	22.6	21.0	14.7	9.1	6.9	5.1	3.5	2.1	0.9	1.5
8	24.7	22.7	22.0	23.8	24.1	24.5	24.1	23.7	23.0	21.2	20.2	21.3	19.1	16.7	10.7	7.5	5.2	3.8	2.4	1.5	1.7
7	22.7	21.4	20.7	21.3	22.3	22.9	23.2	23.4	22.8	19.1	19.7	20.9	21.3	17.7	12.5	8.0	5.4	3.9	2.5	2.1	2.3
6	20.7	19.7	19.2	19.7	20.5	21.9	22.8	22.9	22.6	19.5	19.1	20.2	20.9	19.1	13.4	8.4	5.5	4.1	2.7	2.2	2.5
5	18.7	18.5	18.5	18.6	18.6	20.8	21.6	22.5	20.8	17.7	18.4	19.1	21.0	20.6	14.5	8.5	5.8	4.5	3.3	2.7	2.6
4	15.2	16.7	16.4	15.7	16.5	19.0	20.7	20.6	18.7	17.2	17.3	18.4	20.9	20.7	14.7	8.6	4.6	2.7	2.6	2.5	2.4
3	12.6	14.7	14.8	12.9	14.9	17.7	18.8	18.7	16.6	16.3	16.7	17.8	19.9	18.8	13.6	8.4	5.3	4.1	3.6	3.0	2.5
2	10.7	12.0	12.6	11.6	11.8	13.2	13.2	12.5	13.6	14.7	17.1	18.0	18.9	16.8	12.2	7.2	4.5	3.5	2.6	2.5	2.4
1	10.2	10.7	12.7	9.5	10.2	12.9	12.7	11.5	11.5	13.8	15.7	16.6	16.9	14.5	10.6	6.4	3.8	2.5	2.5	2.4	2.4

W_z (m/s)

Node Points	1	3	5	7	9	11	13	15	17	19	21	23	25	27	29	31	33	35	37	39	41
11	1.1	1.0	1.0	0.0	0.5	-2.2	-1.0	-0.9	-1.2	-0.5	0.0	-0.1	1.0	5.1	5.0	3.0	2.0	1.0	0.9	0.8	0.7
10	1.2	0.8	0.4	-0.4	-1.3	-2.0	-0.9	-1.1	-1.0	-0.4	-0.0	-0.1	0.8	4.5	4.7	2.6	1.6	1.1	1.0	0.9	0.8
9	1.1	0.7	0.3	-0.4	-1.1	-1.3	-0.9	-1.0	-1.1	-0.5	-0.1	-0.1	0.8	3.5	4.0	2.0	1.3	0.8	0.5	0.5	0.9
8	1.1	0.5	0.6	-0.4	-1.0	-1.2	-0.9	-1.0	-1.1	-0.5	-0.1	-0.2	0.5	2.5	3.8	1.8	0.8	0.4	0.1	0.3	1.0
7	1.0	0.2	0.3	-0.5	-0.9	-1.0	-0.9	-1.0	-1.1	-0.6	-0.2	-0.1	0.0	1.7	3.0	1.5	0.7	0.3	0.0	0.0	1.1
6	0.7	0.0	0.3	-0.4	-0.8	-0.9	-0.9	-1.0	-1.0	-0.7	-0.3	-0.2	-0.1	0.8	2.3	1.3	0.5	0.3	0.0	0.0	1.0
5	0.4	0.0	0.2	-0.2	-0.5	-0.8	-1.0	-1.2	-1.0	-1.2	-1.1	-0.7	-0.4	0.0	1.4	1.1	0.3	0.0	-0.0	0.0	1.0
4	0.3	-0.1	0.2	-0.1	-0.4	-0.8	-1.2	-1.1	-1.0	-0.3	-0.2	-0.2	-0.1	-0.0	0.5	0.6	-0.1	0.1	-0.1	0.0	0.6
3	0.0	-0.2	0.0	-0.2	-0.5	-0.8	-1.1	-1.1	-0.8	0.0	-0.1	-0.2	-0.1	-0.0	0.4	0.4	-0.1	0.1	-0.1	-0.1	0.5
2	0.0	-0.2	-0.1	-0.2	-0.4	-0.6	-0.7	-0.6	-0.3	0.0	-0.2	-0.3	-0.1	-0.0	0.3	0.1	-0.1	0.1	-0.1	-0.1	0.3
1	0.0	0.0	0.0	0.0	0.0	0.0	0.0	0.0	0.0	0.0	0.0	0.0	0.0	0.0	0.0	0.0	0.0	0.0	0.0	0.0	0.0

TABLE A-6

W_x (m/s) CASE 6 DX = 181.82 DZ = 90.00

Node Points	1	3	5	7	9	11	13	15	17	19	21	23	25	27	29	31	33	35	37	39	41
11	10.3	10.8	12.0	14.0	15.0	15.1	15.1	15.2	15.1	14.6	14.6	15.2	14.6	13.8	13.0	5.0	-1.0	-1.7	-2.4	-2.9	-3.3
10	10.3	11.0	12.3	14.0	14.2	14.4	14.7	14.9	15.1	14.5	14.5	15.1	14.0	13.4	11.5	6.0	0.0	-1.4	-2.3	-2.9	-3.3
9	10.3	11.1	12.5	13.4	13.3	13.3	13.6	14.0	14.0	14.1	14.3	14.8	13.6	12.5	11.5	7.0	0.0	-1.1	-2.2	-2.9	-3.3
8	10.3	11.1	12.4	13.2	12.9	12.8	14.0	13.0	13.6	13.9	14.0	14.0	13.3	12.5	11.5	8.0	0.3	-1.0	-2.2	-3.0	-3.3
7	10.2	11.0	11.9	12.8	12.8	12.9	13.3	12.8	13.2	13.0	13.1	13.1	13.0	11.0	11.1	9.0	0.9	-1.0	-2.3	-3.1	-3.4
6	10.0	10.8	11.3	11.9	12.4	12.9	13.0	12.1	13.2	12.8	12.9	12.9	12.8	10.9	10.0	9.1	1.7	-1.3	-2.4	-3.1	-3.4
5	9.9	10.8	11.5	11.9	12.2	12.6	13.0	11.8	13.0	12.8	12.5	12.3	12.0	11.0	10.1	9.2	3.0	-0.1	-2.0	-3.1	-3.4
4	9.0	10.3	11.1	11.2	11.3	11.3	11.2	11.0	11.0	10.9	10.9	10.9	11.0	11.0	9.8	8.6	5.0	0.3	-1.7	-3.0	-3.3
3	8.0	9.0	9.7	10.3	11.0	11.0	11.1	9.8	9.6	9.4	9.2	9.0	10.1	11.3	9.0	8.7	6.9	1.3	-1.2	-2.1	-3.0
2	7.0	7.9	8.8	8.8	8.7	8.7	7.0	6.5	5.9	5.8	5.8	5.7	7.0	8.7	7.6	7.5	7.0	3.1	0.0	-1.2	-2.0
1	6.7	6.8	6.9	6.9	7.0	5.7	4.9	5.0	4.3	3.0	2.9	3.0	5.6	7.0	5.7	5.0	7.0	5.0	1.2	0.1	-1.0

W_z (m/s)

Node Points	1	3	5	7	9	11	13	15	17	19	21	23	25	27	29	31	33	35	37	39	41
11	-1.0	-1.9	-2.2	-2.0	-0.9	-0.5	-0.2	0.2	0.6	1.1	1.0	-1.1	0.2	1.1	0.8	4.0	6.1	5.0	2.0	1.3	0.8
10	-0.9	-2.1	-2.1	-1.5	-0.8	-0.5	-0.1	0.5	0.8	1.0	1.0	-1.0	0.1	1.0	0.8	3.0	5.8	4.0	1.9	1.0	0.7
9	-0.8	-2.0	-2.0	-1.0	-0.7	-0.3	0.0	0.8	0.7	0.8	0.5	-0.9	0.0	0.9	0.9	2.7	5.0	3.8	1.8	0.9	0.7
8	-0.8	-1.4	-1.4	-0.9	-0.6	-0.3	0.2	1.0	0.9	0.8	0.4	-0.3	0.0	0.5	1.0	2.4	4.2	3.5	1.6	0.9	0.6
7	-0.7	-1.3	-1.3	-0.8	-0.3	0.2	0.7	1.1	0.9	0.8	0.3	-0.3	-0.3	0.0	1.0	2.0	3.5	3.0	1.5	0.9	0.6
6	-0.5	-1.0	-1.0	-0.4	-0.1	-0.2	0.4	1.2	0.8	0.5	0.2	-0.1	-0.4	0.0	1.1	1.7	2.5	2.5	1.3	0.7	0.5
5	-0.4	-0.7	-0.5	0.0	0.0	-0.1	0.5	1.2	0.8	0.5	0.2	-0.2	-0.3	0.0	1.1	1.1	2.0	2.0	1.0	0.8	0.5
4	-0.3	-0.2	-0.1	0.1	0.1	0.0	0.5	1.1	0.8	0.3	-0.1	-0.2	-0.3	0.0	0.8	1.1	1.5	1.5	0.9	0.7	0.5
3	-0.2	-0.1	-0.0	0.0	0.1	0.1	0.5	1.0	0.7	0.5	0.2	-0.1	0.0	0.0	0.5	0.8	1.0	0.8	0.7	0.5	0.4
2	-0.1	-0.1	-0.0	0.0	0.1	0.2	0.3	0.4	0.3	0.3	0.2	0.1	0.0	0.0	0.2	0.5	0.7	0.7	0.6	0.5	0.4
1	0.0	0.0	0.0	0.0	0.0	0.0	0.0	0.0	0.0	0.0	0.0	0.0	0.0	0.0	0.0	0.0	0.0	0.0	0.0	0.0	0.0

TABLE A-7

W_x (m/s) CASE 7 DX = 196.08 DZ = 50.00

Node Points	1	3	5	7	9	11	13	15	17	19	21	23	25	27	29	31	33	35	37	39	41
11	18.3	18.0	17.8	19.8	21.1	22.2	23.0	23.9	23.4	21.6	19.8	15.8	13.9	7.8	1.8	-0.9	-3.7	-6.4	-7.5	-8.6	-9.7
10	18.3	17.6	17.8	19.1	20.8	22.1	22.8	23.5	23.2	22.0	20.8	17.5	14.3	9.8	3.8	-0.4	-2.8	-5.1	-6.9	-8.2	-9.4
9	18.0	17.8	17.8	19.5	19.8	21.8	22.2	22.6	22.6	22.2	21.8	18.5	14.8	9.8	3.8	1.1	-1.4	-3.8	-6.2	-7.2	-8.2
8	17.8	17.7	17.6	18.3	19.8	20.9	22.0	22.3	21.8	22.8	21.8	15.8	15.1	12.8	6.8	2.3	-0.7	-2.8	-4.0	-5.2	-6.4
7	16.9	17.2	17.5	17.8	19.8	20.7	21.6	21.7	21.0	21.9	21.8	15.8	16.5	14.9	6.8	3.8	0.8	-2.2	-3.3	-4.3	-5.4
6	16.3	16.8	17.3	17.8	19.1	20.3	21.3	21.5	21.0	20.5	20.0	18.8	16.8	14.1	10.6	6.2	1.8	0.3	-1.2	-2.7	-4.2
5	16.0	16.6	17.2	17.8	18.6	19.4	20.4	20.7	19.8	19.8	19.9	18.1	16.3	15.4	10.8	8.5	6.1	3.8	1.5	-0.9	-3.2
4	15.8	16.5	17.1	17.8	18.6	19.4	20.3	19.8	17.8	15.8	15.8	15.8	17.2	15.9	11.8	8.5	5.1	1.8	0.5	-0.9	-2.2
3	14.8	15.5	16.1	16.6	17.2	17.7	19.8	19.8	17.4	15.0	13.9	14.0	15.9	16.3	13.3	10.3	7.3	4.3	1.3	-0.5	-1.2
2	13.8	14.5	15.1	15.8	16.6	17.4	19.0	18.1	13.8	12.3	10.8	12.1	15.2	15.9	12.5	9.5	7.0	4.5	2.0	0.4	-0.3
1	12.8	13.5	14.1	14.7	15.2	15.8	18.8	19.8	12.8	8.8	8.7	9.8	15.8	15.8	11.8	9.8	7.8	5.8	3.8	1.8	0.8

W_z (m/s)

Node Points	1	3	5	7	9	11	13	15	17	19	21	23	25	27	29	31	33	35	37	39	41
11	1.0	0.0	-1.0	0.0	-0.5	-1.0	-1.3	-1.5	-1.8	-2.0	-2.0	-1.2	-0.4	4.0	4.1	3.0	2.0	1.0	0.8	0.7	0.5
10	1.0	0.0	-1.0	0.0	-1.0	-1.0	-1.0	-1.0	-1.0	-1.0	-2.0	-1.5	-1.0	1.8	3.1	2.3	1.6	0.8	0.7	0.6	0.5
9	1.0	0.0	-1.0	0.0	-1.0	-1.1	-1.2	-1.4	-1.7	-1.9	-2.2	-1.3	-0.4	1.5	2.7	2.0	1.3	0.9	0.8	0.6	0.5
8	1.0	0.0	-0.4	-0.1	-0.4	-0.7	-1.0	-1.3	-1.5	-1.8	-2.1	-1.7	-1.2	0.0	2.0	1.5	1.0	0.9	0.8	0.6	0.5
7	1.0	0.0	-0.4	-0.1	-0.4	-0.7	-1.0	-1.7	-1.4	-1.3	-2.1	-2.0	-1.9	-0.9	0.2	0.7	1.1	0.9	0.7	0.5	0.3
6	1.0	-0.2	-0.3	-0.1	-0.4	-0.7	-1.3	-2.0	-1.2	-1.2	-2.1	-1.3	-1.4	-1.0	0.3	0.6	0.5	0.4	0.3	0.2	0.1
5	1.0	-0.3	0.0	0.0	0.1	-0.5	-1.0	-1.5	-1.3	-1.0	-2.0	-1.2	-1.2	-2.0	0.0	0.1	0.1	0.2	0.2	0.1	0.1
4	0.5	-0.2	0.0	0.0	0.0	-0.3	-1.0	-2.0	-1.5	-1.1	-1.5	-0.8	-1.6	-1.3	0.0	0.0	0.0	0.1	0.2	0.2	0.2
3	0.0	-0.2	-0.3	-0.3	-0.2	-0.5	-1.0	-1.6	-1.4	-0.9	-1.0	-0.8	-1.4	-2.0	-1.4	-0.9	-0.3	0.1	0.2	0.1	0.0
2	0.0	-0.1	-0.1	0.0	-0.3	-0.7	-1.0	-1.0	-1.0	-0.1	0.1	-0.3	-0.8	-0.9	-0.7	-0.4	-0.2	0.0	0.1	0.0	0.0
1	0.0	0.0	0.0	0.0	0.0	0.0	0.0	0.0	0.0	0.0	0.0	0.0	0.0	0.0	0.0	0.0	0.0	0.0	0.0	0.0	0.0

TABLE A-8

W_x (m/s) CASE 8 DX = 138.89 DZ = 50.00

Node Points	1	3	5	7	9	11	13	15	17	19	21	23	25	27	29	31	33	35	37	39	41
11	6.3	7.2	8.1	9.5	6.0	5.4	7.5	9.5	10.6	10.6	9.5	8.5	3.5	-1.6	-2.4	-3.1	-3.6	-3.7	-4.6	-5.5	-5.7
10	6.4	7.2	8.1	10.2	6.7	7.6	8.5	10.4	10.5	10.6	9.4	8.1	5.2	0.5	-1.5	-2.1	-2.8	-3.5	-4.3	-5.0	-5.7
9	6.4	7.5	8.5	10.5	7.7	7.4	10.5	11.0	11.5	10.7	9.8	9.0	6.6	2.6	-0.2	-1.9	-2.4	-3.0	-3.5	-4.5	-5.5
8	6.4	7.5	8.5	10.6	8.3	8.6	11.2	12.2	12.3	11.8	10.5	9.4	8.4	3.5	2.6	1.7	-1.6	-1.7	-1.7	-3.2	-4.7
7	6.7	7.7	8.7	10.5	8.0	8.7	12.6	12.6	12.7	12.1	11.0	9.9	9.0	6.7	3.1	-0.5	-0.9	-1.2	-1.6	-3.0	-4.5
6	7.5	8.0	8.5	9.5	7.8	8.5	10.1	11.8	12.3	11.5	10.8	10.4	9.4	6.9	3.6	0.3	-0.2	-0.7	-1.2	-2.3	-4.0
5	6.8	7.6	8.5	8.0	7.5	8.5	10.2	11.9	12.5	12.0	11.4	10.9	9.6	6.7	2.6	1.6	0.5	-0.5	-1.5	-2.5	-3.5
4	6.5	6.5	6.4	6.4	6.3	8.5	10.2	11.9	12.5	12.0	11.5	11.0	10.5	7.1	4.9	3.8	2.7	1.7	0.6	-0.9	-2.5
3	6.3	6.4	5.8	4.5	5.8	8.0	10.5	12.5	12.1	11.0	10.5	10.6	9.9	8.5	6.5	4.5	2.5	1.5	0.5	-0.5	-1.5
2	6.0	5.8	5.5	2.7	4.8	7.3	9.5	11.6	12.1	11.0	10.5	10.6	10.6	8.5	7.1	5.6	4.1	2.7	1.2	-0.1	-1.2
1	5.5	5.0	4.5	2.0	4.5	6.5	8.5	12.5	11.5	10.6	10.6	10.6	10.1	9.1	7.9	6.4	4.9	3.5	2.0	0.5	-0.5

W_z (m/s)

Node Points	1	3	5	7	9	11	13	15	17	19	21	23	25	27	29	31	33	35	37	39	41
11	3.0	-1.0	-1.0	1.2	-1.5	-0.9	0.5	1.4	2.2	1.3	0.4	1.7	5.0	4.4	2.8	1.9	1.6	1.3	1.0	0.6	0.3
10	3.5	-1.0	-1.0	1.2	-1.0	-1.4	0.0	0.8	1.7	0.8	0.0	0.2	3.1	3.9	2.6	1.5	1.0	1.1	0.8	0.6	0.3
9	4.0	-1.0	-1.0	1.1	-1.1	-1.4	-0.3	0.5	1.1	-0.4	0.0	0.1	2.0	4.1	3.0	1.6	0.9	0.7	0.5	0.4	0.2
8	4.1	-1.0	-1.0	1.0	-1.7	-1.8	-0.4	0.3	0.9	0.3	-0.1	-0.0	1.0	3.1	3.0	1.1	0.8	0.6	0.5	0.3	0.2
7	3.8	-1.0	-0.9	0.6	-1.9	-1.9	-1.0	0.0	0.5	0.0	-0.1	-0.1	0.0	2.0	2.3	0.9	0.8	0.6	0.5	0.3	0.2
6	3.0	-1.0	-0.8	0.5	-2.5	-1.9	-1.1	-0.3	0.1	0.0	-0.1	0.2	0.7	1.8	2.2	1.5	0.8	0.5	0.4	0.3	0.2
5	2.0	-1.0	-1.1	0.4	-2.0	-1.2	-1.1	-0.4	-0.0	-0.1	-0.2	-0.1	-0.0	1.0	1.5	0.9	0.7	0.4	0.2	0.4	0.9
4	1.5	-1.0	-1.0	-0.3	-1.3	-1.0	-1.0	-0.5	-0.3	-0.2	-0.1	-0.1	-0.0	0.8	1.3	1.0	0.8	0.4	0.1	0.0	0.0
3	1.0	-1.0	-0.9	-0.2	-1.0	-1.0	-0.7	-0.6	-0.5	-0.4	-0.2	-0.1	-0.0	0.1	0.8	0.6	0.5	0.3	0.2	0.0	0.1
2	0.2	-0.1	-0.0	0.0	-0.2	-0.2	-0.2	-0.1	-0.1	-0.1	-0.1	-0.0	-0.0	0.0	0.0	0.1	0.1	0.1	0.0	0.0	0.0
1	0.0	0.0	0.0	0.0	0.0	0.0	0.0	0.0	0.0	0.0	0.0	0.0	0.0	0.0	0.0	0.0	0.0	0.0	0.0	0.0	0.0

TABLE A-9

W_x (m/s) CASE 9 DX = 185.19 DZ = 50.00

Node Points	1	3	5	7	9	11	13	15	17	19	21	23	25	27	29	31	33	35	37	39	41
11	13.8	14.2	14.6	14.9	15.3	16.5	17.8	18.3	18.8	19.3	19.6	19.5	16.8	13.5	11.5	9.5	1.5	-0.9	-1.4	-2.0	-2.5
10	13.7	14.1	14.4	14.8	15.1	15.5	16.2	16.8	17.5	18.0	18.5	17.6	15.5	13.0	11.8	10.5	1.8	-1.0	-2.0	-2.5	-2.6
9	13.7	13.7	14.1	14.5	14.9	15.3	15.8	16.3	16.8	17.3	17.5	17.5	14.8	13.1	12.3	11.3	3.5	-1.1	-2.4	-2.4	-2.5
8	13.6	13.3	13.8	13.8	13.7	13.7	13.6	14.7	16.0	16.3	16.7	16.1	14.3	12.9	12.2	11.5	2.5	-1.5	-2.5	-2.5	-2.5
7	13.5	12.6	13.0	13.5	13.5	13.6	13.5	14.4	15.5	15.6	15.4	14.8	13.4	12.8	12.1	11.5	3.0	-1.5	-2.5	-2.5	-2.5
6	12.5	12.5	12.5	12.5	12.6	12.6	12.6	13.5	14.0	14.6	15.1	14.4	12.6	11.7	11.8	9.0	3.4	-1.3	-2.6	-2.6	-2.6
5	12.5	12.3	12.0	11.8	11.5	12.1	12.7	13.3	13.8	14.1	14.5	13.3	12.0	11.5	11.7	9.1	3.6	-1.3	-2.6	-2.6	-2.6
4	11.8	11.6	11.7	11.4	10.3	11.1	11.7	12.9	13.6	13.7	13.9	12.7	11.5	11.3	11.6	9.4	4.5	-1.2	-2.5	-2.6	-2.6
3	11.7	11.3	11.4	9.9	9.5	10.2	10.8	11.5	13.5	13.2	13.7	12.2	11.3	11.2	11.5	11.6	5.3	0.1	-2.5	-2.6	-2.6
2	11.6	10.8	10.1	9.3	8.0	8.9	9.9	11.0	11.9	12.8	13.6	11.4	11.0	11.0	11.4	11.6	5.5	0.2	-2.4	-2.5	-2.6
1	11.5	10.7	9.9	7.5	7.4	8.5	9.5	10.8	11.8	11.5	13.5	12.3	11.1	10.8	11.3	11.5	5.7	-2.2	-2.5	-2.6	-2.7

W_z (m/s)

Node Points	1	3	5	7	9	11	13	15	17	19	21	23	25	27	29	31	33	35	37	39	41
11	0.0	0.3	0.6	0.9	1.2	0.9	0.7	1.5	2.5	3.3	4.0	3.2	1.0	0.1	-0.1	1.9	4.2	1.9	1.2	0.7	0.3
10	0.3	0.5	0.7	0.9	1.1	1.0	0.7	1.6	2.6	3.5	4.0	3.0	1.0	0.1	-0.1	1.0	4.2	1.5	0.8	0.3	0.2
9	0.3	0.1	0.0	0.5	1.0	1.1	0.8	1.0	2.3	3.5	4.4	2.8	1.1	0.1	-0.1	0.8	3.9	1.2	0.9	0.5	0.2
8	0.3	0.1	-0.1	0.3	0.8	1.1	0.8	1.1	2.0	2.9	3.8	2.9	1.0	0.0	-0.1	0.5	3.0	1.0	0.7	0.5	0.2
7	0.3	0.1	-0.1	0.2	0.7	1.1	0.8	0.9	2.0	3.5	4.2	1.9	0.9	0.0	-0.2	0.0	2.4	0.8	0.6	0.3	0.1
6	0.2	0.0	-0.2	0.2	0.4	0.7	0.6	0.8	1.8	3.3	3.4	2.1	1.0	0.0	-0.2	0.6	1.9	1.4	1.0	0.5	0.1
5	0.2	-0.1	0.0	0.4	0.3	0.1	0.0	0.5	1.0	3.0	3.8	2.3	1.0	0.0	-0.2	0.3	0.9	1.1	0.8	0.4	0.1
4	0.1	-0.1	-0.1	0.1	0.1	-0.1	-0.2	0.1	1.0	2.1	2.5	1.8	1.0	0.0	-0.3	-0.1	0.3	0.8	0.8	0.4	0.0
3	0.1	-0.1	-0.1	0.1	0.1	-0.1	-0.3	0.0	0.0	1.5	2.0	1.5	1.0	0.0	-0.1	0.0	0.5	0.4	0.3	0.1	0.0
2	0.0	-0.1	-0.0	0.0	0.0	-0.1	-0.2	-0.1	0.0	0.9	0.8	0.8	0.7	0.3	-0.2	-0.1	0.1	0.2	0.1	0.1	0.0
1	0.0	0.0	0.0	0.0	0.0	0.0	0.0	0.0	0.0	0.0	0.0	0.0	0.0	0.0	0.0	0.0	0.0	0.0	0.0	0.0	0.0

TABLE A-10

W_x (m/s) CASE 10 DX = 212.77 DZ = 50.00

Node Points	1	3	5	7	9	11	13	15	17	19	21	23	25	27	29	31	33	35	37	39	41
11	21.3	19.5	17.7	16.5	15.9	15.4	16.1	17.1	17.1	16.4	15.7	15.0	14.3	13.6	12.9	4.6	2.7	2.0	1.2	0.3	-0.5
10	21.2	19.1	17.1	16.5	15.9	15.3	15.5	16.6	16.8	16.3	15.7	15.2	16.2	17.2	13.1	5.1	2.6	1.7	0.8	0.1	-0.6
9	21.1	19.5	16.9	16.3	15.6	15.0	15.1	15.8	16.0	15.7	15.4	15.7	16.5	17.3	13.9	5.6	3.3	1.1	0.5	-0.1	-0.7
8	19.1	17.7	16.5	15.6	15.1	15.1	15.1	15.3	15.6	15.9	16.3	16.6	17.0	17.3	11.9	6.6	2.6	0.9	0.3	-0.3	-0.9
7	17.1	17.3	16.1	15.1	14.3	14.1	14.6	15.1	15.5	15.8	16.2	16.6	16.9	17.3	15.1	7.1	3.1	0.8	-0.3	-0.4	-0.9
6	15.9	16.7	15.7	14.5	13.1	13.7	14.2	14.8	15.3	15.7	16.0	16.4	16.8	17.2	15.1	8.9	2.8	1.3	-0.2	-0.9	-1.0
5	15.1	16.1	15.4	14.3	12.8	13.0	13.2	14.0	14.7	15.2	15.5	15.8	16.0	16.3	13.8	9.4	3.1	1.1	-0.3	-0.9	-1.0
4	14.1	14.8	14.4	13.1	12.1	12.5	12.9	13.5	14.5	15.1	15.2	15.3	15.4	14.5	13.6	10.2	4.3	0.8	-0.3	-0.9	-1.0
3	13.1	12.7	12.3	12.0	11.6	12.1	12.7	13.2	14.5	15.1	15.1	15.1	15.1	14.3	13.5	10.2	4.5	1.0	-0.3	-0.9	-1.0
2	11.1	9.8	9.3	9.7	10.1	10.5	10.9	12.1	12.1	11.1	11.1	11.1	11.0	11.0	11.0	8.7	4.1	0.9	-0.3	-0.9	-1.0
1	9.1	7.1	7.8	9.1	9.6	10.1	10.6	11.1	13.1	10.8	9.6	9.1	9.1	9.0	9.3	9.1	4.0	0.6	-1.1	-1.1	-1.1

W_z (m/s)

Node Points	1	3	5	7	9	11	13	15	17	19	21	23	25	27	29	31	33	35	37	39	41
11	0.4	1.0	0.9	-0.1	0.1	0.5	1.1	0.0	-0.1	0.2	-0.8	-1.0	-1.2	-0.3	1.8	5.2	3.1	1.5	0.9	0.6	0.3
10	0.3	0.8	0.7	0.0	-0.1	0.4	1.0	0.2	-0.6	0.2	-0.7	-1.1	-1.2	-0.4	1.7	5.0	3.4	1.8	0.8	0.5	0.2
9	0.3	0.4	0.3	-0.1	0.1	0.4	0.6	-0.3	-0.9	0.1	-0.5	-1.1	-1.2	-1.0	2.7	4.1	2.8	1.5	0.7	0.4	0.2
8	0.3	0.2	0.1	0.0	-0.1	0.3	0.1	-0.6	-0.9	0.0	-0.7	-1.1	-0.9	-0.3	1.2	3.5	2.4	1.3	0.6	0.4	0.2
7	0.2	0.1	-0.0	-0.1	-0.1	0.2	0.0	-1.0	-1.1	-0.2	-0.7	-1.1	-0.6	0.6	1.8	3.0	2.0	1.0	0.7	0.5	0.2
6	0.2	0.1	-0.0	-0.1	-0.1	0.2	-0.5	-0.9	-1.2	-0.7	-0.7	-1.1	-1.1	-1.0	0.4	1.7	2.1	1.6	1.1	0.6	0.1
5	0.1	0.0	-0.1	-0.2	-0.1	0.0	-0.4	-0.9	-0.9	-0.6	-0.7	-1.2	-1.0	-0.3	0.5	1.4	1.4	0.9	0.6	0.4	0.1
4	0.0	-0.0	-0.1	-0.1	-0.2	-0.2	-0.6	-1.1	-1.0	-0.9	-0.9	-1.2	-0.8	-0.5	0.2	0.8	1.0	0.8	0.5	0.3	0.1
3	0.0	-0.0	-0.1	-0.1	-0.2	-0.5	-0.8	-1.0	-0.9	-0.9	-0.9	-1.0	-0.7	-0.3	0.0	0.2	0.7	0.5	0.4	0.2	0.0
2	0.0	-0.0	-0.0	-0.1	-0.1	-0.3	-0.4	-0.5	-0.4	-0.3	-0.3	-0.4	-0.3	-0.2	-0.1	0.0	0.2	0.1	0.1	0.0	0.0
1	0.0	0.0	0.0	0.0	0.0	0.0	0.0	0.0	0.0	0.0	0.0	0.0	0.0	0.0	0.0	0.0	0.0	0.0	0.0	0.0	0.0

TABLE A-11

W_x (m/s) CASE 11 DX = 204.08 DZ = 50.00

Node Points	1	3	5	7	9	11	13	15	17	19	21	23	25	27	29	31	33	35	37	39	41
11	26.9	24.1	21.4	20.7	18.4	14.8	15.6	16.4	16.5	16.3	15.0	14.4	14.5	14.4	12.4	7.1	3.4	1.2	-1.2	-3.6	-3.8
10	26.6	23.5	20.5	20.7	17.5	14.4	14.4	15.8	16.4	15.9	14.8	14.4	13.9	13.1	12.6	8.6	4.7	1.8	-0.0	-1.9	-3.7
9	26.5	23.2	19.9	20.6	18.2	15.8	15.0	15.7	16.5	15.8	14.7	14.4	13.4	12.7	11.2	7.3	4.4	2.4	0.4	-1.6	-3.6
8	25.4	22.4	19.4	20.4	18.4	16.4	14.8	15.2	15.6	15.1	14.6	14.4	13.4	12.5	11.2	8.1	4.9	2.5	0.8	-0.9	-2.6
7	24.4	20.4	16.4	18.3	17.4	16.5	14.8	15.1	15.4	15.0	14.5	14.3	13.3	12.5	11.2	8.0	5.6	3.9	2.3	0.3	-1.8
6	22.4	18.4	15.9	15.7	16.3	15.9	14.6	14.5	14.5	14.4	14.1	13.6	12.9	12.6	10.1	6.6	5.3	3.9	2.3	0.4	-1.6
5	20.4	18.4	14.4	14.5	16.3	15.8	14.4	14.3	14.3	14.2	12.4	12.6	12.8	13.0	12.4	9.7	7.1	4.4	2.6	0.7	-1.1
4	18.4	15.7	14.1	15.4	14.7	14.8	14.0	13.5	12.9	12.4	10.8	11.4	12.1	12.8	11.5	8.8	6.6	4.8	3.2	1.4	-0.6
3	16.4	15.1	12.3	12.4	12.9	13.1	12.4	12.4	12.4	11.4	10.6	11.2	11.8	12.4	10.7	9.0	7.2	5.4	3.9	2.4	0.4
2	15.1	11.9	10.3	10.3	10.3	10.4	10.4	10.4	10.4	10.4	9.9	10.3	10.7	10.6	9.7	8.4	6.9	5.7	4.8	3.4	1.7
1	14.9	12.4	9.5	8.3	7.0	6.8	7.5	8.3	8.3	8.4	8.9	9.8	10.9	9.3	6.4	4.4	6.3	5.7	5.0	4.4	2.4

W_z (m/s)

Node Points	1	3	5	7	9	11	13	15	17	19	21	23	25	27	29	31	33	35	37	39	41
11	-1.1	-0.8	-0.6	-0.9	-1.0	-0.4	-0.5	-1.2	-1.3	-1.5	-1.7	-1.8	-2.0	-1.7	0.5	2.5	2.7	2.0	1.3	1.1	1.3
10	-1.1	-0.7	-0.7	-0.7	-1.1	-0.4	-0.5	-1.2	-1.4	-1.5	-1.6	-1.7	-2.3	-1.8	0.0	2.0	2.6	1.9	1.3	1.0	1.3
9	-1.1	-0.8	-0.8	-0.7	-1.1	-0.4	-0.5	-1.1	-1.3	-1.4	-1.6	-1.7	-2.6	-2.0	0.0	2.0	2.4	1.5	0.9	1.0	1.3
8	-1.1	-0.8	-0.9	-0.8	-1.1	-0.6	-0.7	-1.1	-1.2	-1.3	-1.4	-1.8	-2.5	-2.2	-0.5	1.4	2.1	1.2	0.8	0.9	1.2
7	-1.2	-0.9	-1.0	-0.9	-1.1	-1.0	-0.5	-1.0	-1.2	-1.3	-1.3	-1.2	-2.5	-2.5	-1.0	1.0	1.8	1.0	0.7	0.8	1.2
6	-1.2	-1.1	-1.0	-0.9	-1.1	-1.0	-0.5	-0.9	-1.2	-1.1	-1.2	-1.4	-2.4	-2.5	-1.4	0.5	1.4	0.8	0.7	0.8	1.2
5	-1.2	-1.2	-1.2	-1.1	-1.1	-1.1	-0.5	-1.0	-1.1	-1.0	-1.0	-1.0	-2.1	-2.2	-1.5	0.0	1.0	0.8	0.5	0.8	1.1
4	-1.1	-1.1	-1.1	-1.1	-1.1	-1.1	-0.2	-0.8	-1.0	-0.9	-1.0	-0.8	-2.0	0.3	0.4	0.5	0.6	0.7	0.8	0.9	1.0
3	-1.0	-1.0	-1.0	-1.0	-1.0	-1.0	-0.2	-0.7	-0.9	-0.8	-1.0	-1.0	-1.4	-1.7	-1.1	-0.3	0.2	0.0	0.3	0.5	0.8
2	-0.4	-0.4	-0.4	-0.5	-0.5	-0.4	-0.2	-0.4	-0.7	-0.8	-0.8	-0.8	-0.9	-1.0	-0.9	-0.4	0.0	0.0	-0.0	0.1	0.2
1	0.0	0.0	0.0	0.0	0.0	0.0	0.0	0.0	0.0	0.0	0.0	0.0	0.0	0.0	0.0	0.0	0.0	0.0	0.0	0.0	0.0

TABLE A-12

W_x (m/s) CASE 12 DX = 90.90 DZ = 90.00

Node Points	1	3	5	7	9	11	13	15	17	19	21	23	25	27	29	31	33	35	37	39	41
11	9.3	8.6	7.9	7.1	6.3	5.5	3.4	5.5	6.3	5.7	1.5	-2.4	-2.4	-2.4	-2.6	-3.9	-5.1	-6.0	-6.5	-6.6	-6.7
10	9.6	9.5	8.5	7.4	7.6	6.3	5.0	6.3	6.0	5.7	3.5	-0.5	-1.7	-2.0	-2.3	-3.4	-4.5	-5.2	-5.8	-6.5	-6.7
9	10.6	9.7	8.8	7.7	7.6	6.9	5.8	7.5	6.8	6.1	4.3	1.5	-0.5	-0.7	-1.6	-3.0	-4.1	-4.7	-4.9	-5.5	-6.5
8	11.5	10.4	9.3	8.8	8.4	7.9	7.5	7.6	6.9	6.3	5.6	3.5	-0.2	-0.5	-0.8	-2.5	-3.3	-4.1	-4.4	-4.9	-5.7
7	11.6	10.5	9.4	8.9	8.5	8.0	7.6	7.6	7.1	6.5	5.9	4.0	1.2	0.4	-0.5	-1.5	-2.6	-3.2	-3.8	-4.4	-5.5
6	11.7	10.6	9.5	7.7	7.7	7.6	7.6	7.6	7.1	6.6	6.0	5.5	2.4	1.3	0.1	-1.0	-2.1	-2.9	-3.5	-4.2	-5.0
5	11.1	10.5	9.5	7.4	7.5	7.6	7.7	7.5	7.1	6.6	6.1	5.6	3.5	2.0	0.9	-0.0	-1.1	-2.4	-2.6	-3.8	-4.7
4	11.0	10.7	9.3	6.6	6.5	7.5	7.7	7.6	7.0	6.5	6.1	5.7	5.0	3.4	1.3	0.5	-0.2	-1.0	-2.3	-3.7	-4.5
3	10.6	11.5	8.8	5.5	5.5	6.5	7.5	7.4	7.0	6.7	6.5	6.4	6.4	4.2	1.5	1.4	0.4	-1.1	-2.3	-3.5	-4.5
2	10.4	11.5	8.8	6.1	3.5	6.2	7.4	7.1	6.7	6.4	6.8	7.3	6.8	5.4	3.0	2.0	0.8	-0.5	-2.0	-3.5	-4.5
1	10.3	11.6	8.8	3.9	3.3	5.5	5.7	6.0	6.2	6.4	6.7	7.3	7.8	5.5	3.0	2.3	1.5	0.0	-1.7	-3.6	-4.3

W_z (m/s)

Node Points	1	3	5	7	9	11	13	15	17	19	21	23	25	27	29	31	33	35	37	39	41
11	2.1	1.0	-0.1	-1.0	-1.1	-1.1	-1.1	-1.2	-0.8	-0.3	1.5	3.1	3.2	3.3	2.5	1.9	1.6	1.2	0.9	1.0	1.1
10	2.1	1.1	0.1	-0.8	-0.9	-1.0	-1.1	-1.0	-0.8	-0.3	1.0	2.9	3.0	3.1	2.4	1.8	1.5	1.3	0.9	1.0	1.1
9	2.0	1.2	0.4	-0.1	-0.4	-0.6	-0.9	-1.1	-0.7	-0.3	0.4	2.0	2.0	2.9	2.0	1.5	1.0	1.1	0.9	1.0	1.1
8	1.5	1.0	0.5	0.0	-0.3	-0.5	-0.8	-1.0	-0.7	-0.3	0.0	1.0	1.5	2.5	1.8	1.3	0.9	0.9	0.9	1.0	1.1
7	1.2	1.0	0.6	0.2	0.0	-0.2	-0.5	-0.8	-0.5	-0.3	-0.0	0.4	1.1	2.1	1.5	1.0	0.9	0.8	0.8	0.9	0.9
6	1.1	0.8	0.6	0.3	0.1	-0.1	-0.4	-0.6	-0.4	-0.3	-0.1	0.0	0.9	1.8	1.3	0.9	0.8	0.6	0.5	0.4	0.4
5	0.9	0.4	0.2	0.1	0.0	-0.1	-0.2	-0.4	-0.3	-0.2	-0.1	-0.0	0.5	1.5	1.3	1.0	0.8	0.5	0.3	0.0	0.0
4	0.5	0.2	0.0	0.1	0.1	-0.0	-0.1	-0.2	-0.2	-0.1	-0.1	-0.0	0.3	1.0	0.7	0.4	0.1	0.0	0.1	0.0	-0.1
3	0.3	0.0	-0.0	0.1	0.1	-0.0	-0.1	-0.1	-0.2	-0.1	-0.1	-0.0	0.2	0.5	0.4	0.2	0.1	0.0	0.0	-0.0	-0.1
2	0.0	-0.1	-0.0	0.0	0.0	-0.0	-0.1	-0.1	-0.2	-0.1	-0.1	-0.0	0.1	0.3	0.2	0.1	0.0	-0.0	-0.0	-0.1	-0.1
1	0.0	0.0	0.0	0.0	0.0	0.0	0.0	0.0	0.0	0.0	0.0	0.0	0.0	0.0	0.0	0.0	0.0	0.0	0.0	0.0	0.0

TABLE A-13

W_x (m/s) CASE 13 DX = 138.73 DZ = 50.00

Node Points	1	3	5	7	9	11	13	15	17	19	21	23	25	27	29	31	33	35	37	39	41
11	9.3	10.1	10.8	11.6	11.7	11.5	11.7	11.7	11.5	12.7	13.9	12.6	6.6	3.3	2.6	1.8	1.0	0.0	-0.2	0.3	0.9
10	8.8	10.1	10.6	11.1	11.2	11.2	11.3	11.5	11.6	12.2	13.1	11.6	7.6	3.5	2.6	1.6	1.2	0.7	0.6	0.9	1.1
9	8.6	9.7	10.2	10.1	10.0	10.0	10.3	10.6	10.8	11.7	12.7	12.6	8.6	3.9	2.7	1.5	1.2	0.9	0.9	1.2	1.4
8	8.3	9.6	9.9	9.5	9.4	9.6	10.0	9.7	10.8	11.7	12.5	11.9	9.5	5.4	2.7	1.5	1.5	1.6	1.6	1.5	1.4
7	7.7	9.0	9.6	9.2	9.9	9.2	9.6	9.5	9.9	11.6	11.7	11.6	9.6	5.6	2.6	1.5	1.4	1.3	1.6	1.6	1.4
6	7.6	8.5	8.8	8.5	8.3	8.6	8.8	9.2	9.6	10.9	11.5	11.4	9.6	6.1	3.0	1.5	1.4	1.3	2.0	1.7	1.4
5	6.3	7.8	7.7	7.7	7.6	7.8	8.1	8.3	8.6	10.4	10.6	10.0	9.5	6.4	3.6	2.6	2.8	1.6	2.3	2.3	1.6
4	6.3	6.8	7.2	7.0	6.8	7.3	7.6	7.5	8.1	9.2	9.7	9.5	8.6	6.6	4.5	3.6	3.4	3.2	2.8	2.3	1.9
3	5.6	5.8	5.9	5.8	5.8	6.3	6.7	6.6	6.6	8.1	8.5	8.1	7.8	6.6	5.1	4.4	3.9	3.6	3.3	2.8	2.3
2	5.4	5.4	5.5	5.4	5.1	6.0	6.0	5.8	6.2	6.6	7.5	7.4	7.4	5.6	5.0	4.5	4.1	3.8	3.4	2.9	2.4
1	5.3	4.8	4.2	3.7	3.5	4.1	5.6	5.5	5.4	5.4	5.6	5.6	5.5	5.2	5.3	5.6	5.2	4.1	3.5	3.3	3.1

W_z (m/s)

Node Points	1	3	5	7	9	11	13	15	17	19	21	23	25	27	29	31	33	35	37	39	41
11	0.2	0.3	0.3	0.4	0.1	-0.2	-1.1	-1.0	-0.9	-1.2	-1.2	-1.0	2.5	4.2	4.1	4.1	3.0	3.1	2.9	2.4	2.0
10	0.1	0.2	0.4	0.5	0.1	-0.2	-0.6	-0.8	-0.7	-1.0	-1.1	-0.4	1.5	4.0	4.1	3.8	3.0	2.6	2.4	1.8	1.5
9	0.1	0.3	0.4	0.4	0.1	-0.2	-0.7	-0.8	-0.8	-1.0	-0.9	-0.2	1.5	3.0	3.1	3.6	2.7	2.4	2.0	1.6	1.0
8	0.1	0.3	0.5	0.5	0.2	-0.1	-0.3	-0.5	-0.6	-0.7	-0.6	-0.2	1.0	2.5	3.0	3.4	2.4	1.8	1.7	1.3	0.9
7	0.0	0.3	0.6	0.4	0.1	-0.1	-0.2	-0.3	-0.4	-0.6	-0.5	-0.2	0.7	2.0	2.7	2.7	2.0	1.2	1.3	1.2	0.9
6	0.0	0.2	0.4	0.3	0.1	0.0	-0.0	-0.1	-0.1	-0.4	-0.2	0.0	0.2	1.3	2.0	2.8	1.6	0.9	1.0	1.0	0.8
5	0.0	0.1	0.3	0.3	0.2	0.2	0.1	0.1	0.0	-0.4	-0.1	-0.0	0.0	0.8	1.7	1.8	1.2	0.9	0.9	0.9	0.6
4	0.0	0.1	0.1	0.0	0.0	0.1	0.2	0.1	0.0	-0.3	-0.1	-0.1	0.0	0.4	0.9	1.3	1.0	0.8	0.7	0.5	0.4
3	0.0	0.1	0.1	0.0	0.0	0.1	0.1	0.0	0.0	-0.2	-0.1	-0.0	0.1	0.4	0.7	1.0	0.8	0.7	0.5	0.4	0.2
2	0.0	0.1	0.1	0.0	0.0	0.1	0.0	0.0	-0.0	-0.1	-0.0	0.0	0.0	0.1	0.2	0.3	0.3	0.2	0.2	0.1	0.1
1	0.0	0.0	0.0	0.0	0.0	0.0	0.0	0.0	0.0	0.0	0.0	0.0	0.0	0.0	0.0	0.0	0.0	0.0	0.0	0.0	0.0

TABLE A-14

W_x (m/s) CASE 14 DX = 128.21 DZ = 50.00

Node Points	1	3	5	7	9	11	13	15	17	19	21	23	25	27	29	31	33	35	37	39	41
11	8.8	9.4	10.0	10.0	9.8	9.9	10.0	10.0	10.0	10.0	10.0	10.0	8.0	4.0	0.1	-0.2	0.1	0.1	0.1	0.0	0.0
10	8.9	9.6	10.0	10.1	10.0	10.0	10.0	10.1	10.1	10.1	10.0	9.9	8.4	5.1	1.3	-0.3	-0.2	-0.3	-0.5	-0.7	-0.9
9	8.9	9.7	10.1	10.1	10.1	10.1	10.2	10.2	10.2	10.2	10.1	10.0	9.0	6.0	2.0	-0.1	-0.5	-0.9	-1.2	-1.6	-2.0
8	8.8	9.6	10.0	10.1	10.1	10.1	10.1	10.2	10.2	10.2	10.0	9.9	9.7	6.9	3.0	0.0	-0.8	-1.6	-2.0	-2.1	-2.1
7	8.8	9.3	9.8	10.0	9.9	9.9	10.1	10.1	10.2	10.2	10.2	10.1	10.0	7.0	4.0	0.1	-0.9	-2.0	-2.1	-2.1	-2.2
6	8.4	8.7	8.9	9.2	9.5	9.7	10.0	10.1	10.1	10.2	10.2	10.1	10.0	8.0	4.8	1.6	-0.5	-1.6	-2.1	-2.1	-2.1
5	8.0	8.0	8.3	8.5	8.8	9.0	9.7	10.0	10.1	10.1	10.2	10.1	10.0	8.3	5.1	1.9	0.0	-1.0	-2.0	-2.0	-2.1
4	7.0	7.7	8.0	8.0	8.1	8.1	8.8	9.5	9.9	9.9	10.0	10.0	9.3	7.9	5.8	3.0	0.8	-0.4	-1.1	-1.9	-2.1
3	6.0	6.4	6.7	7.1	7.4	7.8	8.1	8.4	8.6	8.9	8.6	8.3	8.0	8.0	6.0	4.0	2.0	0.0	-0.6	-1.2	-1.8
2	3.9	3.9	4.0	4.7	6.0	6.5	6.8	7.0	7.3	7.2	6.6	6.0	6.1	6.1	6.0	4.5	2.0	0.9	-0.2	-0.8	-1.5
1	3.8	3.9	3.9	4.0	4.8	5.7	6.0	5.7	6.0	5.9	4.9	3.9	4.0	5.0	6.2	4.7	3.2	1.6	0.0	-0.6	-1.3

W_z (m/s)

Node Points	1	3	5	7	9	11	13	15	17	19	21	23	25	27	29	31	33	35	37	39	41
11	1.2	-0.1	-0.9	-1.0	0.1	-0.2	-0.6	-1.0	-1.1	-1.0	-0.6	0.1	1.5	3.0	3.2	3.0	1.7	1.1	0.8	0.4	0.1
10	1.1	-0.3	-0.8	-1.0	0.0	-0.2	-0.6	-1.0	-1.1	-1.0	-0.7	0.0	1.0	2.0	3.2	2.5	1.8	1.1	0.8	0.4	0.1
9	1.1	-0.3	-0.8	-0.7	0.0	-0.1	-0.2	-0.9	-1.0	-1.1	-0.5	-0.0	0.6	1.7	3.0	2.3	1.7	1.0	0.7	0.4	0.1
8	1.1	-0.2	-0.5	-0.5	-0.2	-0.4	-0.7	-0.9	-1.0	-1.0	-0.6	-0.1	0.6	1.5	2.0	2.1	1.6	0.9	0.6	0.4	0.1
7	1.0	-0.1	-0.4	-0.4	-0.2	-0.4	-0.6	-0.7	-0.9	-0.8	-0.5	-0.2	0.3	1.0	1.7	1.9	1.4	0.9	0.6	0.4	0.1
6	0.3	-0.4	-0.7	-0.6	-0.4	-0.3	-0.3	-0.5	-0.8	-0.7	-0.4	-0.1	0.1	0.7	1.3	1.5	1.2	0.9	0.6	0.4	0.1
5	0.0	-0.3	-0.4	-0.3	-0.2	-0.3	-0.5	-0.6	-0.8	-0.6	-0.4	-0.2	0.0	0.4	0.8	1.2	0.9	0.7	0.5	0.3	0.1
4	0.0	-0.1	-0.3	-0.4	-0.3	-0.3	-0.2	-0.4	-0.6	-0.6	-0.4	-0.3	-0.1	0.2	0.6	1.0	0.8	0.6	0.5	0.3	0.1
3	0.0	-0.1	-0.2	-0.3	-0.3	-0.4	-0.4	-0.4	-0.5	-0.5	-0.5	-0.4	-0.4	-0.3	0.2	0.6	0.5	0.4	0.2	0.1	0.0
2	0.0	-0.1	-0.2	-0.2	-0.3	-0.3	-0.3	-0.3	-0.4	-0.4	-0.4	-0.3	-0.2	-0.1	0.0	0.2	0.2	0.1	0.1	0.0	0.0
1	0.0	0.0	0.0	0.0	0.0	0.0	0.0	0.0	0.0	0.0	0.0	0.0	0.0	0.0	0.0	0.0	0.0	0.0	0.0	0.0	0.0

TABLE A-15

W_x (m/s) CASE 15 DX = 185.19 DZ = 90.00

Node Points	1	3	5	7	9	11	13	15	17	19	21	23	25	27	29	31	33	35	37	39	41
11	13.5	13.5	13.5	13.4	13.4	13.4	13.4	12.7	12.1	11.4	8.1	5.5	4.4	3.3	-0.7	-2.9	-3.4	-3.9	-4.4	-4.6	-4.6
10	13.5	13.5	13.5	13.4	13.4	13.4	13.4	13.1	12.4	11.7	10.4	8.4	6.4	4.3	1.2	-2.6	-3.3	-3.9	-4.6	-4.6	-4.7
9	13.5	13.4	13.4	13.5	13.6	13.5	13.5	13.4	12.7	12.1	11.4	10.1	8.4	5.7	2.3	-0.6	-2.7	-3.9	-4.7	-4.7	-4.7
8	13.4	13.3	13.3	13.5	13.5	13.5	13.5	13.2	12.8	12.3	11.9	11.5	9.5	7.4	3.6	0.8	-1.7	-3.4	-4.7	-4.7	-4.7
7	12.0	13.1	13.4	13.4	13.5	13.4	13.4	13.0	12.7	12.3	12.0	11.6	11.3	8.6	5.4	2.4	-0.6	-2.7	-4.6	-4.6	-4.7
6	12.2	12.6	13.0	13.4	12.9	12.8	12.5	11.8	11.7	11.6	11.5	11.4	11.3	9.9	6.7	3.4	0.7	-1.6	-3.0	-3.9	-4.7
5	11.4	11.7	12.0	12.3	12.2	11.8	11.4	11.5	11.6	11.5	11.5	11.6	11.5	10.4	7.5	5.2	2.5	-0.2	-1.7	-2.6	-2.7
4	10.4	11.4	11.6	11.6	11.4	11.0	10.6	11.1	11.4	11.4	11.4	11.5	11.4	10.4	8.4	6.0	3.4	1.4	-0.4	-1.0	-1.6
3	9.4	10.7	11.3	11.3	10.9	10.2	9.5	10.3	11.1	10.4	10.9	11.4	11.3	10.0	8.4	6.7	5.2	3.3	1.4	0.9	0.3
2	9.3	9.8	9.2	8.9	9.5	9.4	9.3	9.4	9.4	9.4	9.6	9.6	9.4	9.3	8.3	6.4	5.7	4.9	3.9	3.0	2.3
1	9.2	9.4	8.4	7.4	8.8	8.9	9.1	9.2	9.4	9.3	9.4	9.4	8.6	7.8	6.9	6.7	7.3	5.6	4.1	3.2	2.7

W_z (m/s)

Node Points	1	3	5	7	9	11	13	15	17	19	21	23	25	27	29	31	33	35	37	39	41
11	-0.2	-0.6	-1.0	-0.8	-0.4	0.0	0.0	0.0	0.0	0.3	0.6	0.9	2.0	2.5	3.0	3.2	3.0	1.9	1.1	0.7	0.3
10	-0.2	-0.5	-0.8	-0.8	-0.3	0.1	0.1	0.0	0.0	0.2	0.5	0.7	1.4	2.2	2.7	3.2	0.9	0.8	0.6	0.5	0.3
9	-0.2	-0.5	-0.8	-0.5	-0.2	0.0	0.3	0.0	-0.1	0.2	0.5	0.8	1.1	1.7	2.3	3.0	2.3	1.5	0.8	0.5	0.2
8	-0.2	-0.4	-0.6	-0.4	-0.1	0.1	0.2	0.0	-0.0	0.3	0.5	0.4	0.9	1.4	2.0	2.5	2.0	1.2	0.7	0.4	0.2
7	-0.2	-0.3	-0.3	-0.2	-0.1	0.1	0.3	0.0	-0.0	0.5	0.1	0.4	0.7	1.0	1.5	2.0	1.5	1.0	0.7	0.5	0.2
6	-0.3	-0.3	-0.3	-0.2	-0.1	0.2	0.3	0.0	-0.1	0.4	0.0	0.0	0.2	0.6	1.0	1.4	1.1	0.9	0.6	0.4	0.1
5	-0.2	-0.3	-0.4	-0.2	-0.1	0.2	0.6	0.0	-0.1	0.5	-0.0	-0.1	0.2	0.7	1.1	1.1	1.0	0.9	0.6	0.4	0.1
4	-0.1	-0.3	-0.5	-0.3	-0.1	0.2	0.6	-0.1	-0.4	0.2	-0.2	-0.2	0.1	0.4	0.7	1.0	0.8	0.6	0.4	0.2	0.0
3	0.0	-0.1	-0.3	-0.2	-0.1	0.0	0.1	-0.1	-0.1	0.2	-0.1	-0.2	0.1	0.3	0.4	0.6	0.5	0.4	0.2	0.1	0.0
2	0.0	-0.1	-0.1	-0.0	-0.0	0.0	0.0	-0.0	-0.0	0.0	0.0	0.0	0.0	0.0	0.0	0.1	0.1	0.1	0.1	0.0	0.0	0.0
1	0.0	0.0	0.0	0.0	0.0	0.0	0.0	0.0	0.0	0.0	0.0	0.0	0.0	0.0	0.0	0.0	0.0	0.0	0.0	0.0	0.0

TABLE A-16

W_x (m/s) CASE 16 DX = 111.11 DZ = 50.00

Node Points	1	3	5	7	9	11	13	15	17	19	21	23	25	27	29	31	33	35	37	39	41
11	9.0	8.4	7.8	7.2	6.9	6.9	8.9	8.9	8.6	7.9	7.2	5.9	3.9	0.9	-0.1	-1.1	-1.1	-1.1	-1.2	-1.2	-1.3
10	9.0	8.4	7.8	7.2	6.9	7.4	8.5	8.8	8.3	7.8	7.4	6.9	4.8	2.9	1.5	0.8	0.4	0.0	-0.3	-0.7	-1.1
9	8.9	8.4	7.9	7.4	6.9	7.7	8.5	8.7	8.3	7.9	7.5	7.1	5.9	3.0	2.0	1.0	0.6	0.5	0.4	0.3	0.2
8	8.5	8.2	7.8	7.5	7.1	7.3	7.6	7.6	7.5	7.3	7.2	7.1	6.3	4.9	3.6	2.2	0.9	0.9	0.8	1.0	0.8
7	8.1	7.9	7.6	7.4	7.2	7.2	7.2	7.2	7.3	7.4	7.3	7.2	7.0	5.6	4.2	2.8	1.6	1.5	1.4	1.3	1.2
6	7.8	7.7	7.5	7.4	7.2	7.1	7.0	7.0	7.1	7.3	7.4	7.2	7.0	6.2	4.9	3.4	2.8	2.9	2.5	2.2	1.8
5	7.4	7.3	7.2	7.1	7.1	7.0	6.9	6.8	6.9	7.0	7.1	7.1	7.0	7.0	5.5	4.2	2.9	3.3	2.8	2.4	2.1
4	7.3	7.2	7.2	7.1	7.1	7.0	6.5	6.4	7.0	7.0	7.0	7.1	7.1	6.7	5.9	5.2	4.6	3.9	3.2	2.8	2.6
3	7.2	7.1	7.1	7.0	7.0	6.9	6.3	5.9	6.4	6.9	6.9	7.0	7.0	6.8	6.4	5.5	4.8	4.2	3.5	2.9	2.7
2	7.2	7.0	6.9	6.9	6.9	6.4	5.4	5.1	5.5	5.9	6.0	6.2	6.7	6.6	6.6	6.2	4.9	4.2	3.6	2.9	2.7
1	7.2	6.9	6.7	6.4	6.2	3.9	4.9	4.8	4.8	4.8	4.9	5.2	5.9	6.4	6.9	6.9	5.0	4.3	3.6	2.9	2.8

W_z (m/s)

Node Points	1	3	5	7	9	11	13	15	17	19	21	23	25	27	29	31	33	35	37	39	41
11	-1.2	-1.1	-1.1	-1.0	-0.9	-0.6	-0.4	-0.1	0.1	0.3	0.6	0.8	1.0	3.0	2.8	2.4	2.0	2.0	2.0	1.7	1.2
10	-1.2	-1.1	-1.1	-1.0	-0.8	-0.6	-0.4	-0.2	0.0	0.2	0.4	0.7	0.9	3.0	2.6	2.2	1.8	1.9	1.8	1.5	1.2
9	-1.1	-1.1	-1.0	-0.8	-0.5	-0.3	-0.3	-0.2	-0.1	0.1	0.3	0.6	0.8	2.0	2.0	2.1	1.5	1.7	1.6	1.3	1.0
8	-1.0	-1.1	-1.0	-0.6	-0.3	-0.1	-0.1	-0.2	-0.1	0.1	0.4	0.6	0.9	1.5	1.8	2.1	1.1	1.3	1.3	1.1	0.7
7	-0.9	-1.0	-0.8	-0.5	-0.2	-0.0	-0.1	-0.2	-0.1	0.1	0.2	0.3	0.6	1.0	1.5	2.0	1.0	1.1	1.0	1.0	0.5
6	-0.6	-0.7	-0.6	-0.3	0.0	0.1	0.0	-0.1	-0.1	0.1	0.2	0.1	0.0	0.6	1.1	1.7	0.7	1.0	0.9	0.6	0.1
5	-0.4	-0.5	-0.5	-0.2	0.0	0.2	0.1	-0.1	-0.1	0.1	0.2	0.1	0.0	0.5	1.0	1.1	0.9	0.8	0.5	0.3	0.0
4	-0.3	-0.4	-0.3	-0.1	0.1	0.3	0.1	0.0	-0.2	0.0	0.0	0.1	0.0	0.2	0.7	1.1	0.8	0.4	0.3	0.2	0.0
3	-0.2	-0.1	-0.1	-0.0	0.0	0.1	0.1	0.0	-0.1	0.0	0.0	0.0	0.0	0.0	0.4	0.8	0.6	0.5	0.3	0.2	0.0
2	-0.2	-0.1	-0.1	-0.0	0.0	0.1	0.1	0.0	-0.1	-0.0	0.0	0.0	0.0	0.0	0.1	0.2	0.2	0.1	0.1	0.0	0.0
1	0.0	0.0	0.0	0.0	0.0	0.0	0.0	0.0	0.0	0.0	0.0	0.0	0.0	0.0	0.0	0.0	0.0	0.0	0.0	0.0	0.0

TABLE A-17

W_x (m/s) CASE 17 DX = 285.71 DZ = 50.00

Node Points	1	3	5	7	9	11	13	15	17	19	21	23	25	27	29	31	33	35	37	39	41
11	20.8	21.5	21.6	21.6	20.8	19.4	18.1	15.5	14.2	12.8	11.5	7.5	5.5	3.5	1.5	1.5	1.5	1.5	1.4	1.4	1.4
10	20.8	21.5	21.6	21.6	20.8	19.5	18.2	7.4	7.1	6.8	6.5	6.2	5.9	5.6	2.5	1.8	1.5	1.4	1.4	1.3	1.3
9	20.9	21.6	21.7	21.6	20.9	19.6	18.4	17.3	16.1	14.8	13.3	10.5	8.4	6.3	4.4	2.9	1.7	1.6	1.5	1.4	1.3
8	20.9	21.4	21.6	21.5	21.0	19.9	18.8	17.5	16.2	14.8	13.5	11.5	10.2	7.6	4.8	3.3	2.7	2.0	1.4	1.4	1.3
7	20.6	21.3	21.5	20.9	20.2	19.5	18.7	17.8	16.6	14.9	13.3	11.6	10.5	9.4	5.6	4.5	3.4	2.5	1.5	1.5	1.4
6	20.4	21.5	20.9	20.4	19.8	19.2	18.6	18.1	17.5	16.0	14.3	12.2	10.7	9.6	6.6	5.9	4.8	3.5	2.7	1.9	1.4
5	20.3	19.9	19.5	19.4	19.4	18.7	18.0	17.8	17.6	16.2	13.5	12.0	10.5	9.0	7.5	7.4	5.6	4.1	2.5	2.0	1.5
4	20.0	19.7	18.5	18.0	18.4	18.1	17.9	17.7	17.6	16.3	13.9	11.5	10.7	9.8	8.9	8.0	6.5	4.5	3.3	3.0	2.8
3	19.8	19.6	17.5	17.5	17.5	17.5	17.5	17.5	17.7	16.0	13.0	10.6	9.7	9.5	9.5	9.4	7.5	5.0	3.5	3.4	3.4
2	19.8	18.3	16.5	15.7	16.2	16.6	17.1	17.5	17.5	16.2	13.5	10.8	9.8	10.3	10.0	9.8	9.5	5.5	3.5	3.5	3.6
1	19.8	19.5	15.5	15.5	15.5	16.1	16.6	17.2	17.5	15.5	11.5	10.1	9.7	10.4	10.1	9.9	9.6	5.5	4.2	3.6	3.7

W_z (m/s)

Node Points	1	3	5	7	9	11	13	15	17	19	21	23	25	27	29	31	33	35	37	39	41
11	-0.2	-0.1	0.0	0.0	-0.0	-0.1	0.0	0.0	0.5	1.1	1.4	1.7	2.0	2.1	2.1	2.0	1.5	1.0	0.7	0.4	0.1
10	-0.2	-0.1	0.1	0.1	-0.0	-0.1	0.4	0.0	0.3	1.1	1.1	1.1	1.1	1.9	1.8	1.5	1.2	0.9	0.6	0.4	0.1
9	-0.2	0.0	0.1	0.0	-0.0	-0.0	0.5	-0.1	0.1	1.0	1.1	1.2	1.3	1.1	1.1	1.4	1.0	0.9	1.0	0.5	0.0
8	-0.2	0.0	0.1	0.0	-0.0	-0.1	0.1	-0.3	0.1	0.4	0.6	0.9	1.0	1.1	1.0	1.0	1.0	0.9	1.1	0.5	0.0
7	-0.2	0.0	0.0	0.0	-0.1	-0.1	0.0	-0.5	0.0	0.3	0.5	0.8	1.0	0.9	0.9	1.0	0.9	0.8	1.0	0.0	0.0
6	-0.3	0.0	0.0	-0.1	-0.2	-0.3	0.0	-0.5	-0.2	0.1	0.3	0.6	0.8	0.4	0.4	0.7	0.8	0.8	0.9	0.4	0.0
5	-0.5	0.0	-0.0	-0.3	-0.5	-0.4	-0.1	-0.4	-0.3	0.0	0.3	0.5	0.3	0.1	0.1	0.4	0.6	0.5	0.5	0.3	0.0
4	-1.0	0.0	0.0	-0.3	-0.6	-0.7	-0.6	-0.5	-0.4	-0.2	0.0	0.4	0.1	0.0	0.1	0.3	0.2	0.2	0.1	0.1	0.0
3	-1.0	-0.3	-0.1	-0.3	-0.4	-0.4	-0.4	-0.3	-0.2	-0.1	0.0	0.3	0.1	0.0	0.0	0.1	0.2	0.1	0.1	0.0	0.0
2	-0.5	-0.3	0.0	-0.1	-0.2	-0.3	-0.2	-0.2	-0.1	-0.0	0.0	0.2	0.0	0.0	0.0	0.1	0.1	0.1	0.0	0.0	0.0
1	0.0	0.0	0.0	0.0	0.0	0.0	0.0	0.0	0.0	0.0	0.0	0.0	0.0	0.0	0.0	0.0	0.0	0.0	0.0	0.0	0.0

TABLE A-18

W_x (m/s) CASE 18 DX = 400.00 DZ = 30.00

Node Points	1	3	5	7	9	11	13	15	17	19	21	23	25	27	29	31	33	35	37	39	41
11	13.7	15.0	15.0	16.0	17.7	19.0	16.1	12.8	13.0	15.6	15.9	14.7	14.0	13.3	13.0	13.0	13.0	13.0	13.0	12.7	12.2
10	13.5	13.8	14.4	15.3	17.1	18.0	15.8	11.2	13.0	15.7	15.8	14.2	13.7	13.2	12.9	12.9	12.9	13.0	12.7	12.2	11.6
9	12.9	13.0	14.0	15.0	17.0	17.5	17.0	11.4	12.9	15.6	15.7	13.0	13.0	13.0	11.0	11.4	11.9	12.3	12.8	12.1	11.5
8	12.8	12.9	13.5	14.6	15.6	16.5	15.0	12.3	12.9	15.0	14.5	12.0	11.9	11.8	10.8	11.3	11.2	11.1	11.1	11.2	11.2
7	12.2	12.6	13.1	15.0	15.4	15.8	14.5	12.4	12.9	14.3	13.7	11.0	10.9	10.8	10.7	10.9	11.1	11.0	11.0	11.1	11.0
6	11.8	12.2	12.6	13.0	13.8	14.6	14.0	12.1	13.0	13.1	12.0	10.6	10.0	10.1	10.3	10.4	10.6	10.7	10.8	10.9	10.5
5	11.5	11.8	12.1	12.4	12.7	13.0	12.9	12.8	12.7	12.6	11.0	9.0	9.1	9.3	9.6	10.0	10.3	10.2	10.1	10.0	9.9
4	11.3	11.1	11.0	11.0	11.0	11.0	12.2	12.5	11.8	11.0	9.7	8.5	8.3	8.5	9.3	9.2	9.1	9.1	9.0	8.9	8.9
3	10.9	10.3	9.6	9.0	9.0	10.0	11.7	13.0	11.1	9.7	8.4	7.1	8.1	9.0	9.4	9.2	9.0	9.6	8.7	7.8	7.0
2	9.1	9.0	9.0	7.0	5.8	7.1	10.9	13.0	9.0	7.0	6.9	6.8	7.6	7.8	7.4	7.0	8.3	9.5	7.8	6.3	5.0
1	7.0	7.0	7.8	5.9	6.0	8.0	11.0	13.1	7.0	6.8	6.7	6.8	7.1	7.2	7.0	7.0	7.0	9.0	8.0	6.3	5.0

W_z (m/s)

Node Points	1	3	5	7	9	11	13	15	17	19	21	23	25	27	29	31	33	35	37	39	41
11	-0.9	-0.0	-0.1	-0.1	0.0	0.0	0.0	0.1	0.0	0.0	-1.0	0.1	0.4	0.6	0.9	1.1	1.7	2.1	2.0	0.8	0.4
10	-1.0	0.0	0.0	0.0	0.1	0.1	0.0	0.2	0.1	0.0	-1.0	0.1	0.3	0.6	0.8	1.0	1.5	2.1	1.2	0.7	0.4
9	-1.0	-0.1	-0.2	0.0	0.1	0.1	0.1	0.4	0.1	0.0	-1.0	0.1	0.3	0.5	0.7	0.9	1.4	1.9	1.0	0.7	0.4
8	-1.0	-0.6	-0.3	0.0	0.1	0.3	0.5	0.6	0.5	0.0	-1.0	0.1	0.3	0.4	0.6	0.8	0.9	1.3	1.0	0.0	0.3
7	-1.0	-0.6	-0.2	-0.0	0.0	0.4	0.8	1.0	1.0	0.0	-0.4	0.1	0.2	0.4	0.5	0.6	0.8	0.9	0.7	0.0	0.0
6	-1.0	-0.2	-0.1	-0.1	0.0	0.4	0.8	1.1	1.0	0.0	-0.7	0.1	0.2	0.3	0.4	0.5	0.6	0.7	0.5	0.0	0.0
5	-1.0	-0.1	-0.0	-0.1	-0.1	0.3	0.8	1.1	0.9	0.0	-0.3	0.0	0.1	0.3	0.3	0.4	0.5	0.6	0.5	0.0	0.0
4	-0.5	0.0	-0.1	-0.2	-0.1	0.2	0.6	1.0	0.3	0.0	-0.3	0.0	0.1	0.1	0.2	0.3	0.3	0.4	0.3	0.0	0.0
3	0.0	-0.1	0.0	-0.1	-0.0	0.1	0.4	0.7	0.2	-0.1	-0.2	0.0	0.0	0.1	0.1	0.1	0.2	0.2	0.1	0.0	0.0
2	0.0	0.1	0.0	-0.1	0.0	0.1	0.1	0.2	0.1	-0.0	-0.1	0.0	0.0	0.0	0.0	0.1	0.1	0.1	0.1	0.0	0.0
1	0.0	0.0	0.0	0.0	0.0	0.0	0.0	0.0	0.0	0.0	0.0	0.0	0.0	0.0	0.0	0.0	0.0	0.0	0.0	0.0	0.0

TABLE A-19

W_x (m/s) CASE 19 DX = 178.57 DZ = 50.00

Node Points	1	3	5	7	9	11	13	15	17	19	21	23	25	27	29	31	33	35	37	39	41
11	0.7	0.9	1.0	3.0	4.9	2.9	4.3	6.0	8.0	10.0	11.1	11.2	11.3	11.1	11.0	8.0	5.0	5.0	1.0	0.9	0.7
10	0.7	1.0	2.3	3.7	5.2	3.9	6.0	8.0	10.0	11.9	11.7	11.6	11.4	11.3	11.1	9.6	7.0	6.3	3.0	1.0	0.9
9	1.0	2.3	4.0	6.0	6.3	5.0	7.0	9.0	11.0	13.0	13.0	12.6	12.2	11.8	11.4	11.0	9.0	6.0	3.0	2.0	1.0
8	3.0	4.0	5.0	7.1	7.7	7.0	8.5	20.2	12.1	13.1	13.0	12.1	11.3	11.5	11.8	11.3	10.0	7.5	4.5	2.7	2.0
7	5.0	5.8	6.6	8.0	9.0	9.1	10.0	11.7	13.0	13.1	12.9	11.9	11.0	11.1	11.2	11.3	11.0	9.0	5.2	3.7	2.5
6	6.0	7.0	8.3	9.2	9.8	10.3	10.9	11.7	12.6	12.9	12.4	11.5	11.0	11.0	11.0	10.6	9.8	9.0	7.0	5.0	2.7
5	7.0	7.8	8.6	9.3	9.9	10.4	11.0	11.6	12.2	12.1	11.4	10.7	10.0	10.3	10.7	11.0	10.0	9.0	7.7	5.7	3.0
4	7.1	7.9	8.6	9.3	9.9	10.4	11.0	11.5	12.0	11.3	10.5	9.6	9.2	9.1	9.1	9.1	9.0	8.6	7.8	7.0	3.5
3	7.2	7.2	8.1	9.1	9.2	9.9	11.0	11.3	11.3	10.5	9.4	8.4	8.5	9.1	9.2	9.1	8.8	8.5	9.0	7.0	4.1
2	7.2	7.0	7.0	9.0	9.0	9.5	10.5	11.1	10.9	9.8	8.3	6.8	6.6	7.8	9.0	9.1	8.7	8.2	9.0	7.0	4.2
1	7.2	7.0	7.0	8.0	8.5	9.0	9.8	10.6	11.0	9.0	7.0	5.0	5.7	7.2	8.4	9.0	8.8	8.3	9.0	7.0	4.3

W_z (m/s)

Node Points	1	3	5	7	9	11	13	15	17	19	21	23	25	27	29	31	33	35	37	39	41
11	-1.3	-1.6	-2.0	-2.0	-0.8	-2.0	-1.0	-2.2	-2.0	-1.2	-0.5	1.0	1.0	-0.9	-1.8	-1.4	0.3	2.2	2.8	2.3	1.5
10	-1.3	-1.6	-1.9	-1.5	-0.8	-2.0	-1.0	-1.7	-1.7	-1.0	0.0	0.8	0.5	-0.6	-1.7	-1.4	0.3	1.9	2.8	2.1	1.5
9	-1.2	-1.4	-1.6	-1.3	-0.8	-1.7	-0.9	-2.0	-1.3	-0.6	0.1	0.7	0.4	-0.6	-1.7	-1.6	0.0	1.6	2.6	2.1	1.5
8	-1.2	-1.1	-1.1	-1.0	-0.7	-1.5	-0.9	-1.4	-1.0	-0.4	0.2	0.7	0.4	-0.5	-1.6	-1.5	-0.2	1.3	2.0	2.1	1.2
7	-1.2	-1.1	-1.1	-1.0	-0.7	-1.3	-0.8	-1.2	-0.8	-0.3	0.2	0.6	0.2	-0.7	-1.6	-1.4	-0.2	1.0	1.5	2.0	1.0
6	-1.1	-1.1	-1.1	-1.1	-0.7	-1.1	-0.8	-1.2	-0.7	-0.2	0.2	0.6	0.2	-0.6	-1.3	-1.3	-0.4	0.9	1.3	1.8	0.9
5	-1.0	-1.1	-1.1	-1.0	-0.6	-1.0	-0.6	-1.0	-0.6	-0.2	0.2	0.5	0.1	-0.6	-1.3	-1.3	-0.5	0.5	1.1	1.4	0.9
4	-1.0	-1.0	-1.0	-0.8	-0.5	-0.6	-0.6	-0.6	-0.4	-0.1	0.1	0.3	0.1	-0.6	-1.0	-0.9	-0.2	0.3	0.7	1.1	0.8
3	-0.5	-0.9	-0.8	-0.7	-0.4	-0.3	-0.2	-0.3	-0.2	-0.1	0.0	0.2	0.0	-0.5	-1.0	-0.9	0.0	0.3	0.6	0.9	0.6
2	-0.2	-0.2	-0.2	-0.2	-0.1	-0.2	-0.2	-0.1	-0.1	-0.0	0.0	0.1	0.0	-0.2	-0.3	-0.3	0.0	0.1	0.2	0.3	0.1
1	0.0	0.0	0.0	0.0	0.0	0.0	0.0	0.0	0.0	0.0	0.0	0.0	0.0	0.0	0.0	0.0	0.0	0.0	0.0	0.0	0.0

TABLE A-20

W_x (m/s) CASE 20 DX = 333.33 DZ = 50.00

Node Points	1	3	5	7	9	11	13	15	17	19	21	23	25	27	29	31	33	35	37	39	41
11	9.9	11.9	13.9	14.2	14.5	14.5	14.6	14.6	15.8	18.5	19.9	19.9	17.9	15.5	13.0	10.8	8.9	6.9	5.5	4.8	4.1
10	9.7	11.2	12.7	13.9	14.4	14.1	13.9	13.9	15.9	18.7	19.9	19.3	18.0	15.9	13.2	10.9	8.8	6.8	5.5	4.7	3.9
9	9.9	10.6	12.1	12.8	13.6	13.7	13.7	13.8	16.0	18.8	19.9	19.2	17.6	16.0	13.9	11.6	9.4	7.5	5.7	4.5	3.9
8	9.7	9.9	11.2	12.1	12.4	12.7	13.2	13.8	16.4	18.9	19.9	18.8	17.7	16.1	14.0	11.9	9.3	7.2	5.6	4.0	3.8
7	7.9	9.2	10.2	10.8	11.3	11.9	12.8	13.8	16.6	18.9	19.9	18.9	17.8	16.2	14.1	11.9	9.9	7.9	5.9	4.0	3.8
6	7.4	8.4	9.4	10.2	10.9	11.5	12.6	13.9	16.6	18.5	19.5	18.6	17.7	16.2	14.1	11.9	9.8	7.7	5.9	4.4	3.7
5	6.7	7.5	8.4	9.4	10.3	11.2	12.0	13.9	16.6	18.2	18.9	18.4	17.9	15.9	14.0	11.9	9.8	7.7	5.8	4.5	3.8
4	5.9	6.9	7.9	8.8	9.7	10.6	11.6	13.3	15.8	17.9	18.7	17.9	16.9	15.9	13.9	11.7	9.2	7.4	5.7	4.5	3.8
3	5.8	6.4	7.4	8.3	9.1	9.9	11.4	12.9	13.9	16.4	17.2	16.3	15.9	14.9	12.9	10.9	8.9	7.2	5.9	4.6	3.8
2	5.8	5.9	6.3	6.3	6.9	8.4	9.4	10.9	11.9	13.9	15.4	14.4	13.9	13.9	11.9	9.9	7.9	6.6	5.3	3.9	3.7
1	5.7	5.8	5.9	5.9	5.9	7.9	8.9	9.9	9.6	11.9	13.1	11.9	11.9	11.9	9.9	8.6	7.4	6.5	4.9	3.8	3.7

W_z (m/s)

Node Points	1	3	5	7	9	11	13	15	17	19	21	23	25	27	29	31	33	35	37	39	41
11	-0.6	-1.1	-1.2	-1.2	-1.1	-1.1	-1.1	-2.0	-3.0	-2.8	-1.7	-1.0	-0.6	-0.2	0.0	0.0	0.0	0.1	0.1	0.1	0.1
10	-0.5	-1.1	-1.2	-1.2	-1.1	-1.1	-1.1	-1.8	-2.4	-2.3	-1.4	-0.8	-0.5	-0.2	0.0	0.0	0.0	0.1	0.2	0.2	0.2
9	-0.4	-0.9	-1.1	-1.0	-1.0	-1.0	-0.9	-1.4	-2.0	-1.9	-1.0	-0.7	-0.4	-0.1	0.0	0.0	0.1	0.2	0.2	0.2	0.1
8	-0.2	-0.6	-1.0	-0.9	-0.8	-0.9	-0.8	-1.0	-1.4	-1.3	-0.9	-0.6	-0.4	-0.1	0.0	0.0	0.1	0.2	0.2	0.1	0.1
7	0.0	-0.2	-0.5	-0.6	-0.5	-0.5	-0.6	-0.9	-1.1	-1.0	-0.7	-0.4	-0.2	0.0	0.0	0.0	0.1	0.2	0.2	0.1	0.1
6	0.1	-0.1	-0.4	-0.5	-0.4	-0.3	-0.5	-0.7	-0.9	-0.6	-0.4	-0.1	-0.2	0.0	0.0	0.1	0.1	0.2	0.1	0.1	0.0
5	0.1	0.0	-0.2	-0.3	-0.2	-0.1	-0.3	-0.6	-0.8	-0.5	-0.3	0.0	-0.1	0.0	0.0	0.1	0.1	0.2	0.1	0.1	0.0
4	0.1	0.0	0.0	0.0	0.0	0.0	-0.1	-0.3	-0.4	-0.4	-0.2	0.0	0.0	0.0	0.0	0.1	0.1	0.1	0.1	0.0	0.0
3	0.1	0.0	0.0	0.0	0.0	0.0	-0.0	-0.1	-0.2	-0.2	-0.1	0.0	0.0	0.0	0.0	0.0	0.0	0.0	0.0	0.0	0.0
2	0.0	0.0	0.0	0.0	0.0	0.0	0.0	-0.0	-0.1	-0.1	-0.1	-0.1	-0.0	-0.0	-0.0	0.0	0.0	0.0	0.0	0.0	0.0
1	0.0	0.0	0.0	0.0	0.0	0.0	0.0	0.0	0.0	0.0	0.0	0.0	0.0	0.0	0.0	0.0	0.0	0.0	0.0	0.0	0.0

REFERENCES

REFERENCES FOR CHAPTER 1

1-1. Etkin, Bernard. Dynamics of Atmospheric Flight, John Wiley and Sons, New York, (1973).

1-2. McRuer, Duane, Irving Ashkenas, and Dunstan Graham. Aircraft Dynamics and Automatic Control, Princeton University Press, Princeton, New York, (1973).

1-3. Dobrolenskey, Y. P. "Flight Dynamics in Moving Air," NASA TT F-600 (1971).

1-4. Bromley, Edmund, Jr., "Aeronautical Meteorology - Progress and Challenges - Today and Tomorrow," 57th Annual Meeting of the AMS, Jan. 1977, Tucson, Arizona.

1-5. Wyatt, S. V. "Weather Involvement in General Aviation Accidents, "Fifth Annual International Seminar, The Society of Air Safety Investigators, Washington, D. C., October 1-3, (1974).

1-6. Laynor, W. G., Performance Study DCA-74-A-14, NTSB, Bureau of Aviation Safety, Washington, D. C., (1974).

1-7. Aircraft Accident Report, FAA, Report No. NTSB-AAR-71-11, (1971).

1-8. Sowa, Daniel. "Low-Level Wind Shear," D. C. Flight Approach, No. 20, Douglas Aircraft Co., Long Beach, California, (1974).

1-9. Chambers, E. "BOAC Experience with Turbulence," Flight in Turbulence, AGARD-CP-140 (1973), 6. 1-6.13.

1-10. Low Level Wind Shear, Department of Transportation, Federal Aviation Administration, Advisory Circular AC No: 00-50, (1976).

REFERENCES FOR CHAPTER 4

4-1 Kropfli, R. A. and L. J. Miller, "Kinematic Structure and Flux Quantities in a Convective Storm from Dual-Doppler Radar Observations," J. Atmos. Sci. 3 (1976) 520-529.

4-2 Goff, R. C., "Thunderstorm Outflow Kinematics and Dynamics," NOAA Tech. Memo. ERL NSSL-75 (1975).

4-3 Colmer, M. "On the Character of Thunderstorm Gust Fronts" Proceeding International Conference on Atmospheric Turbulence Roy. Aeronautical Soc., (1971).

4-4 Sinclair, R. W., R. A. Anthes and H. A. Panofsky, "Variation of the Low Level Winds During the Passage of A Thunderstorm Gust Front," NASA CR-2289 (1973).

4-5 Frank, H.W., "Notes on the 8 August 1972 Haswell Gravity Flow Event," personal communication.

4-6 Clarke, R.H., Mesostructure of Dry Cold Fronts over Featureless Terrain," J. Meteor., 18 (1961) 715-735.

4-7 Byers, H.R. and R.R. Braham, Jr., The Thunderstorm, U.S. Government Printing Office, Washington, D.C., (1949) 287.

4-8 Ward, N.B., and A.B. Arnett, "Some Relationships Between Surface Wind Fields and Radar Echoes," Proc. of the third Conf. on Severe Storms, Champaign, Ill. (1962).

4-9 Browning, K.A. and T.W. Harold, "Air Motion and Precipitation Growth of a Cold Front," Quart. J. Roy. Meteor. Soc., 96 (1970) 369-398.

4-10 Fichtl, G.H., and D. Camp, Personal Communications (1976).

4-11 Mitchell, K.E., "A Numerical Investigation of Severe Thunderstorm Gust Fronts," NASA CR-2635, (1975).

REFERENCES FOR CHAPTER 5

5-1 Fichtl, G.H., "Problems in the Simulation of Atmospheric Simulation of Atmospheric Boundary Layer Flows, Flight in Turbulence," AGARD-CP-140 (1973) 2-1.

5-2 Busch, Niels E., "The Surface Boundary Layer," Boundary Layer Meteorology, 4 (1973) 213-240.

5-3 Monin, A.S., "The Atmospheric Boundary Layer," Annual Review of Fluid Mech., Annual Reviews, Palo Alto, Calif. (1970) 225-250.

5-4 Leurs, J.K., "A Model of Wind Shear and Turbulence in the Surface Boundary Layer," NASA CR-2288 (1973).

5-5 Barr, N.M., Dagfinn Gangaas and D.R. Schaeffer, "Wind Models for Flight Simulator Certification of Landing and Approach Guidance and Control Systems," Report No. FAA-RD-74-206 (1974).

5-6 Businger, J.A. "Turbulent Transfer in the Atmospheric Surface Layer," Workshop on Micrometeorology, Ed. Duane A. Haugen, Published by American Meteorology Society, (1973) 67-100.

5-7 Blackadar, A.K., J.A. Dutton, H.A. Panofsky and A. Chaplin, "Investigation of Turbulent Wind Fields Below 150 m Altitude at the Eastern Test Range," NASA-CR-1410 (1972).

5-8 Fiedler, F., and H.A. Panofsky, "The Geostrophic Drag Coefficient and the Effective Roughness Length," Quart. J. Roy. Meteor. Soc., 98 (1972), 213-306.

5-9 Thuiller, R.H. and V.O. Lappe, "Wind and Temperature Profile Characteristics from Observations on a 1400 ft. Tower," J. Appl. Meteor., 3 (1964) 299-306.

5-10 Tennekes, H. "Similarity Laws and Scales Relations in Planetary Boundary Layers," Workshop on Micrometeorology Ed. Duane A. Haugen, Published by American Meteorology Society, (1973) 177-216.

5-11 Hana, S.R., "Characteristics of Wind and Turbulence in the Planetary Boundary Layer," ERLTM-ARL Tech. Memo. 8, Oak Ridge, Tenn. (1969).

5-12 Estoque, M.A., "Numerical Modeling of the Planetary Layer," Workshop on Micrometeorology, Ed., Duane A. Haugen, Published by American Meteorology Society, (1973) 217-270.

5-13 Blackadar, A.K., and H. Tennekes, "Asymptotic Similarity in Neutral Barotropic Atmospheric Boundary Layers," J. Amos. Sci. 25 (1968), 1015-1020.

5-14 Hess, G.D. "On Rossby-Number Similarity Theory for a Baroclinic Boundary Layer," J. Atmos. Sci., 30, (1973), 1722-1723.

5-15 Yamada, Tetsuji, "On the Similarity Functions A, B and C of the Planetary Boundary Layer," J. Atmos. Sci., 5 (1976) 781-793.

5-16 Clarke, R.H., and G.D. Hess, "Geostrophic Departure and the Function A and B of the Rossby-Number Similarity Theory," Boundary Layer Meteorology 3 (1974) 267-288.

5-17 Deardorff, J.W., "Numerical Investigation of Neutral and Unstable Planetary Boundary Layer," J. Atmos. Sci., 30, (1972) 91-115.

5-18 Blackadar, A.K., "The Vertical Distribution of Wind and Turbulent Exchange in a Neutral Atmosphere," J. Geophys. Res. 67 (1962) 3095-3102.

5-19 Ohmstede, W.D. and J.F. Appleby, Numerical Solution of the Distribution of Wind and Turbulence in the Planetary Boundary Layer," Meteor. Res. Note No. 8 DA Task 1-A-0-1101-B-021-08 USAERDAA-MET-5-64, (1964) 43.

5-20 Blackadar, A.K. and J. Ching, "Wind Distribution in a Steady State Planetary Boundary Layer of the Atmosphere With Upward Heat Flux," Final Rept. Contract AF (604)-6641, Dept. of Meteor., Penn. State Univ. (1965) 23-48.

5-21 Yamamoto, G., N. Yasuda and A. Shimanuke, "Effects of Thermal Statification on the Ekman Layer," J. Meteor. Soc., Japan, 46, (1969) 442-455.

5-22 Blackadar, A.K., "A Single Theory of the Vertical Distribution of the Wind in a Baroclinic Neutral Atmospheric Boundary Layer," Final Rept., Contract AF (604)-6641, Dept. of Meteor., Penn. State Univ. (1965) 1-22.

5-23 Plate, E.J., Aerodynamic Characteristics of Atmospheric Boundary Layers. AEC Critical Review Series, TID-25465, (1971) 137-160.

5-24 Huang, Chin, Hua and E.C. Nickerson, "Stratified Flow Over Non-Uniform Surface Conditions: Mixing Length Model," Boundary Layer Meteorology 4 (1974) 395-418.

5-25 Panchev. S., E. Donev and N. Godev, "Wind Profile and Vertical Motions above an Abrupt Change in Surface Roughness and Temperature," Boundary Layer Meteorology 1 (1971) 52-63.

5-26 Bradley, E.F., "A Micrometeorological Study of Velocity Profiles and Surface Drag in the Region Modified by a Change in Surface Roughness," Quart. J. Roy. Meteor. Soc. 94 (1968) 361-379.

5-27 Munro, D.S. and T.R. Oke, "Aerodynamic Boundary Layer Adjustment Over a Crop in Neutral Stability," Boundary Layer Meteorology, 9 (1975) 53-61.

5-28 Antonia, R.A. and R.E. Luxton, "The Response of a Turbulent Boundary Layer to a Step Change in Surface Roughness. Part 2 Rough-to-Smooth," J. Fluid Mech. 53 (1972) 737-757.

5-29 Merony, R.N., "Characteristics of Wind and Turbulence in and Above Model Forests," J. Appl. Meteor., 7 (1968) 780-788.

5-30 Elliott, W.P., "The Growth of the Atmospheric Internal Boundary Layer," Trans. Amer. Geophys. Union 39, (1958) 1048-1054.

5-31 Rao, K.S., "Effect of Thermal Stratification of the Internal Boundary Layer," Boundary Layer Meteorology, 2 (1975) 227-234.

5-32 Huang, Chin-Hua and E.C. Nickerson, "Stratified Flow Over Non-Uniform Surfaces: Turbulent Energy Model," Boundary Layer Meteorology, 1, (1974) 107-124.

5-33 Rao, K.S., J.C. Wyngaard and O.R. Cote, "The Structure of the Two-Dimensional Internal Boundary Layer Over a Sudden Change in Surface Roughness," J. Atmos. Sci. 31 (1974) 738-746.

5-34 Bitte, Juergen, and Walter Frost, "Numerical Solution of Turbulent Flow over Surface Roughness Transition: Two Equation Turbulence Model," paper in preparation, Univ. of Tenn. Space Institute.

5-35 Logan, Earl, Jr., and G.H. Fichtl, "Rough to Smooth Transition of an Equilibrium Neutral Constant Stress Layer," NASA TM X-3322, (1975).

5-36 Geiger, Rudolf, The Climate Near the Ground, Harvard University Press, Cambridge, Mass. (1950).

5-37 Windbreaks and Shelterbelts WMO-No. 147.TP.70, (1964).

5-38 Munn, R.E., Descriptive Micrometeorology, Academic Press, (1966).

5-39 Ogawa, Yasushi, Richard Griffiths and W.G. Hoydysh, "A Wind Tunnel Study of Sea Breeze Effects," Boundary Layer Meteorology 2 (1975) 141-162.

5-40 Vukovich, F.M., J.W. Dunn III and B.W. Cressman, "A Theoretical Study of the St. Louis Heat Island: The Wind and Temperature Distribution," J. Appl. Meteor. 5 (1976) 417-440.

5-41 Taylor, P.A., "A Model of Airflow above Changes in Surface Heat Flux, Temperature and Roughness for Neutral and Unstable Conditions." Boundary Layer Meteorology, 1 (1970) 18-39.

REFERENCES FOR CHAPTER 6

6-1. Houbolt, J. C., Roy Steiner, and K. G. Pratt. "Dynamic Response of Airplanes to Atmospheric Turbulence Including Flight Data on Input and Response," NASA TR R-199, National Aeronautics and Space Administration, Washington, D.C., June 1964.

6-2. Houbolt, J. C. "Gust Design Procedures Based on Power Spectral Techniques," Technical Report AFFDL-TR-67-74, Wright-Patterson Air Force Base, Ohio, August 1967.

6-3. Reeves, P. M., G. S. Campbell, V. M. Ganzer, and R. G. Joppa. "Development and Application of a Non-Gaussian Atmospheric Turbulence Model for Use in Flight Simulators," NASA CR-2451, National Aeronautics and Space Administration, Washington, D.C., September 1974.

6-4. Reeves, P. M., R. G. Joppa, and V. M. Ganzer. "A Non-Gaussian Model of Continuous Atmospheric Turbulence for Use in Aircraft Design," NASA CR-2639, National Aeronautics and Space Administration, Washington, D.C., January 1976.

6-5. Jones, J. G. "A Unified Discrete Gust and Power Spectrum Treatment of Atmospheric Turbulence," Paper presented at the Royal Aeronautical Society International Conference on Atmospheric Turbulence, May 18-21, 1971.

6-6. Tomlinson, B. N. "Developments in the Simulation of Atmospheric Turbulence," Tech. Memo FS 46, Royal Aircraft Establishment, September 1975.

6-7. Frost, Walter, and M. Perlmutter. "Three Velocity Component Atmospheric Boundary Layer Turbulence," Contract No. NAS8-29548 Report, University of Tennessee Space Institute, Tullahoma, Tennessee 37388, 1976.

6-8. Munn, R. E., editor. "Turbulence Spectra, Length Scales and Structure Parameters in the Stable Surface Layer." Boundary-Layer Meteorology, Vol. 4, Nos. 1, 2, 3 and 4, April 1973.

6-9. Jernigan, P. L. Douglas Aircraft Company, personal communications.

6-10. Bray, R. S. NASA Ames Research Center, personal communications.